University of South Carolina
Scholar Commons

Theses and Dissertations

12-14-2015

Supramolecular Coordination Networks of s- and f-Block Metals Featuring the 1,8-Naphthalimide Tecton

Andrew Paul Leitner
University of South Carolina - Columbia

Follow this and additional works at: https://scholarcommons.sc.edu/etd

 Part of the Chemistry Commons

Recommended Citation

Leitner, A. P.(2015). *Supramolecular Coordination Networks of s- and f-Block Metals Featuring the 1,8-Naphthalimide Tecton.* (Doctoral dissertation). Retrieved from https://scholarcommons.sc.edu/etd/3251

This Open Access Dissertation is brought to you by Scholar Commons. It has been accepted for inclusion in Theses and Dissertations by an authorized administrator of Scholar Commons. For more information, please contact digres@mailbox.sc.edu.

Supramolecular Coordination Networks of s- and f-Block Metals Featuring the 1,8-Naphthalimide Tecton

by

Andrew Paul Leitner

Bachelor of Science
Georgia Institute of Technology 2010

Submitted in Partial Fulfillment of the Requirements

For the Degree of Doctor of Philosophy in

Chemistry

College of Arts and Sciences

University of South Carolina

2015

Accepted By:

Daniel L. Reger, Major Professor

Hans-Conrad zur Loye, Committee Member

John J. Lavigne, Committee Member

John Van Zee, Committee Member

Michael A. Matthews, Committee Member

Lacy Ford, Senior Vice Provost and Dean of Graduate Studies

© Copyright by Andrew Paul Leitner, 2015.

All Rights Reserved.

Dedication

To Eryn, Justin, Riley and Frankleton.

Our real discoveries come from chaos, from going to the place that looks wrong and stupid and foolish.

Acknowledgements

Thank you so much to the following people who have helped me immensely along my journey without whose support I would not be here today. Dr. Reger has been an excellent advisor who has encouraged me to be creative and adventurous in my experiements and who has the patience to teach me how to write and do proper science. Dr. Mark Smith had the patience to solve over 90 of my crystal structures, many with extensive disorder, and rejected several times that many submissions. My committee members Drs. Hans-Conrad zur-Loye, John Lavigne and John Van Zee, had valuable input on my research plan and proposal and a thanks to Dr. Michael Matthews for serving in Dr. Van Zee's absence.

Thank you to the past members of the Reger group who laid the groundwork that made my research possible. Drs. Radu Semeniuc and Jacob Horger developed the ligands that I used extensively. Drs. Ágota Debreczeni and Andrea Pascui made me feel welcome in the lab and were an invaluable part of my graduate experience. The past members of Dr. zur-Loye's group, Drs. Shae Vaughn, Rachel Severance, Michael Chance taught me to use their instruments with care and how crystal growth worked. Some of the present members Dr. Greg Morrison and Allison Latshaw for help with magnetism. Derek Williams and others from Dr. Natalia Shustova's group who allowed me to use their instruments and provided me with some company in this big empty lab.

A big thank you to my parents who raised me with a love of science and a curiosity to seek answers to the big questions. Thank you to my non-chemistry friends Justin Thaker, Riley Chapman, Andrew and Elizabeth Park-Floyd, Paul Priest and Santiago Azpúrua-Borrás who kept me sane and showed me a great time in Columbia, South Carolina. The biggest thank you of all to Eryn Jacobson for being so patient and loving with me while I worked on chemistry. You have a kind heart and have taught me a lot about life.

Abstract

The reactions of (*S*)-2-(1,8-naphthalimido)propanoic acid (H$\mathbf{L_{ala}}$), and (*S*)-2-(1,8-naphthalimido)-3-hydroxypropanoic acid (H$\mathbf{L_{ser}}$), protonated forms of ligands that contain a carboxylate donor group, an enantiopure chiral center and a 1,8-naphthalimide $\pi^{\cdots}\pi$ stacking supramolecular tecton and in the case of H$\mathbf{L_{ser}}$ an alcohol functional group, with the appropriate alkali metal hydroxide followed by a variety of crystallization methods leads to the formation of crystalline K($\mathbf{L_{ala}}$)(MeOH) (**1**), K($\mathbf{L_{ala}}$)(H_2O) (**2**), Na($\mathbf{L_{ala}}$)(H_2O) (**3**), K$\mathbf{L_{ser}}$ (**4**), Cs$\mathbf{L_{ser}}$ (**5**) and Cs$\mathbf{L_{ala}}$ **(6)**. Each of these new complexes has a solid state structure based on six-coordinate metals linked into homochiral helical rod SBU central cores. In addition to the bonding of the carboxylate and solvent (in the case of $\mathbf{L_{ser}}$ the ligand alcohol) to the metals, both oxygens on the 1,8-naphthalimide act as donor groups. One naphthalimide oxygen bonds to the same helical rod SBU as the carboxylate group of that ligand forming a chelate ring. The other naphthalimide oxygen bonds to adjacent SBUs. In complexes **1**-**3**, this inter-rod link has a square arrangement bonding four other rods forming a three-dimensional enantiopure MOF structure, whereas in **4**-**6** this link has a linear arrangement bonding two other rods forming a two-dimensional, sheet structure. In the latter case, the third dimension is supported exclusively by interdigitated $\pi^{\cdots}\pi$ stacking interactions of the naphthalimide supramolecular tecton, forming enantiopure supramolecular MOF solids. Compounds **1**-**3** lose the coordinated solvent when heating above 100 °C. For **1**, the polycrystalline powder reverts to **1** only by recrystallization from methanol, whereas compounds **2** and **3**

undergo gas/solid, single-crystal to single-crystal transformations to form dehydrated compounds **2*** and **3***, and rehydration occurs when crystals of these new complexes are left out in air. The reversible single-crystal to single-crystal transformation of **2** involves the dissociation/coordination of a terminal water ligand, but the case of **3** is remarkable considering the water that is lost is the only bridging ligand between the metals in the helical rod SBU and a carboxylate oxygen that is a terminal ligand in **3** moves into a bridging position in **3*** to maintain the homochiral helical rods. Both **2*** and **3*** contain five-coordinate metals. There are no coordinated solvents in compounds **4-6**, in two cases by designed ligand modification, which allows them to have high thermal stability. Compounds **1**-**3** did not exhibit observable SHG efficiency at an incident wavelength of 1064 nm, but compounds **4**-**6** did exhibit modest SHG efficiency for MOF-like compounds in the range of 30 x α-SiO_2.

The reactions of the potassium salts of the ligands (*S*)-2-(1,8-naphthalimido)propanoate (K$\mathbf{L_{ala}}$) and (*S*)-2-(1,8-naphthalimido)-3-hydroxypropanoate (K$\mathbf{L_{ser}}$) and (*R*)-2-(1,8-naphthalimido)propanoate (K$\mathbf{L_{ala}}$*), enantiopure carboxylate ligands containing a 1,8-naphthalimide π...π stacking supramolecular tecton and in the case of $\mathbf{L_{ser}}^-$ an alcohol functional group, with calcium or strontium nitrate under solvothermal conditions produce crystalline [Ca($\mathbf{L_{ala}}$)$_2$(H_2O)]·(H_2O) (**1**), [Ca($\mathbf{L_{ser}}$)$_2$]·(H_2O)$_2$ (**2**), [Sr($\mathbf{L_{ala}}$)$_2$(H_2O)]·(H_2O)$_3$ (**3**), [Sr($\mathbf{L_{ala}}$*)$_2$(H_2O)]·(H_2O)$_3$ (**3***) and [Sr($\mathbf{L_{ser}}$)$_2$(H_2O)] (**5**). Placing **3** under vacuum removes the interstitial waters to produce [Sr($\mathbf{L_{ala}}$)$_2$(H_2O)] (**4**) in a single-crystal to single-crystal transformation; introduction of water vapor to **4** leads to the reformation of crystalline **3**. Each of these new complexes has a solid-state structure based on homochiral rod secondary building units (SBUs)

central cores. Supramolecular π···π stacking interactions between 1,8-naphthalimide rings link adjacent rod SBUs into 3D structures for **1**, **3**, **4** and **5** and 2D structure for **2**. Compounds **1** and **3** have open 1D channels along the crystallographic *c* axis that are occupied by disordered solvent. For **3**, these channels close and open in the reversible single-crystal conversion to **4**; the π···π stacking interactions of the naphthalimide rings facilitate this process by rotating and slipping. IR spectroscopy demonstrated that the rehydration of **4** with D_2O leads to $\mathbf{3d_8}$ and the process of dehydration and rehydration of $\mathbf{3d_8}$ with H_2O leads to **3**, thus showing exchange of the coordinated water in this process. These forms of **3** and **4** were characterized by ^1H, ^2H and ^{13}C solid-state NMR spectroscopy and thermal and luminescence data are reported on all of the complexes.

The reactions of (1,8-naphthalimido)ethanoic acid ($H\mathbf{L_{gly}}$), and (*S*)-2-(1,8-naphthalimido)-3-hydroxypropanoic acid ($H\mathbf{L_{ser}}$), protonated forms of ligands that contain a carboxylate donor group and a 1,8-naphthalimide π···π stacking supramolecular tecton, with cesium hydroxide followed by solvothermal treatment in ethanol led to the formation of crystalline Cs($\mathbf{L_{gly}}$) (**1**) and Cs($\mathbf{L_{ene}}$) (**2**), where the $\mathbf{L_{ene}}^-$ ligand, 2-(1,8-naphthalimido)acrylate, is formed from the dehydration of the $H\mathbf{L_{ser}}$ starting material. The X-ray studies show that **1** crystallizes in the monoclinic space group *C2/c* with unit cell dimensions *a* = 30.430(7) Å, *b* = 4.9820(12) Å, *c* = 16.566(4) Å, β = 101.951(4)^o and **2** in the monoclinic space group $P2_1/n$ with unit cell dimensions *a* = 13.6049(15) Å, *b* = 6.8100(8) Å, *c* = 14.4187(16) Å, β = 105.345(2)^o. The solid state structure of **1** contains two types of 6-coordinate cesium cations linked into sheets by bridging carboxylate oxygen atoms. One cation has a distorted octahedral environment, while the other is in an unusual planar, hexagonal O_6-coordination geometry. The latter geometry is stabilized

on both sides of the plane by η^2-coordination of naphthalimide rings. The 1,8-naphthalimide rings are involved in intra-sheet $\pi\cdots\pi$ stacking interactions. The O_6 coordination sphere of complex **2** is distorted and only half-filled with the oxygen atoms, which link the cations into rods that are further linked into sheets by bridging interactions of naphthalimide carbonyls with cesium cations from adjacent rods. The open face on the cation has unique η^2:η^1 interactions with two methylene groups in the ligands. These sheets are linked into a 3D supramolecular structure by interdigitated 1,8-naphthalimide rings involved in strong $\pi\cdots\pi$ interactions. Both complexes show naphthalimide based fluorescence.

The reactions of the lithium salt of (*S*)-2-(1,8-naphthalimido)-3-hydroxypropanoate ($\mathbf{L_{ser}}^-$), an enantiopure carboxylate ligand containing a 1,8-naphthalimide $\pi\cdots\pi$ stacking supramolecular tecton and an alcohol functional group, with $La(NO_3)_3$, $Ce(NO_3)_3$, $SmCl_3$, $Eu(NO_3)_3$, $Gd(NO_3)_3$, $Tb(NO_3)_3$ and $Dy(NO_3)_3$ under solvothermal conditions (water/ethanol) produced single crystals (characterized by single crystal X-ray crystallography) of $[La_3(\mathbf{L_{ser}})_8(OH)(H_2O)]\bullet(H_2O, EtOH)_x$ (**1**), $[Ce_3(\mathbf{L_{ser}})_8(OH)(H_2O)]\bullet(H_2O, EtOH)_x$ (**2**), $[Sm_3(\mathbf{L_{ser}})_8(OEt)]\bullet(H_2O, EtOH)_x$ (**3**), $[Eu_3(\mathbf{L_{ser}})_8(OEt)]\bullet(H_2O, EtOH)_x$ (**4**), $[Gd_3(\mathbf{L_{ser}})_8(OEt)]\bullet(H_2O, EtOH)_x$ (**5**), $[Tb_3(\mathbf{L_{ser}})_8(OEt)]\bullet(H_2O, EtOH)_x$ (**6**) and $[Dy_3(\mathbf{L_{ser}})_8(OEt)]\bullet(H_2O, EtOH)_x$ (**7**), respectively. Mixed-metal complexes $[Ce_{2.3}Tb_{0.7}(\mathbf{L_{ser}})_8(OH)]\bullet(H_2O, EtOH)_x$ (**8**), $[Gd_{0.4}Tb_{2.6}$ $(\mathbf{L_{ser}})_8(OEt)]\bullet(H_2O, EtOH)_x$ (**9**) and $[Ce_{1.4}Gd_{0.3}Tb_{1.3}(\mathbf{L_{ser}})_8(OH)]\bullet(H_2O, EtOH)_x$ (**10**) were prepared by using two or more types of lanthanides in the solvothermal reactions (additional mixed-metal complexes were prepared and characterized by ICP-MS). Single crystals of compounds **1**-**10** are isostructural: trinuclear, carboxylate-bonded

helicates organized by the noncovalent, π···π stacking interactions of the 1,8-naphthalimide groups into *intertwined M* helices, with a pitch of 56 Å, that are further arranged into a three dimensional supramolecular framework by additional π···π stacking interactions. Magnetic measurements of several compounds were as expected for the metal(s) present, indicating no significant interactions between metals within the helicates. The Ce complex **2** showed weak antiferromagnetic ordering below 50 K. All of the complexes, with the exception of **2**, showed luminescence based on the 1,8-naphthalimide group. Complex **2** has no emission and complexes with mixed Ce/Tb ratios showed significant quenching of the naphthalimide-based luminescence, as quantitated with solid state, absolute quantum yield measurements of these mixed-metal and the pure metal complexes. Lanthanide based luminescence was only observed for the Eu complex **4**.

The new ligand 5-(1,8-naphthalimido)isophthalate ($\mathbf{L_{135}}^{2-}$), containing two carboxylate donor groups and the 1,8-naphthalimide supramolecular tecton, has been used under solvothermal conditions to prepare a series of group 2, lanthanide and actinide metal complexes: $[Ca_4(\mathbf{L_{135}})_4(H_2O)_8]\cdot(H_2O)_{9.5}(DMF)_{2.6}$ (**1**), $Ba(\mathbf{L_{135}})(H_2O)_{1.5}(DMF)_{0.5}$ (**2**), $La_2(\mathbf{L_{135}})_3(DMF)_4$ (**3**), $Ce_2(\mathbf{L_{135}})_3(DMF)_4$ (**4**), $Eu_2(\mathbf{L_{135}})_3(DMF)_4$ (**5**), $Tb_2(\mathbf{L_{135}})_3(DMF)_4$ (**6**), $[UO_2(\mathbf{L_{135}})(DMF)]\cdot(py)_{0.5}(EtOH)_{0.5}$ (**7**) and $Th(\mathbf{L_{135}})(NO_3)_2(DMF)_2]\cdot(DMF)_2$ (**8**). The solid state structure of the calcium complex **1** is based on helical rod-shaped secondary building-units (SBUs) of edge-shared polyhedra bridged by oxygens from the carboxylate groups. The crystals are racemic, with the one-dimensional (1D) helical rods organized by π···π stacking interactions of the naphthalimide group into a 3D supramolecular framework (SMOF) structure. Although the structure of the barium complex **2** also

contains rod-shaped SBUs, the rods are linked through the aryl backbone of the ditopic $\mathbf{L_{135}}^{2-}$ ligands into 2D sheets. The sheets are further engaged in naphthalimide $\pi\cdots\pi$ stacking interactions to build a 3D SMOF. The lanthanide complexes **3**-**6** are isostructural, based on binuclear SBUs linked by the ligands into a square-shaped grid pattern, with π-stacking interactions linking adjacent sheets to generate a 3D SMOF. The uranium(VI) complex **7** contains 7-coordinate pentagonal bipyramid uranyl cations bridged by the ligands into one dimensional ribbons. The solid state structure of the thorium(IV) complex **8** consists of 10-coordinate thorium cations, also bridged by the ligands into one dimensional ribbons. Both of these actinide structures are organized into only 2D supramolecular sheets by π-stacking interactions. Compounds **1**, **2**, **3**, **6** and **8** exhibit solid-state luminescence dominated by the naphthalimide chromophore in the ligand. The group 2 complexes are slightly red-shifted and the lanthanum complex **3** and the thorium complex **8** slightly blue-shifted with respect to the ligand. The terbium compound, **6**, is greatly blue-shifted by ~75 nm and naphthalimide sensitization of the metal emission occurs for the europium complex **5**. The cerium(III) and uranyl(VI) compounds **4** and **7** have no solid state emission.

Table of Contents

List of Tables

List of Figures

List of Schemes

Chapter I

Homochiral helical metal-organic frameworks of group 1 metals [1]

[1]Adapted with permission from Reger, D. L.; Leitner, A.; Smith, M. D.; Tran, T. T.; Halasyamani, P. S. *Inorg. Chem.* **2013**, *52* (17), 10041–10051. DOI: 10.1021/ic401327h.

Copyright 2013 American Chemical Society.

Introduction

The rational design of metal-organic frameworks (MOFs) with diverse architectures and functionalities is a major area for research because of the wide range of potential applications.[1] Secondary building units (SBUs) are the core geometric building blocks of MOFs that are used to assemble desired structures when coupled with appropriately chosen bridging ligands.[2] In addition to the covalent forces from which these network solids are built, supramolecular tectons (e.g. groups that can hydrogen bond or participate in $\pi\cdots\pi$ stacking interactions) can be built into the organic ligands for added functionality and enhanced stability.[3]

We recently designed a series of ligands with up to four functionalities derived from enantiopure amino acids and a 1,8-naphthalimide group (Scheme 1.1).[4] The first functionality comes from the carboxylate anion that acts as a donor to the metal cations and helps constitute the SBU.[2] The second is the chiral center from enantiopure amino acids, which imparts chirality on the crystal structure resulting in noncentrosymmetric space groups.[4,5] The third key feature of the amino acid component is the "side chain" that can contain functional groups such as an alcohol or amide. The fourth, and probably most unique feature of the ligands is the 1,8-naphthalimide group that not only blocks the amine end of the acid from coordination,[6] but has been shown to organize the supramolecular structure through directionally versatile and strong $\pi\cdots\pi$ stacking interactions.[4,7,8]

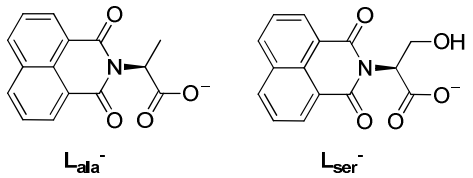

Scheme 1.1. Enantiopure Tri- and Tetrafunctional Ligands

The majority of our previous research on metal complexes of these ligands has dealt with the square paddlewheel SBU adopted by late transition metals.[7] These and related studies have demonstrated that ligands containing the 1,8-naphthalimide group have complex structures frequently organized in at least one dimension by supramolecular interactions, structural types that we have denoted as supramolecular metal-organic frameworks (SMOFs).[7b] These SMOFs have shown very interesting properties, most notably a variety of single-crystal to single-crystal transformations; in one system gas/solid guest exchange takes place in densely packed solids,[4a] in another the gas/solid exchange is enantioselective with a racemic substrate,[7a] and in a third temperature induced phase changes are observed.[4c] In order to investigate additional interesting trends and physical properties imparted by these ligands, we chose to look at complexes with group 1 metals. Although not as extensively studied in this field as transition metals, s-block metals are cheap, nontoxic, essential in many biological processes[9] and their complexes have shown a wealth of interesting properties, ranging from catalysts[10] to ferroelectrics.[11] By using enantiopure ligands the new complexes can also have interesting nonlinear optical applications. Herein we report the syntheses and structures of eight alkali metal complexes of three different group 1 metals with the two ligands pictured in Scheme 1 along with their thermal, fluorescent and non-linear optical properties. In contrast to other studies with these metals,[12] two very similar structural types have emerged from this study, both of which are based on homochiral rod SBUs,

despite changes in metals, ligands, and solvent systems. Two of these compounds are able to undergo reversible single-crystal to single-crystal transformations even though the solids lack channels. Some of these results have been communicated previously.[13]

Experimental

General Considerations. All reactants were used as purchased from Aldrich and Strem. The syntheses of the ligands H$\mathbf{L_{ala}}$ and H$\mathbf{L_{ser}}$ have been reported elsewhere.[4c,8,13] Elemental analyses were performed by Robertson Microlit Laboratories (Ledgewood, NJ). Thermalgravimetric analysis was performed using a Thermal Analysis (TA) SDTQ600 simultaneous DTA/TGA system. The samples were heated in dry air to 800 °C with a heating rate of 10 °C/min. Some samples (compounds **3** and **6**) froth when heated too high, so the experiment was terminated after the decomposition temperature was recorded. The fluorescence measurements were done on a Perkin Elmer Lambda 35 UV-vis spectrometer.

*K(**L**$_{ala}$)(MeOH)* (**1**). H$\mathbf{L_{ala}}$ (2.0 g, 7.4 mmol) was added to a solution of potassium hydroxide (0.42 g, 7.4 mmol) in water and stirred for an hour until homogeneous. The solvent was removed and the precipitate dried in vacuo to produce a light brown powder (1.96 g). A 9 mL thick walled glass tube with a Teflon screw top was charged with a sample of this solid (0.10 g) and methanol (4 mL) and heated at 120 °C overnight or until the solution became homogeneous. The heat was removed and the system was allowed to slowly cool at a rate of about 1°C/min. The reaction vessel was placed in a quiet area. Over the course of 3 days large crystals grew from the solution and were collected from

the tube and washed with diethyl ether to provide 0.063 g of single crystals. Anal. Calcd. (Found) for $C_{16}H_{14}KNO_5$: C 56.62 (56.42); H 4.16 (4.00); N 4.13 (3.97).

*K(**L**$_{ala}$)(H_2O)* (**2**). The light brown powder of K**L**$_{ala}$ (0.086 g, 0.28 mmol) was dissolved in water (1 mL) and acetone vapor was allowed to diffuse into the solution to yield X-ray quality single crystals (0.064 g) after 3 weeks. Anal. Calcd. (Found) for $C_{15}H_{14}KNO_5$: C 55.37 (55.21); H 3.72 (3.58); N 4.31 (4.28).

*Na(**L**$_{ala}$)(H_2O)* (**3**). H**L**$_{ala}$ (1.30 g, 4.83 mmol) was added to a solution of sodium hydroxide (0.20 g, 5.0 mmol) in methanol (30 mL) and the stirred until homogeneous. The solution was filtered through a short celite plug. The solvent was removed and the resulting precipitated dried in vacuo to produce a pale orange powder (1.30 g). A 9 mL thick walled glass tube with a Teflon screw top was charged with the solid (0.05 g), a 40:1 mixture of 1-butanol and water (4 mL) was added and heated at 120 °C overnight or until the solution became homogeneous. The heat was removed and the system was allowed to slowly cool at a rate of about 1°C/min. The reaction vessel was placed in a quiet area. Over the course of 2 days large crystals grew from the solution and were collected from the tube and washed with diethyl ether to provide 0.032 g of single crystals. Anal. Calcd. (Found) for $C_{15}H_{14}NNaO_5$: C 58.26 (58.08); H 3.91 (3.93); N 4.53 (4.44).

*K(**L**$_{ser}$)* (**4**). H**L**$_{ser}$ (1.00 g, 3.5 mmol) was added to a solution of potassium hydroxide (0.20 g, 3.5 mmol) in water and stirred for an hour or until homogeneous. The solvent was removed and the precipitate dried in vacuo to produce a light brown powder (0.89 g). A 9 mL thick walled glass tube with a Teflon screw top was charged with the solid (0.05 g) and methanol (2.0 mL) and heated at 120 °C. Over the course of heating for

3 days, brown crystals grew on the walls of the tube above the solvent line. After no starting material remained at the bottom of the tube, the heat was removed and the system was allowed to slowly cool at a rate of about 1°C/min. Small dark brown crystals were collected from the walls of the tube and washed with diethyl ether to provide 0.032 g of single crystals. Anal. Calcd. (Found) for $C_{15}H_{10}KNO_5$: C 55.72 (55.60); H 3.12 (3.22); N 4.33 (4.21).

*Cs(**L**$_{ser}$)* (**5**). This compound was prepared by the same procedure as for K**L**$_{ser}$, but with CsOH·*x*H_2O (0.50 g) and H**L**$_{ser}$ (0.72 g, 2.5 mmol) to provide a pale brown powder (1.02 g). Small dark brown crystals were collected from the walls of the tube and washed with diethyl ether to provide 0.031 g of single crystals. Anal. Calcd. (Found) for $C_{15}H_{10}CsNO_4$: C 44.91 (44.38); H 2.51 (2.33); N 3.49 (3.31).

*Cs(**L**$_{ala}$)* (**6**). This compound was prepared by the same procedure as for K**L**$_{ser}$, but with CsOH·*x*H_2O (0.50 g) and H**L**$_{ala}$ (0.76 g, 2.5 mmol) to provide an orange powder (1.06 g). Small dark brown crystals were collected from the walls of the tube and washed with diethyl ether to provide 0.037 g of single crystals. Anal. Calcd. (Found) for $C_{15}H_{10}CsNO_5$: C 43.19 (43.10); H 2.42 (2.31); N 3.36 (3.36).

Second Harmonic Generation Studies. Powder SHG measurements were performed on a modified Kurtz-nonlinear optical (NLO) system using a pulsed Nd:YAG laser with a wavelength of 1064 nm.[14] A detailed description of the equipment and methodology has been published.[15] As the powder SHG efficiency has been shown to strongly depend on particle size,[14] **4**, **5** and **6** were ground and sieved into distinct particle size ranges (<20, 20–45, 45–63, 63–75, 75–90, >90 μm). Relevant comparisons with known SHG materials were made by grinding and sieving crystalline α–SiO_2 and

$LiNbO_3$ into the same particle size ranges. No index matching fluid was used in any of the experiments.

Powder X-Ray Diffraction. In order to test for phase purity of the crystalline products, samples for compounds **1**-**5** were collected from the walls of the solvothermal tubes, washed with diethyl ether and ground in air. For compound **6** the single crystals were transported into a dry box and ground in a nitrogen atmosphere. A zero-background slide was loaded with the sample, covered with a Kapton film and sealed with high vacuum grease. All measurements were performed on a Rigaku Ultima 4 instrument using Cu Kα radiation at a scan rate of 1 °/min between 5 and 30 °2θ with a step size of 0.02 °2θ. Powder patterns were analyzed using Microsoft Excel. The powder pattern for **6** initially indicated some lack of phase purity, but two additional short scans (10-15 °2θ at a scan rate of 2 °/min) were performed on compound **6**, before and after the long scan and they show that compound **6** likely undergoes a change when ground.

Recycling Experiments. The repeated single-crystal to single-crystal transformation of compound **3** to **3*** was performed on two selected single crystals. These crystals were collected from the walls of the solvothermal tubes and washed with diethyl ether. After checking the unit cell, they were heated under vacuum to 150 °C for one hour in a Schlenk flask. The flask was refilled with nitrogen and the crystal quickly mounted in a nitrogen stream on the diffractometer; the unit cell parameters were collected and the diffraction peaks monitored for broadening to determine if compound **3*** had formed and retained single crystallinity. These same two single crystals were then returned to a glass vial which was kept in a humid environment for two days and unit cell parameters collected to determine if compound **3** had reformed. This procedure was repeated; at the

end the single crystals started to show broadening in the diffraction pattern indicating some degradation had taken place.

Crystallographic Studies. For all complexes, X-ray diffraction intensity data were measured at 100(2) K using a Bruker SMART APEX diffractometer (Mo Kα radiation, λ = 0.71073 Å).[16] The raw area detector data frames were reduced with the SAINT+ program.[16] Direct methods structure solution, difference Fourier calculations and full-matrix least-squares refinement against F^2 were performed with SHELXS/L, implemented in OLEX2.[17,18] Non-hydrogen atoms were refined with anisotropic displacement parameters. Hydrogen atoms bonded to carbon were placed in geometrically idealized positions and included as riding atoms. For compounds **1**, **2**, **2***, **4**, **5** and **6**, crystal enantiopurity and the "S" configuration of the chiral carbon (C13 in all structures) were established by the absolute structure (Flack) parameters of zero (within experimental error) derived from the X-ray datasets. For **3** and **3***, containing no atoms heavier than sodium in the crystal, the absolute structures were inferred from synthetic information; *i.e.*, enantiopure starting material which does not racemize. Details of data collection are given in Table 1.1.

Table 1.1. Crystallographic Data

	1	**2**	**2***	**3**	**3***
Formula	$C_{16}H_{14}KNO_5$	$C_{15}H_{12}KNO_5$	$C_{15}H_{10.58}KNO_{4.29}$	$C_{15}H_{12}NaNO_5$	$C_{15}H_{10}NaNO_4$
Fw, g mol^{-1}	339.38	325.36	312.58	309.25	291.23
Cryst. Syst.	Orthorhombic	Orthorhombic	Orthorhombic	Orthorhombic	Orthorhombic
Space group	$P2_12_12_1$	$P2_12_12_1$	$P2_12_12_1$	$P2_12_12_1$	$P2_12_12_1$
T, K	100(2) K	100(2) K	100(2) K	100(2) K	100(2) K
a, Å	6.8979(5)	6.9520(7)	6.874(2)	6.9818(7)	6.9329(13)
b, Å	14.3515(10)	13.2676(13)	12.842(4)	11.8361(13)	12.061(2)
c, Å	14.5164(10)	14.9719(15)	15.052(4)	15.5125(17)	14.777(3)
α, deg	90	90	90	90	90
β, deg	90	90	90	90	90
γ, deg	90	90	90	90	90
V, Å^3	1437.05(18)	1381.0(2)	1328.8(7)	1281.9(2)	1235.5(4)
Z	4	4	4	4	4
R1(I>2σ (I))	0.0277	0.0296	0.0439	0.0322	0.0522
wR2(I>2σ (I))	0.0721	0.0748	0.1085	0.0830	0.1306
Flack Parameter	0.01(4)	-0.03(4)	0.05(7)	-0.2(3)	0.5(7)

	4	**5**	**6**
Formula	$C_{15}H_{10}KNO_5$	$C_{15}H_{10}CsNO_5$	$C_{15}H_{10}CsNO_4$
Fw, g mol^{-1}	323.34	417.15	401.15
Cryst. Syst.	Monoclinic	Monoclinic	Monoclinic
Space group	$P2_1$	$P2_1$	$P2_1$
T, K	100(2) K	100(2) K	100(2) K
a, Å	8.7050(5)	9.2965(12)	9.0674(6)
b, Å	6.6081(4)	6.6108(9)	6.5650(5)
c, Å	11.1731(7)	11.2603(15)	11.2571(8)
α, deg	90	90	90
β, deg	99.1048(10)	99.668(2)	95.2910(10)
γ, deg	90	90	90
V, Å^3	634.62(7)	682.20(16)	667.25(8)
Z	2	2	2
R1(I>2σ (I))	0.0311	0.0233	0.0233
wR2(I>2σ (I))	0.0819	0.0552	0.0546
Flack Parameter	0.03(3)	0.01(2)	0.037(16)

Results

Syntheses. The reaction of H$\mathbf{L}_{\mathbf{ala}}$ and H$\mathbf{L}_{\mathbf{ser}}$ with the appropriate alkali metal hydroxide (NaOH, KOH, CsOH) in water or methanol produced Na$\mathbf{L}_{\mathbf{ala}}$, K$\mathbf{L}_{\mathbf{ala}}$, Cs$\mathbf{L}_{\mathbf{ala}}$, K$\mathbf{L}_{\mathbf{ser}}$, and

Cs**L**$_{ser}$. Crystals of K(**L**$_{ala}$)(MeOH) (**1**) and Na(**L**$_{ala}$)(H_2O) (**3**) were obtained by heating the appropriate salt in an alcohol solution to 120° C followed by cooling. Crystals of K**L**$_{ser}$ (**4**), Cs**L**$_{ser}$ (**5**), and Cs**L**$_{ala}$ (**6**) were obtained by solvothermal treatment in alcohol solution at 120° C and grew on the walls of the reaction vessel above the solvent line. Dissolving K**L**$_{ala}$ in water followed by vapor diffusion of acetone into the solution afforded crystals of K(**L**$_{ala}$)(H_2O) (**2**).

Structural Analyses. In K(**L**$_{ala}$)(MeOH) (**1**), the potassium cation is 6-coordinate with two of the sites occupied by μ^2-κ^2 carboxylate oxygens, two by bridging methanols, and two by carbonyls from the naphthalimide rings (Figure 1.1). One of the naphthalimide carbonyls is coordinated to a potassium cation in the same chain as the bridging carboxylate oxygen of that ligand forming a seven-member chelate ring. The noncoordinated oxygen atom from the carboxylate participates in hydrogen bonding to the methanol bridging to the next potassium cation. The irregular potassium polyhedra are edge-shared through the bridging oxygen atoms originating from the methanol and carboxylate, extending in one dimension to generate helical rods. The helical rods are enantiopure, all *P*-handed helicies as defined by the K1-O3-K1-O3 chain (Figure 1.2) with a pitch of 6.90 Å. The second naphthalimide carbonyl of each ligand acts to bridge adjacent helices. These bridging naphthalimide carbonyls form four points of extension from each helical rod generating “squares” which are occupied by the naphthalimide rings (Figure 1.3), generating a three-dimensional uninodal 4*c* net structure.

The naphthalimide rings form extended π···π stacking networks that reinforce the structure. Four parameters were chosen to define the strength of the naphthalimide π···π

stacking interaction: the dipole angle between the two rings, the angle between ring planes, the average perpendicular distance, and the slippage parameter (χ) that is defined as the third side of the right triangle formed with the average perpendicular distance between the two rings and the line between the two central carbon atoms of the rings. The values for these metrics, along with the angles formed by the dipole vectors of the rings, are listed in Table 1.2.

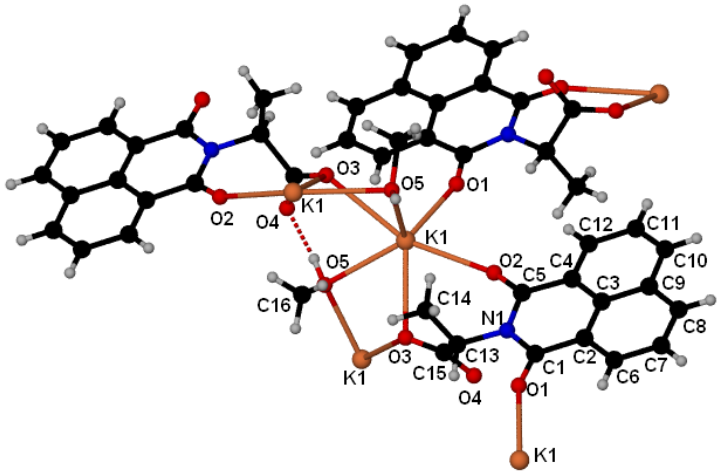

Figure 1.1 The K^+ coordination environment of K(**L**$_{ala}$)(MeOH) (**1**); black C, red O, blue N, white H, orange K.

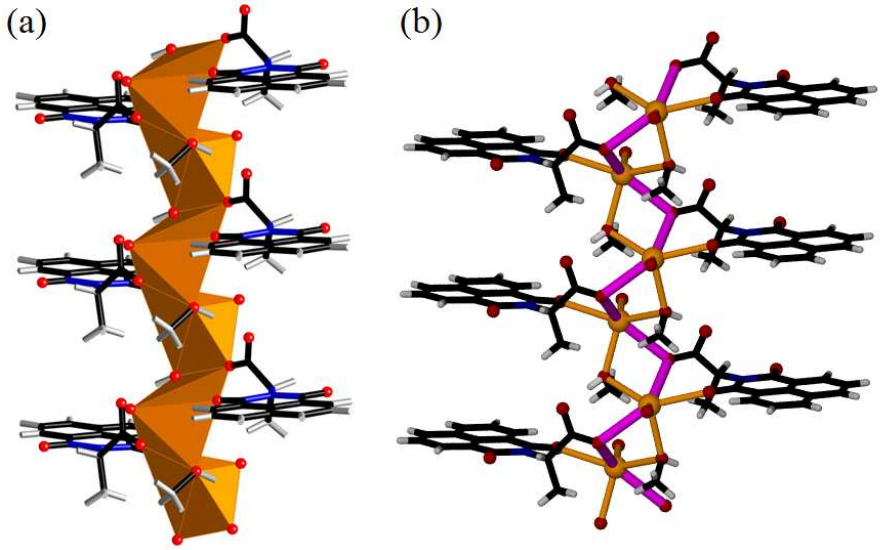

Figure 1.2. (a) The rod-like structure of **1** formed by edge shared K^+ polyhedra and (b) the *P*-handed helix highlighted in purple follows the K1-O3-K1-O3 chain.

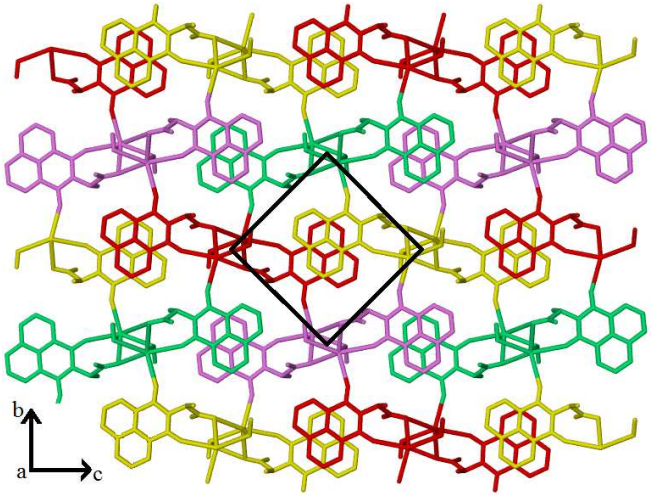

Figure 1.3. View down the crystallographic *a* axis of **1** illustrating the four points of connectivity between rods, where each rod is a different color and the vertices of the square lie in the center of each helical rod.

The structure of K(**L**$_{\mathbf{ala}}$)(H_2O) (**2**) is very similar to **1** with the presence of homochiral helical rods of potassium cations and the uninodal 4*c* net, yet there are important differences in the coordination environment and helical connectivity. The potassium is 6-coordinate with three of the sites occupied by the μ^2-κ^1:κ^2 carboxylate oxygens, one of the sites filled by a terminal water molecule, and the remaining two sites filled by two carbonyls from the naphthalimide rings (Figure 1.4). The terminal water molecule in **2** is hydrogen bonded to the carboxylate O3 involved with bridging the next two potassium cation of the helix. The distorted octahedral potassium polyhedra are corner-shared through the bridging carboxylate and extend in one dimension to generate helical rod SBUs. The *P*-handed helix defined by the K1-O3-K1-O3 chain is shown in Figure 1.5 and has a pitch of 6.95 Å. As with **1**, one of the naphthalimide carbonyls is coordinated to a potassium cation in the same chain as the bridging carboxylate oxygen of that ligand forming a seven-member chelate ring, while the other acts to bridge an adjacent helix. The bridging mode of the naphthalimide carbonyls again creates four

points of extension per rod and the extended interdigitated π···π stacking are similar to compound **1** (Figure 1.6). The metrics for the π···π stacking are listed in Table 1.2.

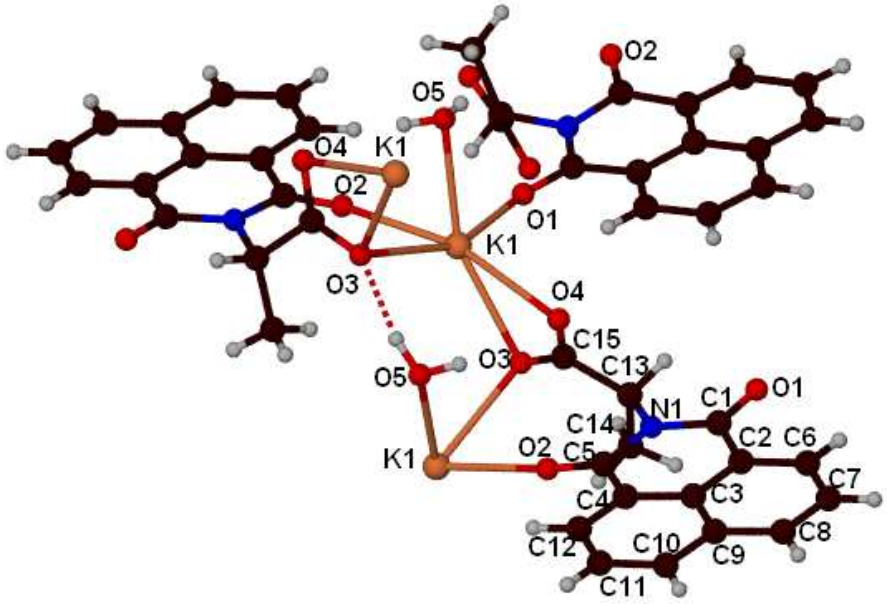

Figure 1.4. The K^+ coordination environment of K(**L**$_{ala}$)(H_2O) (**2**) ; black C, red O, blue N, white H, orange K.

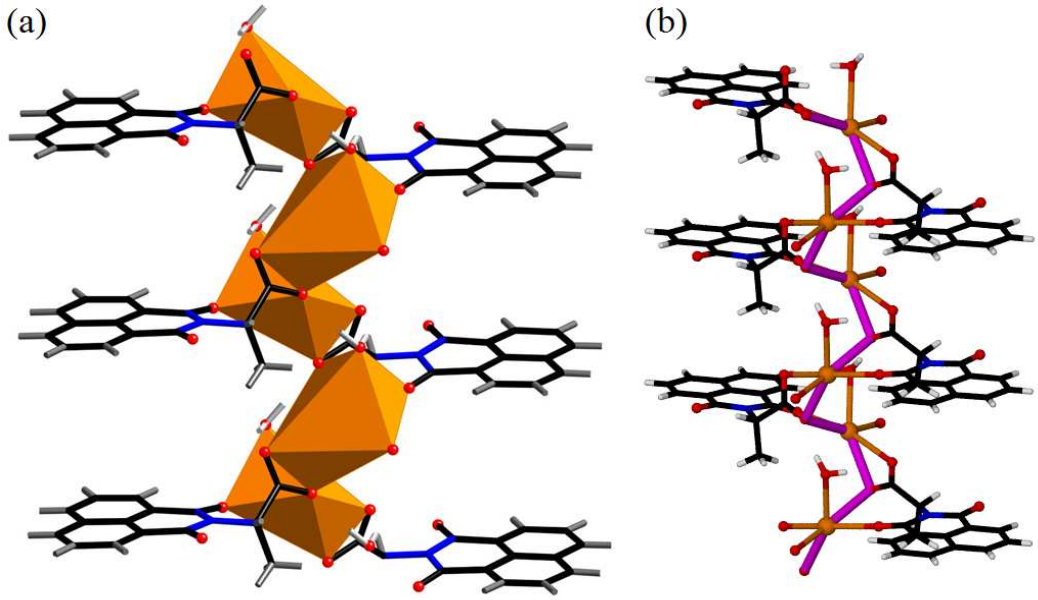

Figure 1.5. (a) The rod-like structure of **2** formed by corner shared K^+ polyhedra and (b) the *P*-handed helix highlighted in purple follows the K1-O3-K1-O3 chain.

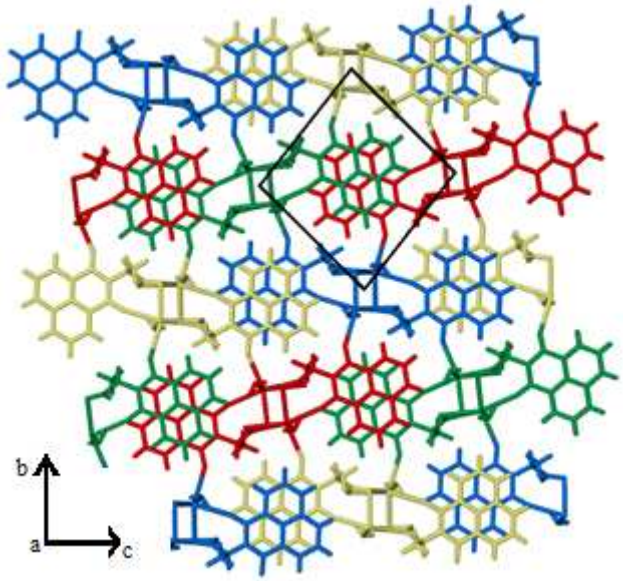

Figure 1.6. View down the crystallographic *a* axis of K(**L**$_{ala}$)(H_2O) (**2**) illustrating the four points of connectivity between rods, where each rod is a different color and the vertices of the square lie in the center of each helical rod.

Compound **2** undergoes a reversible single-crystal to single-crystal transformation at high temperatures by the loss of the coordinated water to form compound **2*** (vide infra). The structure of the dehydrated complex is almost identical to the hydrated form with the exception of the coordination number of potassium changing from six to five (Figure 1.7) and a slight decrease in the unit cell volume (~3%).

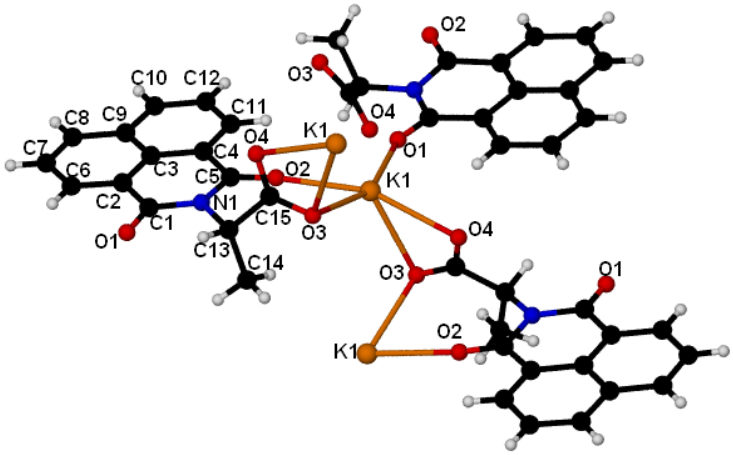

Figure 1.7. The K^+ coordination environment of K(**L**$_{ala}$) (**2***); black C, red O, blue N, white H, orange K.

Na(**L**$_{ala}$)(H_2O) (**3**) again has the same basic structure featuring homochiral helical rods of sodium and a uninodal 4*c* net, but with distinct differences in coordination and helical environment from either **1** or **2**. Sodium is 6-coordinate with two of the sites occupied by a κ^2 carboxylate, two of the sites filled by bridging water molecules, and the remaining two sites filled by two carbonyls from the naphthalimide rings (Figure 1.8). Compound **3** is the only example where the carboxylate does not act as a bridge and the intrachain chelate ring formed by one of the naphthalimide carbonyls involves a sodium located in the next segment of the helix forming nine-member rings. In a similar manner to the methanol in **1**, the bridging water molecule in **3** is hydrogen bonded to the carboxylate O3, but in this case O3 is coordinated to sodium. The distorted octahedral sodium polyhedra are corner shared through the bridging water and extend in one dimension to generate helical rod SBUs (Figure 1.9). The *P*-handed helix is defined by the Na1-O5-Na1-O5 chain and has a pitch of 6.98 Å. Again, the second naphthalimide carbonyls of each ligand bridge to adjacent helices forming four points of extension per rod and extended interdigitated π···π stacking as in compounds **1** and **2** (Figure 1.10) is also present. The metrics for the π···π stacking are listed in Table 1.2.

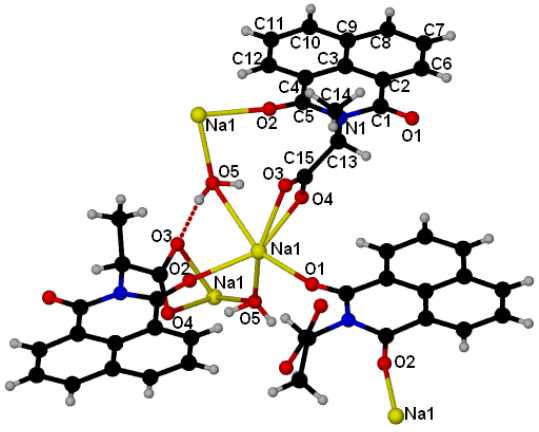

Figure 1.8. The Na^+ coordination environment of Na(**L**$_{ala}$)(H_2O) (**3**) ; black C, red O, blue N, white H, yellow Na.

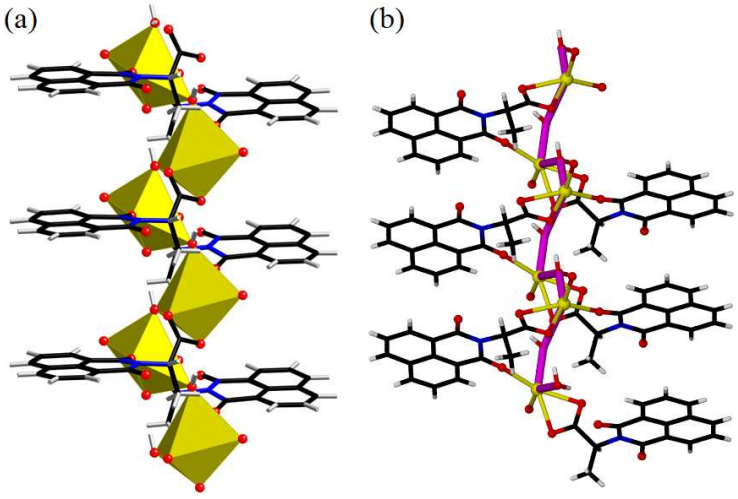

Figure 1.9. (a) The rod-like structure of **3** formed by corner shared Na^+ polyhedra and (b) the *P*-handed helix highlighted in purple follows the Na1-O5-Na1-O5 chain.

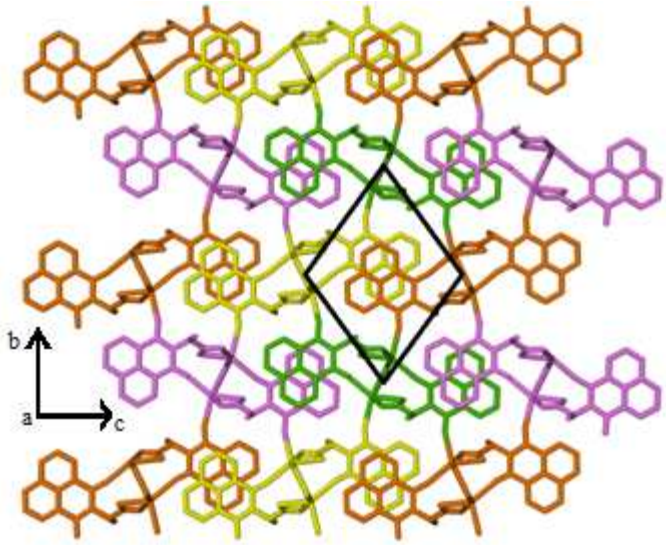

Figure 1.10. View down the crystallographic *a* axis of Na(**L**$_{\mathbf{ala}}$)(H_2O) (**3**) illustrating the four points of connectivity between rods, where each rod is a different color and the vertices of the square lie in the center of each helical rod.

Compound **3** undergoes a reversible single-crystal to single-crystal transformation upon heating with loss of water to form compound **3*** (vide infra) which was characterized by single crystal X-ray diffraction. Sodium is 5-coordinate in compound **3*** with 3 of the sites occupied by the μ^2-κ^1:κ^2 carboxylate oxygens in a similar fashion to compound **2** and the remaining two sites are occupied by the carbonyls of the

naphthalimide rings (Figure 1.11). In comparison to the structure of **3**, the bridging water is lost and one of the oxygens (O3) of the non-bridging, κ^2-carboxylate in **3** moves into a bridging position in the structure of **3***. This change causes the nine-member rings formed by the carboxylate ligand and naphthalimide carbonyls in **3** to become a seven-member ring, similar to that observed in complexes **1** and **2**. Sodium polyhedra are corner-shared through the carboxylate O3 and extend into helical rods (Figure 1.12). The second naphthalimide carbonyl of each ligand is involved with bridging adjacent rods. The overall 3D structures is the same as the previous four compounds where each of the homochiral helical rods of corner-shared sodium atoms are connected to four adjacent rods generating a uninodal 4*c* net (Figure 1.13). The metrics for the $\pi^{\cdots}\pi$ stacking are listed in Table 1.2.

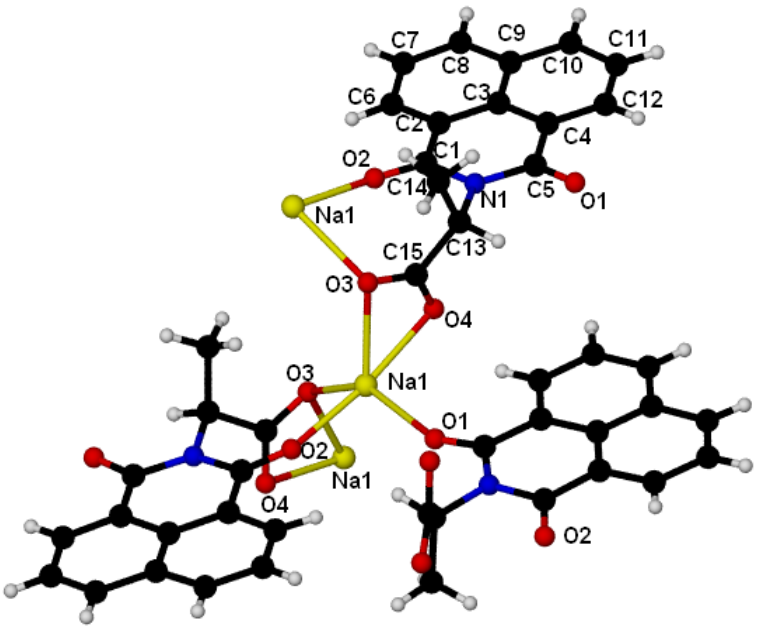

Figure 1.11. The Na^+ coordination environment of Na(**L**$_{\mathbf{ala}}$) (**3***); black C, red O, blue N, white H, yellow Na.

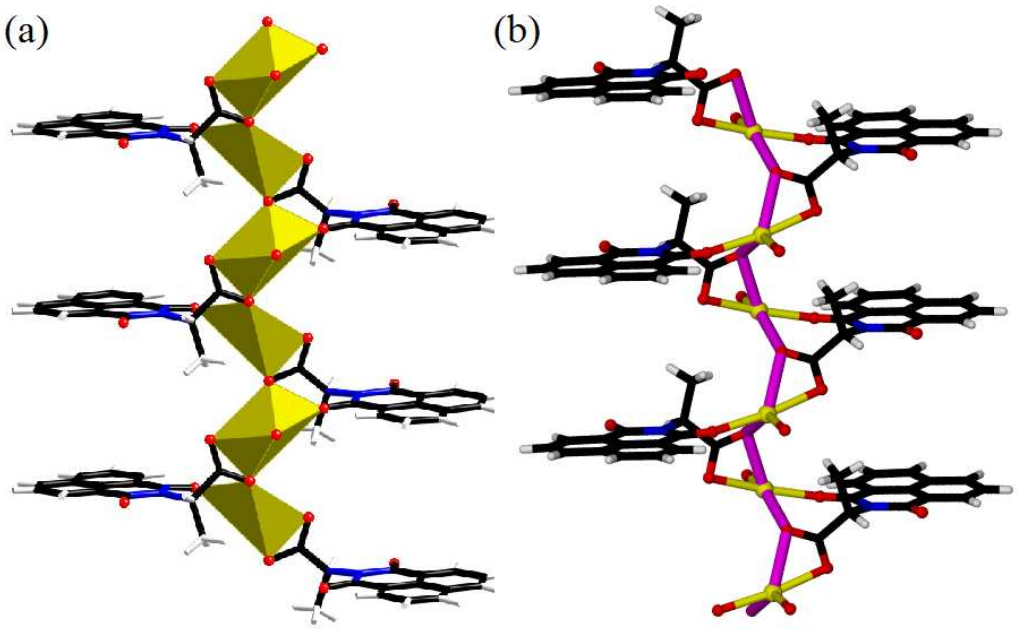

Figure 1.12. (a) The rod-like structure of **3*** formed by corner shared Na^+ polyhedra and (b) the *P*-handed helix highlighted in purple follows the Na1-O3-Na1-O3 chain.

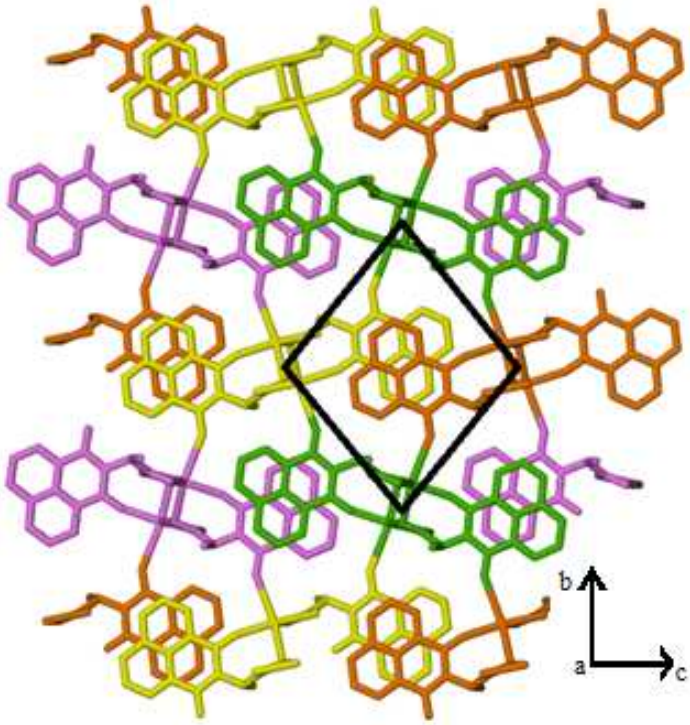

Figure 1.13. View down the crystallographic *a* axis of Na(**L_{ala}**) (**3***) illustrating the four points of connectivity between rods, where each rod is a different color and the vertices of the square lie in the center of each helical rod.

Table 1.2. π···π stacking metrics for compounds **1**-**3**.

	Compound	Cen-Cen(Å)	dipole ∠ (°)	plane ∠ (°)	avg dist (Å)	χ (Å)
1	K(**L**$_{ala}$)(MeOH)	3.70	180	4.8	3.45	1.34
2	K(**L**$_{ala}$)(H_2O)	3.67	180	2.9	3.48	1.16
2*	K(**L**$_{ala}$)(H_2O)$_{0.29}$	3.63	180	3.6	3.45	1.16
3	Na(**L**$_{ala}$)(H_2O)	3.77	180	5.9	3.49	1.43
3*	Na(**L**$_{ala}$)	3.66	180	3.8	3.46	1.18

In the structure of K(**L**$_{ser}$) (**4**), potassium is 6-coordinate with two of the sites occupied by μ^2-κ^2 carboxylate oxygens, two are filled by the bridging alcohol functional groups located in the side-chains, and the last two are occupied by carbonyls of naphthalimide rings (Figure 1.14). The *designed ligand modification* in **L**$_{ser}^-$ when compared to **L**$_{ala}^-$ introduces the alcohol in the side-chain that replaces the solvent molecules in the structures of **1**-**3**. One of the naphthalimide carbonyls in each ligand is bonded to the same potassium cation as the carboxylate and alcohol that each bridge a different potassium cation in the same chain, forming a [3.2.2] bicyclic system. The distorted trigonal prismatic potassium polyhedra are edge-shared through the bridging alcohol and carboxylate oxygens and extend in one dimension to generate helical rods (Figure 1.15). The *P*-handed helical rods are defined by the K1-O4-K1-O4 chain and have a pitch of 6.61 Å. The other naphthalimide carbonyls in each ligand bridge to potassium cations in adjacent helices. In contrast to **1**-**3**, these connections extend in only two directions, connecting the rods into sheets. All of the naphthalimide rings are pointed away from the helices, fixed in position by the tridentate coordination mode of the ligand, and line up in parallel ribbons. The naphthalimide rings are interdigitated through π···π stacking connecting the sheets into a three-dimensional supramolecular metal-organic framework (SMOF) in a "zipper-like" fashion as shown in Figure 1.16. By introducing a

donor group into the ligand sidechain, we successfully exclude coordinated solvents, but the ligand is now locked into a different orientation and a new structure type is formed. The metrics for the π···π stacking are listed in Table 1.3.

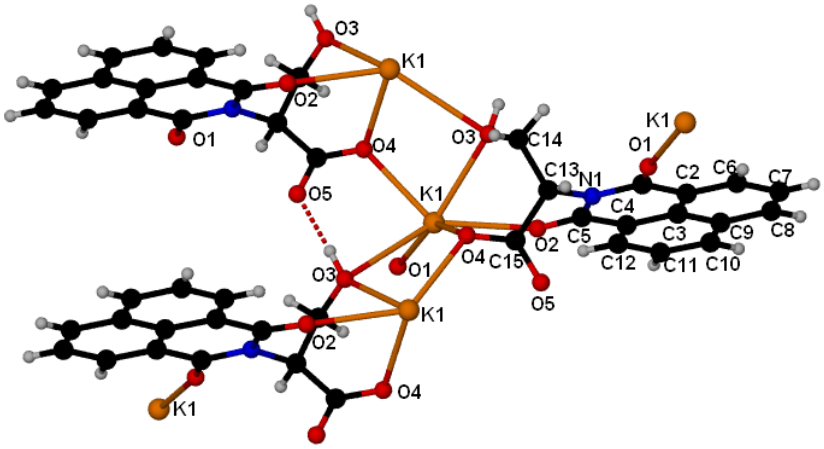

Figure 1.14. The K^+ coordination environment of K**L**$_{ser}$ **(4)** ; black C, red O, blue N, white H, orange K.

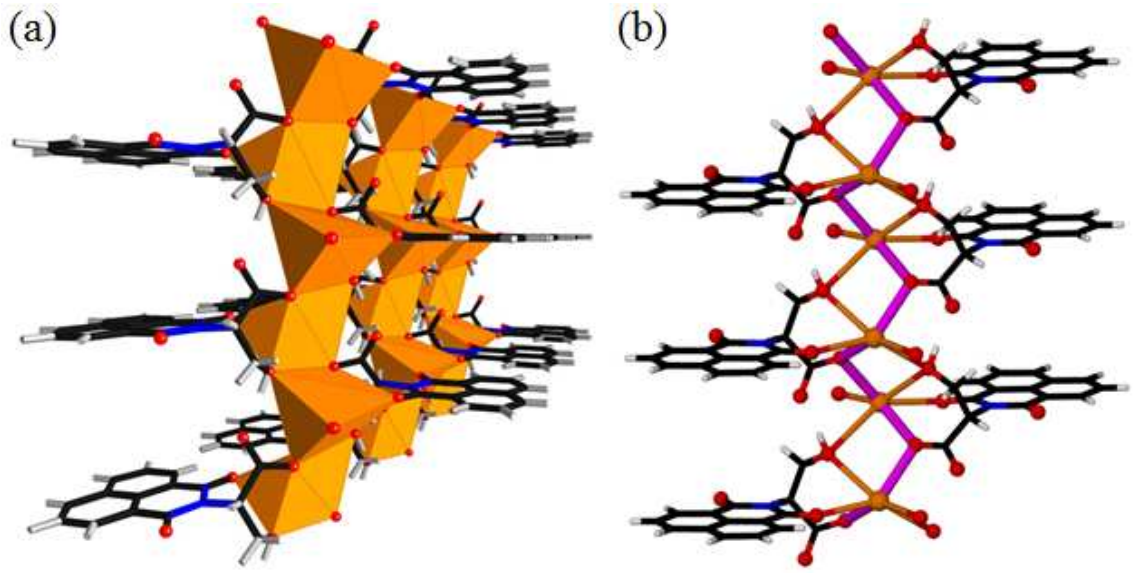

Figure 1.15. (a) A sheet of rods from **4** formed by edge shared K^+ polyhedra bridged together by the carbonyls of the naphthalimide and (b) the *P*-handed helix of each rod highlighted in purple follows the K1-O4-K1-O4 chain.

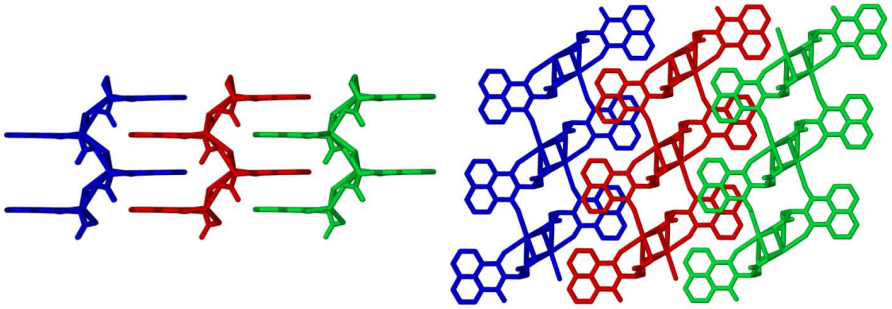

Figure 1.16. Views down the crystallographic *a* (left) and *c* (right) axis of **4** illustrating the zipperlike π···π stacking extending the structure in three dimensions and slippage of the naphthalimide rings. Each sheet is distinguished with a different color. Hydrogen atoms are omitted for clarity.

Cs(**L**$_{\mathbf{ser}}$) (**5**) has a very similar structure to **4**. Cesium has an unusually low coordination number of 6 with two of the sites occupied by μ^2-κ^2 carboxylate oxygens, two are filled by the bridging alcohol side-chains, and the last two are filled by carbonyls of the naphthalimide rings (Figure 1.17). The distorted trigonal prismatic cesium polyhedra are edge-shared through the bridging alcohol and carboxylate oxygens and extend in one dimension to generate helical rods as shown in Figure 1.18. The *P*-handed helical rods are defined by the Cs1-O4-Cs1-O4 chain and have a pitch of 6.61 Å. The rods are bridged together by carbonyls of the naphthalimide groups extending in two directions to form sheets. These sheets are zippered together through π···π stacking in a similar fashion to **4** (Figure 1.19). The metrics for the π···π stacking are listed in Table 1.3.

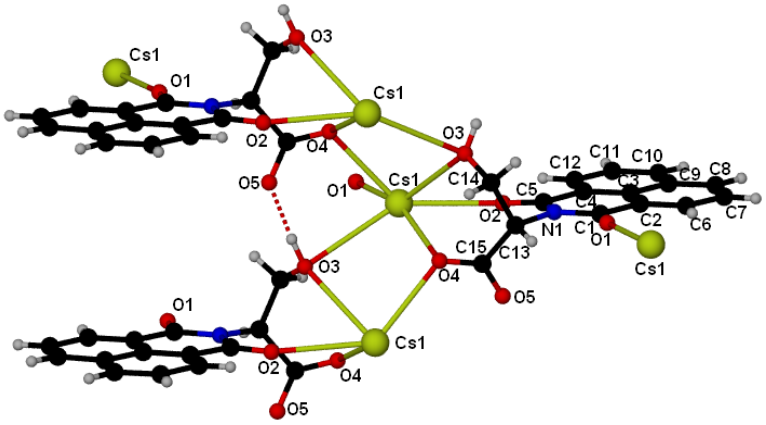

Figure 1.17. The Cs^+ coordination environment of Cs**L**$_{ser}$ (**5**) ; black C, red O, blue N, white H, yellow Cs.

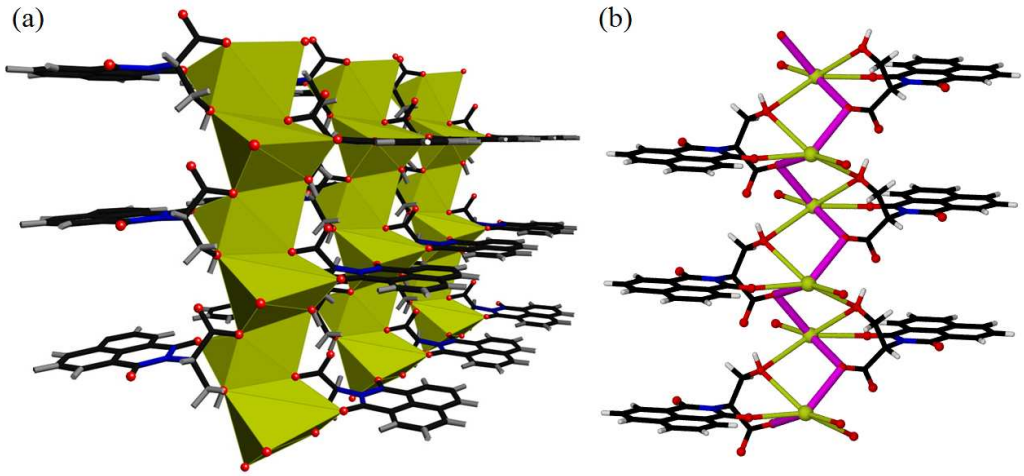

Figure 1.18. (a) A sheet of rods from **5** formed by edge shared Cs^+ polyhedra bridged together by the carbonyls of the naphthalimide and (b) the *P*-handed helix of each rod highlighted in purple follows the Cs1-O4-Cs1-O4 chain.

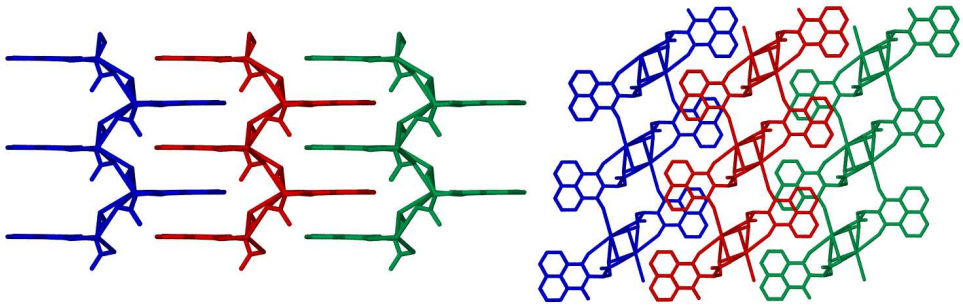

Figure 1.19. Views down the crystallographic *a* (left) and *c* (right) axis of Cs**L**$_{ser}$ (**5**) illustrating the zipperlike $\pi\cdots\pi$ stacking extending the structure in three dimensions and slippage of the naphthalimide rings. Each sheet is distinguished with a different color. Hydrogen atoms are omitted for clarity.

The coordination environment for the alkali cation in Cs($\mathbf{L_{ala}}$) (**6**) is significantly different from **1**-**5**, yet the overall 3D structure is very similar to **4** and **5**. Compound **6** is the only complex with $\mathbf{L_{ala}}^-$ to exclude the solvent molecule in the structure. Cesium is 6-coordinate with four of the sites occupied by μ^2-κ^2:κ^2 carboxylate oxygens and the remaining two filled by carbonyls of the naphthalimide rings (Figure 1.20). The unique μ^2-κ^2:κ^2-bonding of the carboxylate group allow the cesium cations to be six-coordinate without the presence of the solvent molecule in **1**-**3**. The cesium cation is in an extremely distorted, low-coordination environment with all of the oxygen donor atoms on one side leaving an open face on the metal. The distance between cesium and the hydrogen atoms of the methyl group of the ligand is short enough (3.17 Å) to denote a Cs···H interaction (Figure 1.20b). There is also an interaction between cesium and an aromatic hydrogen atom from an adjacent sheet with a distance of 3.32 Å. The irregular cesium polyhedra are edge-shared through both carboxylate oxygens, O3 and O4, and extend in one dimension to generate the helical rod SBU. The *P*-handed helical rods are defined by the Cs1-O4-Cs1-O4 chain and have a pitch of 6.56 Å. One of the carbonyls of the naphthalimide is bonded to the same cesium cation as the carboxylate making the ligand tridentate to one metal as in **4** and **5** and generating a [4.1.1] bicyclic system. As in these two structures, the other naphthalimide carbonyls bridge to potassium cations in adjacent helices, again extending in only two directions forming sheets of helical rods (Figure 1.21). There is π···π stacking between the naphthalimide rings linking sheets together into a SMOF in the same motif as **4** and **5** (Figure 1.22). The metrics for the π···π stacking are listed in Table 1.3.

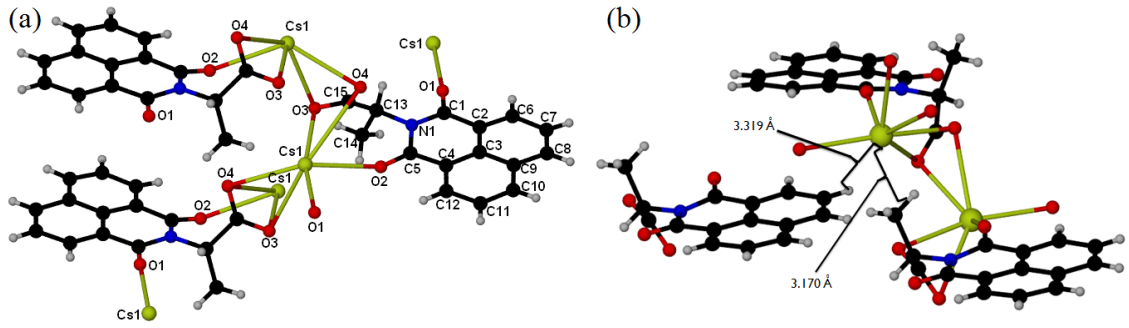

Figure 1.20. (a) The Cs^+ coordination environment of Cs**L**$_{ala}$ **(6)** and (b) possible Cs···H interactions; black C, red O, blue N, white H, yellow Cs.

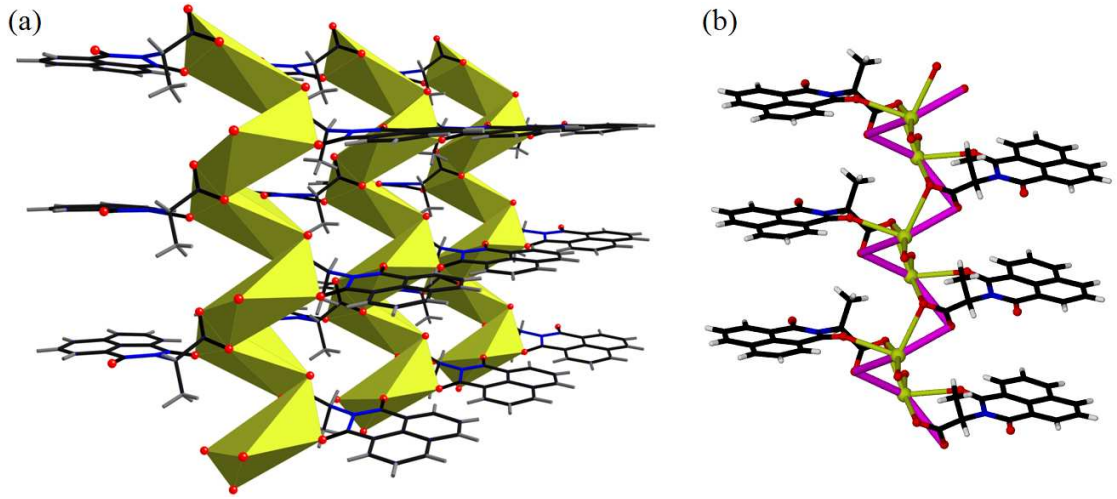

Figure 1.21. (a) A sheet of rods from **6** formed by rods of edge shared Cs^+ polyhedra bridged together by the carbonyls of the naphthalimide and (b) the *P*-handed helix of each rod highlighted in purple follows the Cs1-O4-Cs1-O4 chain.

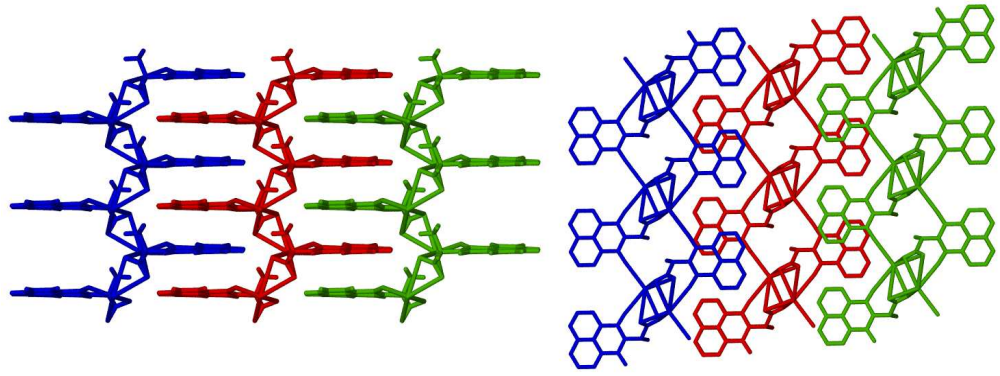

Figure 1.22. Views down the crystallographic *a* (left) and *c* (right) axis of Cs**L**$_{ala}$ (**6**) illustrating the zipperlike π···π stacking extending the structure in three dimensions and slippage of the naphthalimide rings. Each sheet is distinguished with a different color. Hydrogen atoms are omitted for clarity.

Table 1.3. π···π stacking metrics for compounds **4-6**.

	Compound	Cen-Cen(Å)	dipole ∠ (°)	plane ∠ (°)	avg dist (Å)	χ (Å)
4	K(**L**$_{ser}$)	4.18	180	1.6	3.30	2.56
5	Cs(**L**$_{ser}$)	4.32	180	1.5	3.31	2.78
6	Cs(**L**$_{ala}$)	4.53	180	10.3	3.27	3.11

Thermal Analysis. Thermal gravimetric analysis was performed on a TA Instruments SDT 2960 under a steady stream of dry air. Thermal analysis of compounds **1** and **4** are representative of their structure types and are shown in Figure 1.23. Compound **1** showed a weight loss at 128 °C that corresponds with a loss of the coordinated methanol ligand (9.81%, calcd. 9.44%). In addition, a physical change from dark brown single crystals to a white polycrystalline powder (**1p**) was observed at this temperature. The PXRD of this powder reveals that although the solid is polycrystalline, the structure has changed. Single crystals of the **1** can be reformed by recrystallization of this solid from methanol, as indicated in the Synthesis section. The polycrystalline powder remains stable until decomposition sets in starting at 319 °C.

TGA of compound **2** showed a weight loss between 80 and 120 °C corresponding to the loss of the coordinated water ligand (6.00%, calcd. 5.54%), resulting in the formation of a new compound, **2***. Single crystal X-ray analysis of **2***, formed by heating crystals of **2** at 140 °C for 3 hours, showed a partially hydrated compound with a 29% occupancy of coordinated water where the remaining potassium cations are five coordinate. Because the TGA shows a quantitative loss of water, we assume that partial rehydration occurred in the short time transferring the single crystals from the nitrogen atmosphere into the paraffin liquid for the X-ray analysis. PXRD analysis shows **2*** is different from **1p**. Upon further heating, compound **2*** experiences a higher decomposition point (347 °C) than **1p** even though they share the same chemical

formula. After exposure of the single crystal used for the structure of **2*** to air for two days compound **2** is reformed by reuptake of water**,** as confirmed by *single-crystal XRD*.

Upon heating, compound **3** experienced a weight loss between 89 and 177 °C indicative of a loss of the *coordinated* water ligand from the structure (6.40%, calcd. 5.83%). A second TGA experiment was performed where the heat ramp was stopped at 160 °C and after sitting in air at room temperature for three days the compound regained the lost water to reform the original compound, as shown by both PXRD and *single crystal X-ray analysis*. In a third experiment, crystals were heated in a Schlenk tube under vacuum to 150 °C for an hour, cooled under dry nitrogen and mounted quickly in the nitrogen stream of the single crystal diffractometer. Single crystal X-ray structural analysis shows that the crystals of **3** have undergone a single-crystal to single-crystal transformation and form compound **3*** at high temperature. Exposure of these dehydrated crystals to moist air for two day results in the reformation of **3**. This single-crystal to single-crystal transformation experiment was repeated a second time on the same two crystals, and again single crystal X-ray analysis at each stage showed the crystals still diffracted, but showed some signs of decay. It is important to note that in these experiments the single crystal are cooled from ambient temperature to 100 K at each step to collect the X-ray data, again indicating the stability of these crystals. In a separate experiment, single crystals were heated in a Schlenk tube under nitrogen to 200 °C for an hour, cooled under nitrogen and mounted quickly in the nitrogen stream of the single crystal diffractometer and again X-ray structural analysis shows that the crystals of **3** had undergone a single-crystal to single-crystal transformation to form compound **3*.** TGA

experiments show that compound **3*** is stable until 335 °C, well above the decomposition point.

As shown in Fig. 1.23b for **4**, decomposition temperatures for compounds **4**-**6** are 280, 227, and 314 °C, respectively. Compounds **4** and **6** maintain single crystallinity upon heating up until 250 and 215 °C, respectively; single crystals heated to these temperatures *still diffract.* Compound **5** does not retain single crystallinity when heated.

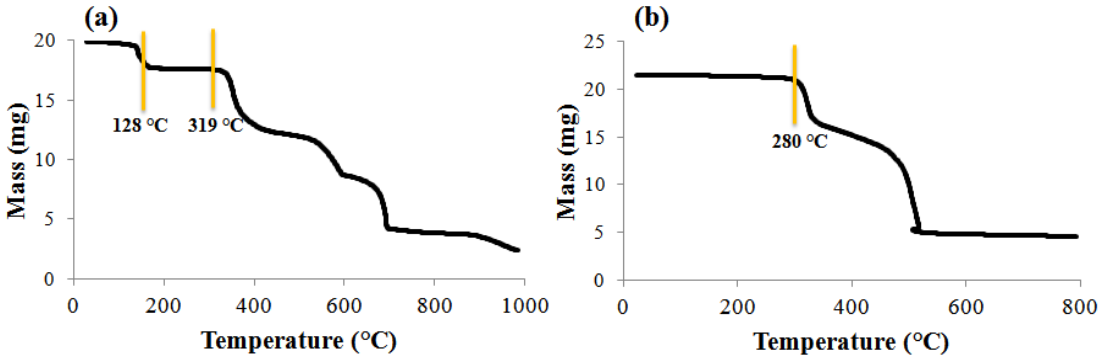

Figure 1.23. Thermal gravimetric analysis for compounds **1** and **4**.

Spectral Analyses. Compounds **1**-**6** all display similar fluorescence spectra. Complexes with the $\mathbf{L_{ala}^-}$ ligand all exhibit red-shifted emission spectra when compared to the protonated form, $\mathbf{HL_{ala}}$, and complexes with the $\mathbf{L_{ser}^-}$ ligand all exhibit blue-shifted emission spectra when compared to the protonated form, $\mathbf{HL_{ser}}$. No trends were found between structure type, cation choice, and fluorescence maxima. Fluorescence excitation and emission maxima are given in Table 1.4.

Table 1.4. Fluorescence excitation and emission maxima for the protonated ligands and their compounds.

	Compound	Excitation Max (nm)	Emission Max (nm)
	H**L**$_{\mathbf{ala}}$	381	450
1	K(**L**$_{\mathbf{ala}}$)(MeOH)	379	469
2	K(**L**$_{\mathbf{ala}}$)(H_2O)	380	462
3	Na(**L**$_{\mathbf{ala}}$)(H_2O)	373	453
6	Cs(**L**$_{\mathbf{ala}}$)	395	465
	H**L**$_{\mathbf{ser}}$	380	470
4	K(**L**$_{\mathbf{ser}}$)	395	438
5	Cs(**L**$_{\mathbf{ser}}$)	412	427

Second Harmonic Generation. Compounds **1**-**3** and **4**-**6** all contain the naphthalimide chomophore and crystallize in the noncentrosymmetric space groups $P2_12_12_1$ and $P2_1$, respectively; space groups that can potentially generate interesting nonlinear optical behavior. We did not detect any SHG with an incident wavelength of 1064 nm from **1**-**3**. It is possible that these materials do show nonlinear optical SHG activity but at different incident wavelengths. For **4**, **5** and **6**, powder SHG measurements indicate a SHG efficiency of approximately $30 \times \alpha$–SiO_2 in the 45–63 μm particle size range. Additional SHG measurements, particle size vs. SHG efficiency, indicate that **4** and **5** exhibit type 1 phase-matching while **6** reveals type 1 non-phase-matching behavior. As such **4**-**5** and **6** fall into the class B and C categories, respectively, of SHG materials, as defined by Kurtz and Perry (Figure 1.24).[14] Based on these measurements, we estimate the average NLO susceptibilities, $\langle d_{eff} \rangle_{exp,}$ of **4, 5** and **6** approximately 6.3, 6.3 and 3.0 pm/V, respectively.

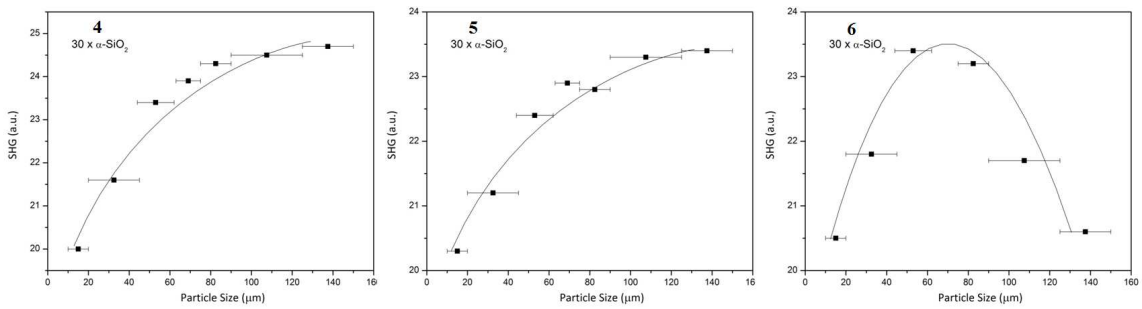

Figure 1.24. SHG efficiency for compounds **4**-**6** exhibiting type I phase- and non-phase-matching responses.

Discussion

Eight new complexes of three different alkali metals (Na^+, K^+ and Cs^+) have been prepared from the two ligands pictured in Scheme 1; ligands that contain a carboxylate donor group, a enantiopure chiral center and a 1,8-naphthalimide $\pi\cdots\pi$ stacking supramolecular tecton. Even though there is a large change in ionic radii with these three metals (six-coordinate ionic radii of 1.02, 1.46 and 1.67 Å for Na^+, K^+, and Cs^+, respectively[17]), each of the new complexes has a solid state structure based on six-coordinate metals linked into homochiral helical rod SBU central cores, with the exception of compounds **2*** and **3*** which have lost solvent upon heating and contain 5-coordinate potassium or sodium cations, respectively. Despite this uniformity of structure, the helical rod SBU cores form from four different, but related bonding arrangements: in **1**, **4** and **5** the metal polyhedra are linked by edge-sharing through bridging oxygens originating from the alcohol and carboxylate; in **2, 2*,** and **3*** by corner-sharing through bridging oxygens originating from the carboxylate; in **3** by corner-sharing through bridging oxygens originating from the water; and in **6** by edge-sharing through bridging oxygens originating only from the carboxylate. Very few homochiral helical rod SBUs have been reported previously.[19] Also, this consistent

formation of a central organizational structural feature in the work described here is uncommon for group 1 carboxylates.[12]

In addition to this consistent formation of a similar type of SBU, only two overall structural arrangements of the eight complexes are observed. The five complexes **1**-**3*** are all three-dimensional rod-packed structures in a uninodal 4*c* net, in which the remaining two dimensions are linked by the interactions of oxygens on the naphthalimide groups bridging to adjacent SBUs forming a "square" arrangement. In contrast, complexes **4**-**6** show polar covalent linkages in only one additional dimension leading to the formation of two-dimensional sheets. This inter-rod bonding to the group 1 metal of the carbonyl oxygens coupled with intra-rod bonding of the same type present in all eight complexes is a new bonding feature of ligands containing the naphthalimide group that was not present in our previous work with transition metal complexes. Such a difference is not unexpected in complexes of these oxophilic metals.

In all of our previous chemistry with these types of naphthalimide-based ligands, we have observed structures strongly influenced by strong $\pi\cdots\pi$ stacking interactions. In addition to complexes **1**-**3*** having three-dimensional "covalent" structures, they are also supported by these supramolecular interactions. More importantly, in the structures of complexes **4**-**6**, the third dimension is supported exclusively by interdigitated $\pi\cdots\pi$ stacking interactions, forming SMOF solids. The overlap of the naphthalimide rings in complexes **4**-**6** is somewhat reduced when compared to complexes **1**-**3***, a result emphasized by the "slippage" parameters in Tables 1.2 and 1.3, but the overlap is still substantial. It is interesting to speculate that these noncovalent forces are instrumental not only in the organization of the third dimension in complexes **4**-**6**, but also in the

consistency of the structures based on homochiral helical SBUs in all eight complexes reported here. This impact of the naphthalimide supramolecular tecton is supported by the fact that all of the metals have low coordination numbers, most notably the five-coordinate potassium cation in **2***, the five-coordinate sodium cation in **3*** and the six-coordinate cesium cations in compounds **5** and **6**, all particularly low for these large cations.[20]

A related interesting result of this chemistry is the limited amount of coordinated solvent in all the structures. In general, group 1 complexes crystallized from polar solvents, especially those of the heavier metals, retain a significant amount of solvent,[12] and this issue has been shown to impact on the dimensionality and thermal stability of the structures.[12] Complexes **1**-**3** contain only one equivalent of solvent in the structures. Heating complexes **2** and **3** formed new complexes, **2*** and **3*** respectively, which have no solvent. Complexes **4** and **5** contain no solvent by design; after obtaining the result of one methanol in the structure of **1** we synthesized the $\mathbf{L_{ser}^-}$ ligand that "builds in" the alcohol functional group to intentionally prepare complexes that contained no solvent. While this *designed ligand modification* is successful in the initial goal of eliminating the solvent, the resulting tridentate bonding of the new ligand also caused a structural change from three- to two-dimensional as described above. The absence of solvent in complex **6** is especially notable as the large cesium cation is only six-coordinate and has a "vacant face" in its structure. We note that although the coordination sphere of **6** has this highly distorted arrangement of the ligands, there are apparently at least two Cs-H interactions (Fig. 1.20 b). Again, as indicated above, it is likely that the large naphthalimide groups

coupled with the π···π stacking interactions strongly influence the amount of solvent and relatively low coordination numbers in these structures.

The presence of solvent makes a substantial impact on the thermal properties. Compound **1** loses the bridging methanol upon heating resulting in a polycrystalline powder (**1p**) which is stable up to the decomposition point around 318 °C. Although this loss of solvent results in collapse of the single crystal structure, this desolvated solid can be recrystallized to reform the starting structure. In the cases of compounds **2** and **3**, coordinated water can be reversibly removed/incorporated into the structure by heating in the absence of water vapor and cooling in the presence of water vapor through *gas/solid, single-crystal to single-crystal transformations*. In the case of compound **2** there is no huge impact on the crystal structure from the transformation, likely a function of the fact that the water molecule is a terminal ligand. The loss of water results in a 5-coordinate potassium cation, which is unusually low, and a slight decrease of the unit cell volume. Upon heating compound **3**, the water that is *the only bridge* between the sodium cations was lost, but the crystals *remain suitable for single crystal X-ray analysis*. In the structure of this new compound, **3***, the role of the carboxylate group changed from κ^2 to μ^2-κ^1:κ^2 and O3 rotates 1.36 Å closer to the adjacent sodium cation to form a direct interaction in order to satisfy the coordination environment of the sodium cations and retain the homochiral helical rod SBU structure (Figure 1.25). Exposure of the single crystals of **3*** to moist air over the course of three days results in a reincorporation of water into the bridging position of the rods reforming **3**, again *without loss of single crystallinity*. This reversible single-crystal to single-crystal transformation can be repeated second time, but with modest degradation of the crystal (note the crystals are cooled to 100 K at each step

for the X-ray analysis). It can be argued that this structural change is supported by the intra-rod chelate rings formed by the carboxylate and naphthalimide carbonyl, which change from a nine-member ring in **3** to a seven member ring in **3***. Remarkably, these reversible single-crystal to single-crystal transformations occur in the absence of channels. In contrast to the solvated crystals, crystals of solvent free compounds **4** and **6** are amazingly stable; they retain single crystallinity up to *ca.* 210 °C, well above the decomposition point of the protonated ligand. This stability is particularly notable for an SMOF solid, where at least one dimension is organized only by noncovalent forces.

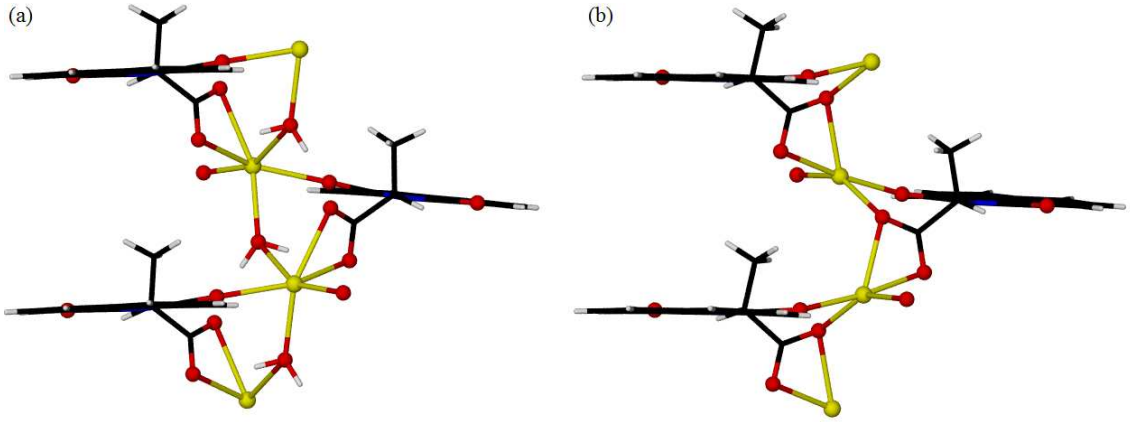

Figure 1.25. A comparison of hydrated **3** (a) and dehydrated **3*** (b) and the differences in carboxylate bonding; black C, red O, blue N, white H, yellow Na.

All of the compounds exhibit luminescence which is known to be derived from the naphthalimide ligand. Compounds containing the $\mathbf{L_{ala}^-}$ ligand (**1**-**3**, **6**) are all red-shifted by 3-19 nm with respect to crystals of the protonated ligand whereas compounds containing the $\mathbf{L_{ser}^-}$ ligand (**4**, **5**) are both blue-shifted by 32-43 nm with respect to the crystals of the protonated ligand.

The second-harmonic generation efficiency of these compounds was studied for several reasons: the naphthalimide ring is a known chromophore, the ligands are enantiopure and lead to the formation of crystals with noncentrosymmetric space groups

and rod shaped SBUs are known to promote interesting electronic properties because of the extended metal-metal interactions.[21] Compounds **1**-**3** did not exhibit observable SHG efficiency at an incident wavelength of 1064 nm, but compounds **4**-**6** did exhibit modest SHG efficiency for MOF-like compounds in the range of 30 x α-SiO_2. Compounds **4** and **5** exhibit type I phase-matching behavior while compound **6** is type I non-phase matchable. The SHG effect in **4-6** is thought to originate from the lower symmetry of these networks because **1-6** contain the same building blocks: enantiopure helical rods of alkali metals and π···π stacking. The strong SHG response coupled with the retention of crystallinity at elevated temperatures makes compounds **4-6** potential candidates for practical applications.

References

(1) (a) Corma, A.; Garcia, H.; Llabrés i Xamena, F. X. *Chem. Rev.* **2010**, *110*, 4606. (b) Lin, W. *Top. Catal.* **2010**, *53*, 869. (c) Natori, Y.; Tsutsui, H.; Sato, N.; Nakamura, H.; Nambu, H.; Shiro, M.; Hashimoto, S. *J. Org. Chem.* **2009**, *74*, 4418.

(2) (a) Tranchemontagne, D. J.; Mendoza-Cortés, J. L.; O'Keefe, M.; Yachi, O. M. *Chem. Soc. Rev.* **2009**, *38*, 1257-1283. (b) Rosi, N. L.; Kim, J.; Eddaoudi, M.; Chem. B.; O'Keeffe, M.; Yaghi, O. M. *J. Am. Chem. Soc.* **2005**, *127*, 1504-1518. (c) O'Keeffe, M.; Yaghi, O. M. *Chem. Rev.* **2012**, *112*, 675-702.

(3) (a) *Design of Organic Solids*; Weber, E., Ed. *Topics in Current Chemistry*; Springer: Berlin, **1998**; Vol. 198. (b) Pidcock, E.; Motherwell, W. D. S. *Cryst. Growth Des.* **2005**, *5*, 2232. (c) Du, M.; Zhang, Z. H.; Zhao, X. J. *Cryst. Growth Des.* **2005**, *5*, 1199. (d) Takahashi, S.; Katagiri, T.; Uneyama, K. *Chem. Commun.* **2005**, 3658. (e) Weatherhead-Kloster, R. A.; Selby, H. D.; Miller, W. B.; Mash, E. A. *J. Org. Chem.* **2005**, *70*, 8693. (f) Zhang, J. P.; Lin, Y.-Y.; Huang, X. C.; Chen, X.-M. *Chem. Commun.* **2005**, 1258. (g) Vangala, V. R.; Bhogala, B. R.; Dey, A.; Desiraju, G. R.; Broder, C. K.; Smith, P. S.; Mondal, R.; Howard, J. A. K.; Wilson, C. C. *J. Am. Chem. Soc.* **2003**, *125*, 14495.

(4) (a) Reger, D. L.; Horger, J. J.; Smith. M. D.; Long, G. J.; Grandjean. F. *Inorg. Chem.* **2011**, *50*, 686-704. (b) Reger, D. L.; Horger, J. J.; Smith, M. D. *Chem. Commun.* **2011**, *47*, 2805-2807. (c) Reger, D. L.; Horger, J. J.; Debreczeni, A.; Smith, M. D. *Inorg. Chem.* **2011**, *50*, 10225-10240.

(5) (a) Qu, Z.-R.; Zhao, H.; Wang, X.-S.; Li, Y.-H.; Song, Y.-M.; Liu, Y.-J.; Ye, Q.; Xiong, R.-G.; Abrahams, B. F.; Xue, Z.-L.; You, X.-Z. *Inorg. Chem.* **2003**, *42*, 7710-7712. (b) Ingleson, M. J.; Bacsa, J.; Rosseinsky, M. J. *Chem. Commun.* **2007**, *29*, 3036-3038.

(6) (a) Rombach, M.; Gelinsky, M.; Vahrenkamp, H. *Inorg. Chim. Acta.* **2002**, *334*, 25-33. (b) Fox, S.; Buesching, I.; Barklage, W.; Strasdeit, H. *Inorg. Chem.* **2007**, *46*, 818-824.

(7) (a) Reger, D. L.; Debreczeni, A.; Smith, M. D. *Inorg. Chem.* **2011**, *50*, 11754-11764. (b) Reger, D. L.; Debreczeni, A.; Smith, M. D..; Jezierska, J.; Ozarowski, A. *Inorg. Chem.* **2012**, *51*, 1068-1083. (c) Reger, D. L.; Debreczeni, A.; Reinecke, B.; Rassolov, V.; Smith, M. D.; Semeniuc, R. F. *Inorg. Chem.* **2009**, *48*, 8911-8924.

(8) Reger, D. L.; Debreczeni, A.; Horger, J. J.; Smith, M. D. *Cryst. Growth Des.* **2011**, *11*, 4068-4079.

(9) Lee, J. D. *Concise Inorganic Chemistry*; Chapman & Hall: New York, **1991**.

(10) (a) Takarada, T.; Nabatame, T.; Ohtsuka, Y.; Tomita, A. *Ind. Eng. Chem. Res.* **1989**, *28*, 505-510. (b) Makosza, M.; Nieczypor, P.; Grela, K. *Tetrahedron*, **1998**, *54*, 10827-10836.

(11) (a) Valasek, J. *Phys. Rev.* **1921**, *17*, 475. (b) Kambay, S.; Brezina, B.; Petzelt, J.; Schaack, G. *J. Phys.: Condens. Matter* **1996**, *8*, 8669.

(12) (a) Fromm, K. M. *Coord. Chem. Rev.* **2008**, *252*, 856-885. (b) Banerjee, D.; Parise, J. B. *Cryst. Growth Des.* **2011**, *11*, 4704-472.

(13) Reger, D. L.; Leitner, A. P.; Smith, M. D. *Inorg. Chem.* **2012**, *51*, 10071-10073.

(14) Kurtz, S. K.; Perry, T. T. *J. Appl. Phys.* **1968**, *39*, 3798.

(15) Ok, K. M.; Chi, E. O.; Halasyamani, P. S. *Chem. Soc. Rev.* **2006**, *35*, 710.

(16) SMART Version 5.630, SAINT+ Version 6.45 and SADABS Version 2.10. Bruker Analytical X-ray Systems, Inc., Madison, Wisconsin, USA, 2003.

(17) Sheldrick, G.M. *Acta Cryst*. **2008**, *A64*, 112.

(18) Dolomanov, O. V., Bourhis, L. J., Gildea, R. J., Howard J. A. K. and Puschmann, H. OLEX2: a complete structure solution, refinement and analysis program. *J. Appl. Cryst*. **2009**, *42*, 339.

(19) (a) Mallick, A.; Saha, S.; Pachfule, P.; Roy, S.; Banerjee, R. *J. Mater. Chem.* **2010**, *20*, 9073. (b) Appelhans, L. N.; Kosa, M.; Radha, A. V.; Simoncic, P.; Navrotsky, A.; Parrinello, M.; Cheetham, A. K. *J. Am. Chem. Soc.* **2009**, *131*, 15375. (c) Yeung, H. H.-M.; Kosa, M.; Parrinello, M.; Forster, P. M.; Cheetham, A. K. *Cryst. Growth Des.*

2011, *11*, 221. (d) Rood, J. A.; Noll, B. C.; Henderson, K. W. *J. Solid State Chem.* **2010**, *183*, 270. (e) Gao, Q.; Wang, X.; Conato, M. T.; Makerenko, T.; Jacobson, A. *J. Cryst. Growth Des.* **2011**, *11*, 4632.

(20) (a) Nichol, G. S.; Clegg, W. *Polyhedron*, **2006**, *25*, 1043-1056. (b) Stein, I.; Ruschewitz, U. *Acta Crystallogr., E* **2007**, *63*, M382-M84. (c) Wiesbrock, F.; Schmidbaur, H. *Inorg. Chem.* **2003**, *42*, 7283-7289. (d) Santra, S.; Das, B.; Baruah, J. *J. Chem. Crystallogr.* **2011**, *41*, 1981-1987.

(21) (a) Xu, X.; Zhang, X.; Liu, X.; Sun, T.; Wang, E. *Cryst. Growth Des.* **2010**, *10*, 2272-2277. (b) Che, C.-M.; Tse, M.-C.; Chan, M. C. W.; Cheung, K.-K.; Phillips, D. L.; Leung, K.-H. *J. Am. Chem. Soc.* **2000**, *122*, 2464-2468.

Chapter II

Framework complexes of group 2 metals organized by homochiral rods and π··π stacking forces: a breathing supramolecular MOF [2]

---

[2]Adapted with permission from Reger, D. L.; Leitner, A.; Pellechia, P. J.; Smith, M. D *Inorg. Chem.* **2014**, *53*(18), 9932-9945. DOI: 10.1021/ic501581c. Copyright 2014 American Chemical Society.

Introduction

The crystal engineering of metal-organic hybrid materials with novel extended structures remains an important goal in synthesis and crystal growth.[1] Metal-organic frameworks (MOFs) are composed of groups of metal ions, also known as secondary building units (SBUs), covalently connected in one-, two- or three-dimensions by organic linkers.[2] Supramolecular tectons (e.g. groups that can hydrogen bond or participate in $\pi^{\cdots}\pi$ stacking interactions) can be built into the bridging ligands for enhanced flexibility and stability.[3] Flexible MOFs can show reversible structural changes based on external stimuli and have shown selective adsorption of substrates that can be used for sensing and separations.[4] The ability to characterize these highly flexible crystalline materials by solid-state NMR spectroscopy has been well established.[4a,5]

We have designed a series of ligands (Scheme 2.1) containing a carboxylate donor group and a naphthalimide $\pi^{\cdots}\pi$ stacking supramolecular tecton. Of interest here are the ligands derived from enantiopure naturally occurring amino acids that all contain a single carboxylate group that coordinates to the metals to create the SBUs and a chiral center that imparts its chirality on the SBU leading to solids in noncentrosymmetric space groups.[3,6,7] Using amino acid precursors provides access to additional functionality made available by the side-chain, varying in the work reported here from a methyl group in the case of L-alanine (in one case R-alanine) to a hydroxyl group in the case of L-serine. Most complexes of amino acid ligands involve coordination of the amine to the metal.[8] We avoid this coordination by protecting the amine with a 1,8-naphthalimide group that

not only blocks it from coordination, but also has a propensity to engage in strong π···π stacking interactions, which have a substantial impact on the 3D structures.[6,9,10] The 1,8-naphthalimide group is also an excellent chromophore that has many biological imaging applications including probing, cellular imaging and DNA-tagging for anti-cancer research because of the ability to form strong intermolecular complexes with nucleic acids.[11]

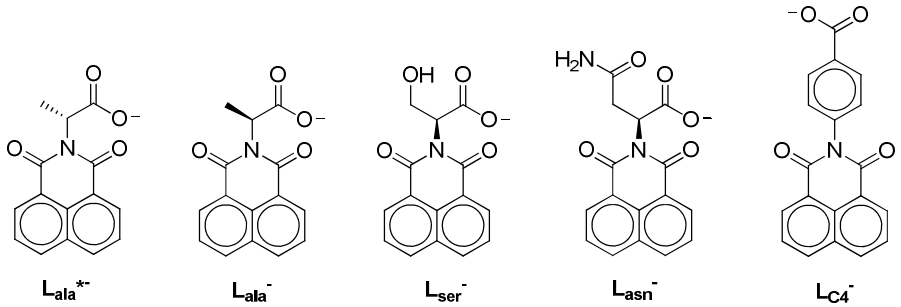

Scheme 2.1 Multifunctional Ligands

When these ligands are combined with transition metals, the three dimensional structures of the new complexes are generally dominated by π···π stacking and contain either open channels or cavities filled with disordered solvent.[6] These solids have interesting and potentially useful properties. For example, in a previous paper we showed a densely packed compound held together by π···π stacking, $[Zn_2(\mathbf{L_{C4}})_4(DMSO)_2]\cdot 2(CH_2Cl_2)$, could exchange interstitial dichloromethane for water despite the lack of pores via a single-crystal to single-crystal transformation.[9a] In a separate paper, we showed enantioselective binding of racemic ethyl lactate to the copper paddlewheel SBU in the compound $[Cu_4(\mathbf{L_{asn}})_8(pyridine)(MeOH)]$, also via a single-crystal to single-crystal transformation.[6c] When $\mathbf{L_{ala}}^-$ and $\mathbf{L_{ser}}^-$ are combined with group 1 metals, the structures are dominated by the consistent formation of helical rod SBUs that are in all cases homochiral.[7] These MOFs have been shown to be thermally stable, retaining single-crystallinity even after

being heated to 200 °C in air. In addition, the compounds Na($\mathbf{L_{ala}}$)(H_2O) and K($\mathbf{L_{ala}}$)(H_2O) show interesting flexibility; bridging water molecules of the rod-shaped SBU can be reversibly removed, despite coordination to two metals, in single-crystal to single-crystal transformations. The combination of the homochiral rod-shaped SBUs and naphthalimide groups opened up the possibilities for unique electronic properties, which we demonstrated with modest solid-state luminescence and second order harmonic generation.

There has only been limited research on the synthesis of MOFs from s-block metals with little previous ability to predict and control the coordination geometry, let alone control the formation of the SBU in MOF type structures.[12] Given our success with group 1 complexes of $\mathbf{L_{ala}}^-$ and $\mathbf{L_{ser}}^-$ (Scheme 2.1), where we showed the consistent formation of rare examples of homochiral rod SBUs,[2] we decided to investigate the dicationic metals in group 2. We report here the syntheses of complexes of calcium and strontium with these same two enantiopure ligands, and in one case with the enantiomeric ligand $\mathbf{L_{ala}}^{*-}$. As observed in the group 1 complexes, the structures of these compounds are dominated by homochiral rod SBUs. In contrast to the group 1 chemistry where both 3D and 2D MOF structures formed, with these group 2 metals only 1D structures form, but the $\pi^{\cdots}\pi$ stacking interactions lead to supramolecular MOFs (SMOFs) where the remaining dimensions are organized by noncovalent forces. In one case, the strontium polyhedra adopt a rare face sharing configuration that composes the rod-shaped SBU.[13] Another of the compounds undergoes a dynamic single-crystal to single-crystal transformation; a breathing SMOF where the 1D channels can be open or closed. The nature of this breathing was investigated by single-crystal X-ray crystallography, IR and

solid-state ^{1}H, ^{13}C and ^{2}H NMR spectroscopy. In addition we report the thermal and luminescent properties of these complexes.

Experimental

General Considerations. All reactants were used as purchased from Aldrich and Strem. The syntheses of the ligand precursors H**L**$_{ala}$ and H**L**$_{ser}$ have been reported elsewhere.[7] H**L**$_{ala}$* is synthesized the same as H**L**$_{ala}$ but starting with D-alanine instead of the naturally occuring L-alanine to produce the protonated ligand with the opposite handed chirality. Elemental analyses were performed by Robertson Microlit Laboratories (Ledgewood, NJ). ^{1}H, ^{13}C and ^{2}H solid-state NMR spectra were recorded on a Bruker Advance III-HD 500 MHz spectrometer. Infrared spectra were recorded on a Thermo Nicolet Avatar 360 FT-IR spectrophotometer. Crystals were collected and transferred to a drybox, ground into a Nujol Mull and placed between NaCl plates. Thermalgravimetric analyses were performed using a Thermal Analysis (TA) SDT Q600 simultaneous DTA/TGA system. The samples were heated in dry air to 800 °C with a heating rate of 10 °C/min. For compound **1**, the experiment was terminated after the decomposition temperature was recorded because it frothed when heated to decomposition. The fluorescence measurements were done on a Perkin Elmer Lambda 35 UV-vis spectrometer.

[Ca(L$_{ala}$)$_2$(H$_2$O)]·(H$_2$O) (**1**). H**L**$_{ala}$ (2.0 g, 7.4 mmol) was added to a solution of potassium hydroxide (0.42 g, 7.4 mmol) in water (25 mL) and stirred for an hour until the solution was homogeneous. The solvent was evaporated and the remaining solid dried in vacuo to produce the potassium salt of the ligand (K**L**$_{ala}$) as a light brown powder (1.96 g). A 9 mL thick walled glass tube with a Teflon screw top was charged with a sample of

this solid (0.055 g), calcium nitrate tetrahydrate (0.017 g, 0.075 mmol), and 1 mL of a 1:1 water/isopropanol solution and heated at 120 °C. Over the course of heating for 3 days, yellow crystals grew on the walls of the tube above the solvent line. After no starting material remained at the bottom of the tube, the heat was removed and the system was allowed to slowly cool at a rate of about 1°C/min. Small yellow crystals were collected from the walls of the tube and washed with diethyl ether to provide 0.031 g of single crystals. Anal. Calcd. (Found) for $C_{30}H_{23}CaN_2O_{10}$: C 58.98(58.92); H 3.79 (4.02); N 4.58 (4.34).

[Ca(L_{ser})$_2$]·(H_2O)$_2$ (**2**). This complex was prepared as for **1** using KL_{ser} (0.050 g), calcium nitrate tetrahydrate (0.010 g, 0.061 mmol) and 1mL of a 1:1 water/isopropanol solution to produce colorless crystals that were washed with methanol to provide 0.026 g of single crystals. Crystals were dried to constant weight before elemental analysis. Anal. Calcd. (Found) for $C_{30}H_{24}CaN_2O_{12}$: C 55.90 (56.29); H 3.75 (4.05); N 4.34 (4.83).

[Sr(L_{ala})$_2$(H_2O)]·(H_2O)$_3$ (**3**). A 9 mL thick walled glass tube with a Teflon screw top was charged with KL_{ala} (0.050 g), anhydrous strontium nitrate (0.015 g, 0.070 mmol), and 1 mL of a 4:1 water/methanol solution and heated at 120 °C. Yellow crystals grew overnight on the walls of the tube above the solvent line. Small yellow crystals were collected and washed with methanol to provide 0.028 g of single crystals. Anal. Calcd. (Found) for $C_{30}H_{28}N_2O_{12}Sr$: C 51.72 (52.09); H 4.06 (3.84); N 4.02 (3.89).

[Sr(L_{ala}*)$_2$(H_2O)]·(H_2O)$_3$ (**3***). This compound was prepared by the same procedure as for **3** but starting with KL_{ala}*.

[Sr(L_{ser})$_2$(H_2O)] (**5**). This compound was prepared by the same procedure as for **2**, but with $Sr(NO_3)_2$ (0.032 g) to produce large colorless needles. Colorless crystals were

collected from the walls of the tube and washed with methanol to provide 0.060 g of single crystals. Crystals were dried to constant weight before elemental analysis. Anal. Calcd. (Found) for $C_{30}H_{22}N_2O_{11}Sr$: C 53.42 (53.45); H 3.02 (3.29); N 4.16 (4.16).

Single-Crystal to Single-Crystal Experiments – Synthesis of [Sr(L_{ala})$_2$(H_2O)] (**4**). Compound **3** undergoes a reversible single-crystal to single-crystal transformation when placed under vacuum to form [Sr(**L_{ala}**)$_2$(H_2O)], **4**. Single crystals of compound **3** were collected from the walls of the solvothermal tubes and washed with methanol. After checking the unit cell with single crystal X-ray diffraction to verify crystallinity, the crystals were held under vacuum for one hour and single crystal X-ray diffraction showed that compound **4** had formed, although the crystallinity was degraded. Anal. Calcd. (Found) for $C_{30}H_{22}N_2O_9Sr$: C 56.11 (56.50); H 3.45 (3.28); N 4.36 (4.41). This same batch of single crystals were then returned to a glass vial that was kept in a humid environment for 24 hours and single crystal X-ray diffraction showed that **3** had reformed and the crystal quality had improved. The experiment was repeated on the same crystals three times with the same results.

Crystallographic Studies. For all complexes, X-ray diffraction intensity data were measured at 100(2) K using a Bruker SMART APEX diffractometer (Mo Kα radiation, λ = 0.71073 Å). The raw area detector data frames were reduced with the SAINT+ program. Direct methods structure solution, difference Fourier calculations and full-matrix least-squares refinement against F2 were performed with SHELXS/L, implemented in OLEX2. Non-hydrogen atoms were refined with anisotropic displacement parameters. Hydrogen atoms bonded to carbon were placed in

geometrically idealized positions and included as riding atoms. For compounds **1**-**5** crystal enantiopurity and the "S" configuration (except 3* where it is "R") of the chiral carbon (C13 in all structures) were established by the absolute structure (Flack) parameters of zero (within experimental error) derived from the X-ray data sets. For compound **1** the data crystal was mounted inside a thin-walled glass capillary along with a drop of the mother liquor. Previous studies indicated some decomposition of the crystals in air. Attempts to cool crystals in a nitrogen cold stream resulted in loss of crystallinity accompanied by clouding of the crystals and broadening of the diffraction maxima. Details of data collection are given in Table 2.1.

Table 2.1 Crystallographic Data

	1	**2**	**3**	**3***	**4**	**5**
Formula	$C_{30}H_{23.82}CaN_2O_{9.91}$	$C_{30}H_{24}CaN_2O_{12}$	$C_{30}H_{28.04}N_2O_{12.02}Sr$	$C_{30}H_{28.10}N_2O_{12.05}Sr$	$C_{30}H_{22}N_2O_9Sr$	$C_{30}H_{22}N_2O_{11}Sr$
Fw, g mol^{-1}	610.97	644.59	696.57	697.03	642.11	674.11
Cryst. Syst.	Tetragonal	Monoclinic	Tetragonal	Tetragonal	Tetragonal	Orthorhombic
Space group	$P4_32_12$	$C2$	$P4_12_12$	$P4_32_12$	$P4_12_12$	$P2_12_12_1$
T, K	296(2) K	100(2) K	100(2) K	100(2) k	100(2) K	100(2) K
a, Å	20.8348(16)	15.585(4)	19.868(3)	19.9415(9)	19.030(5)	7.0910(9)
b, Å	20.8348(16)	21.919(5)	19.868(3)	19.9415(9)	19.030(5)	14.1845(18)
c, Å	14.064(2)	8.214(2)	14.975(4)	14.9995(13)	14.797(7)	26.618(3)
β, deg	90	103.410(4)	90	90	90	90
V, Å^3	6104.9(12)	2729.6(11)	5911.0(18)	5964.8(7)	5359(4)	2677.3(6)
Z	8	4	8	8	8	4
$R_1(I>2\sigma(I))$[a]	0.0564	0.0438	0.0538	0.0325	0.1329	0.0304
$wR_2(I>2\sigma(I))$[b]	0.1428	0.0971	0.1118	0.0841	0.3251	0.0646
Flack Parameter	0.01(5)	-0.01(3)	-0.015(11)	-0.018(2)	0.072(13)	-0.007(4)

[a] $R1 = \Sigma \, ||F_o| - |F_c|| \, / \, \Sigma \, |F_o|$, [b] $wR2 = \{ \Sigma [w(F_o^2 - F_c^2)^2] / \Sigma [w(F_o^2)^2] \}^{1/2}$

Results

Synthesis. Single crystals of $[Ca(\mathbf{L_{ala}})_2(H_2O)]\cdot(H_2O)$ (**1**), $[Ca(\mathbf{L_{ser}})_2]\cdot(H_2O)_2$ (**2**), $[Sr(\mathbf{L_{ala}})_2(H_2O)]\cdot(H_2O)_3$ (**3**), $[Sr(\mathbf{L_{ala}}\mathbf{*})_2(H_2O)]\cdot(H_2O)_3$ (**3***) and $[Sr(\mathbf{L_{ser}})_2(H_2O)]$ (**5**) were synthesized via solvothermal methods by combining the potassium salt of each respective ligand and the appropriate alkaline metal nitrate (2:1 molar ratio) in a mixed solvent

system containing a mixture of either methanol and water or isopropyl alcohol and water. The sealed tubes were heated at 120 °C in an oil bath with the crystals growing slowly just above the solvent line of the hot tube.

Compound **3** undergoes a single-crystal to single-crystal transformation when placed under vacuum to form compound **4**, [Sr($\mathbf{L_{ala}}$)$_2$(H_2O)], where the interstitial waters in **3** are removed, but the coordinated water molecule remains. Placing crystals of **4** in a humid atmosphere leads to the reformation of crystalline **3**, a process that can be repeated at least three times. Monitoring the crystals at each step by single crystal X-ray demonstrates that single crystallinity is retained in this process.

Structure Descriptions. Compound **1**, [Ca($\mathbf{L_{ala}}$)$_2$(H_2O)]·(H_2O), is composed of calcium cations bridged by $\mathbf{L_{ala}}^-$ ligands into a chiral helical rod SBU that is interdigitated with adjacent parallel rods by the supramolecular π···π stacking of the naphthalimide rings to generate a 3D SMOF structure. The coordination number of the calcium cation is seven and the irregular polyhedron most closely resembles a capped octahedron. There are two nonequivalent ligands and each have different coordination modes (Figure 2.1). One carboxylate adopts a μ-κ^1:κ^2 bonding mode (this ligand is disordered over two sites and only one version is shown) while the other adopts a μ-κ^1:κ^1 bonding mode, thus filling five of the seven coordination sites. Another key difference between the two ligands is the orientation of the methyl group at the chiral center, which are oriented in opposite directions with respect to the crystallographic *c*-axis. The last two metal sites are occupied by a bridging water molecule generating the edge shared polyhedra that make up the helical rod SBU. The homochiral, M helices created by the bridged calcium cations have a pitch of 14.06 Å (Figure 2.2). There are two types of π···π stacking in

which the naphthalimide rings are involved: intra-rod π···π stacking where ligands with opposing methyl orientation from the same rod stack together, and inter-rod π···π stacking where ligands from adjacent rods interact with one another to generate the 3D SMOF structure. All of the ligands are involved in both types of π···π stacking creating pairs of 1,8-naphthalimide rings that interdigitated with pairs from an adjacent rod. The metrics used to evaluate the π···π stacking are listed in Table 2.2. The π-stacked pairs of naphthalimide rings of **1** are oriented in a "square" arrangement, Figure 2 (right), so that each rod interacts with four adjacent rods generating a 3D network with square shaped channels (Figure 2.3). These channels are occupied by disordered water molecules.

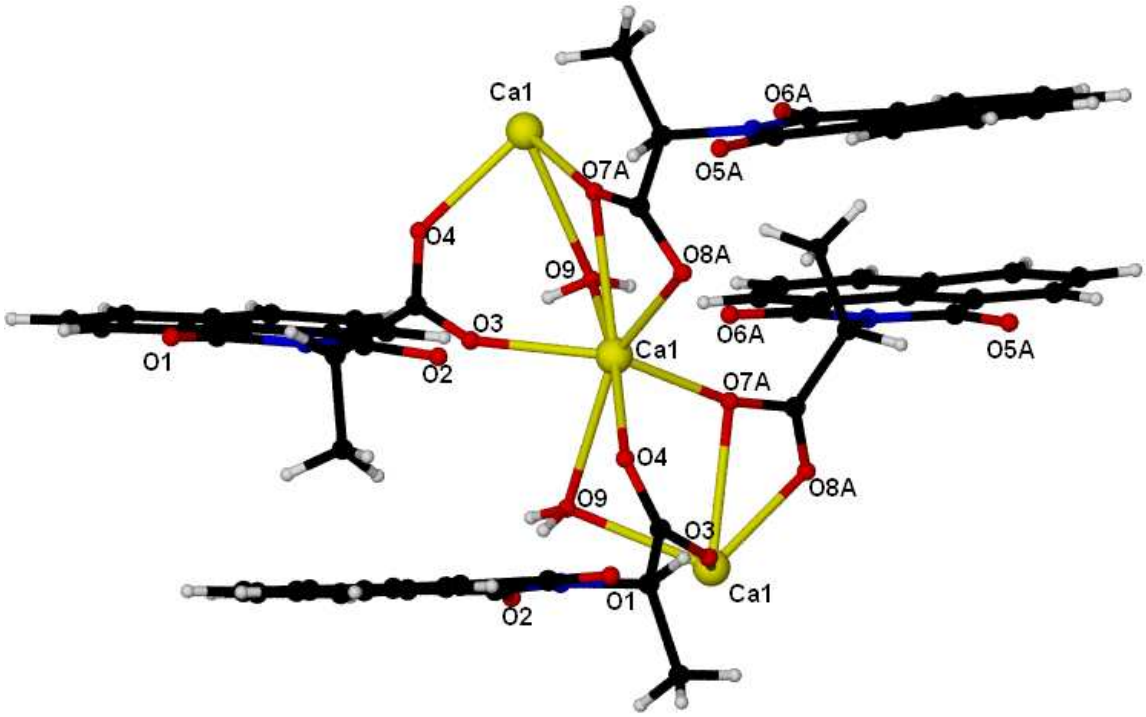

Figure 2.1 The Ca^{2+} coordination environment of $[Ca(\mathbf{L_{ala}})_2(H_2O)]\cdot(H_2O)$ (**1**)

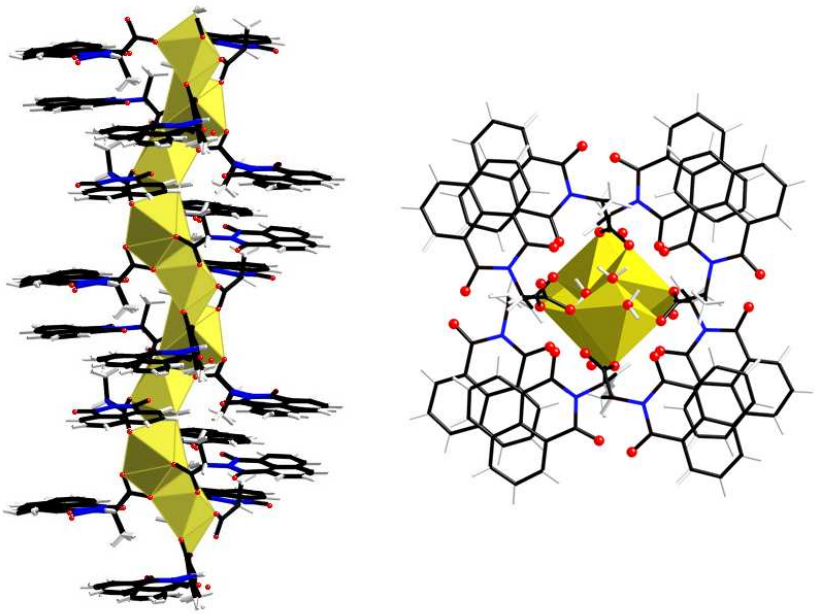

Figure 2.2 Side view of the helical rod formed for **1** by edge shared calcium polyhedra (left) and a top-down view of the helices showing the naphthalimide overlap of intra-rod π···π stacking (right).

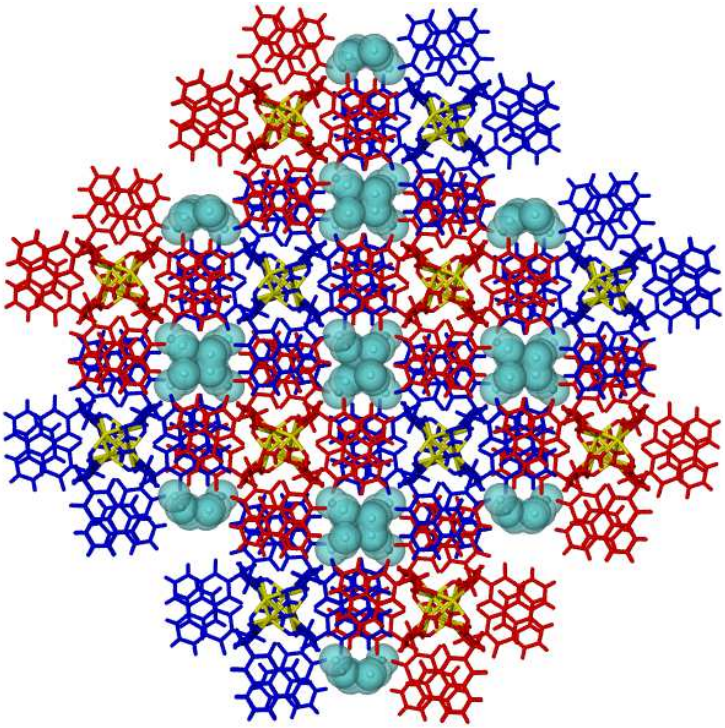

Figure 2.3 A top down view of the 3D supramolecular structure of compound **1** where calcium cations are highlighted in yellow, adjacent helices are either red or blue and the disordered interstitial water molecules are colored teal.

Compound **2**, $[Ca(\mathbf{L_{ser}})_2]\cdot(H_2O)_2$, contains calcium cations bridged by $\mathbf{L_{ser}}^-$ ligands into a homochiral rod SBU that interacts with adjacent parallel rods through supramolecular interactions of the naphthalimide rings. The eight coordinate calcium cations are bridged through μ-κ^1:κ^2 carboxylates which occupy six of the coordination sites (Figure 2.4). The remaining sites are occupied by the alcohol group, an additional donor group designed into the ligand, which chelates the calcium atoms generating 6-member rings. The homochiral zig-zag rods created by bridged calcium cations have a pitch of 8.21 Å (Figure 2.5). There are interstitial water molecules present that are hydrogen bonded to the alcohol, the naphthalimide carbonyl and one of the bridging carboxylates, all within the same SBU. The naphthalimide rings in compound **2** are oriented in a rectangular shape, Figure 2.5 (right), with two pairs of naphthalimide rings interdigitating with two pairs on adjacent rods generating a two dimensional structure of layered sheets (Figure 2.6). There are no strong supramolecular interactions between the sheets. The $\pi^{\cdots}\pi$ stacking metrics for compound **2** are listed in Table 2.2.

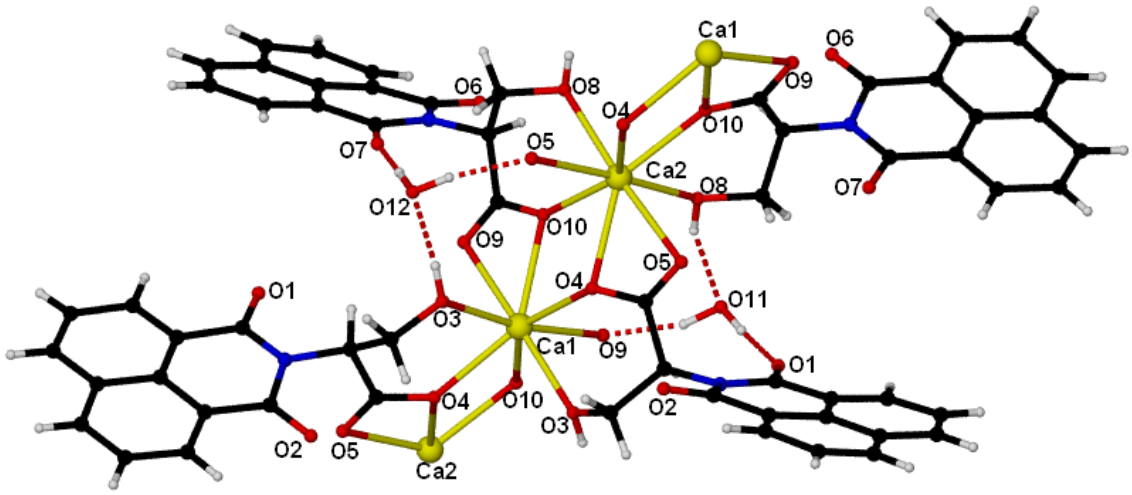

Figure 2.4 The Ca^{2+} coordination environment of $[Ca(\mathbf{L_{ser}})_2]\cdot(H_2O)_2$ (**2**)

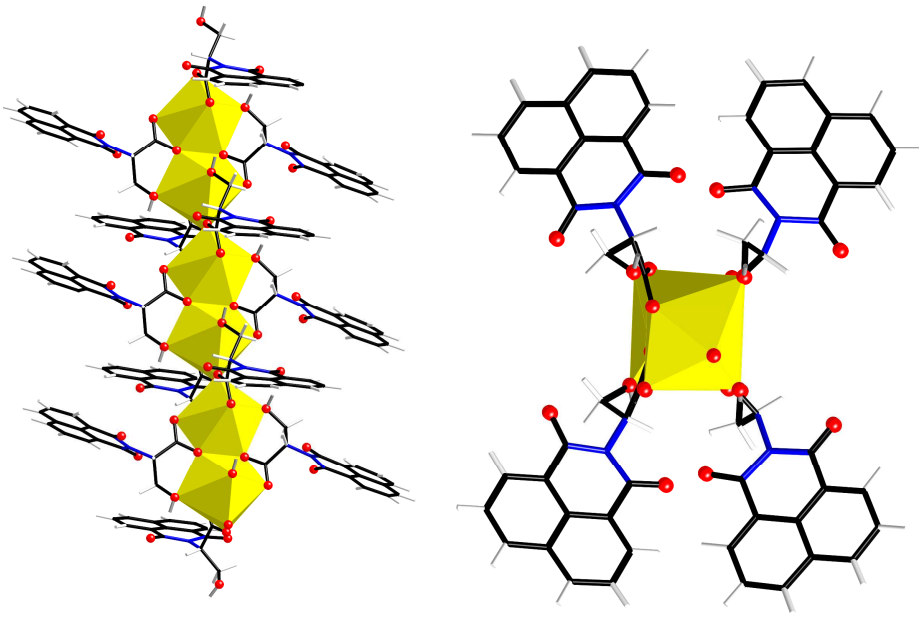

Figure 2.5 Side view of the zig-zag rod in **2** formed by edge shared calcium polyhedra (left) and a top-down view of the rod (right).

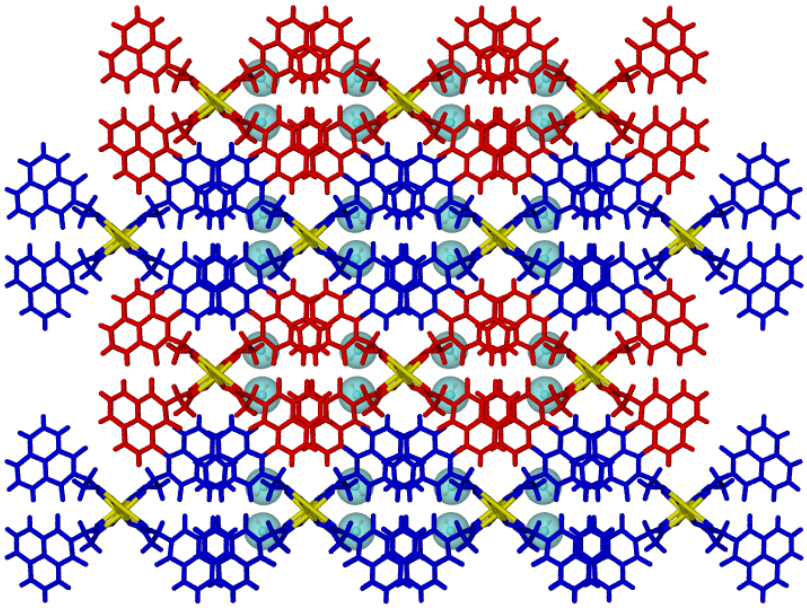

Figure 2.6 A top down view of the supramolecular structure of compound **2** with calcium cations highlighted in yellow and rods involved in π stacking are the same color. The sheets of homochiral rods composed of interdigitated naphthalimide rings extend from left to right and adjacent sheets are different colors. The hydrogen bonded water molecules are colored teal.

Compound **3**, $[Sr(\mathbf{L_{ala}})_2(H_2O)]\cdot(H_2O)_3$, contains strontium cations bridged by $\mathbf{L_{ala}}^-$ ligands into a homochiral helical rod SBU that interacts with adjacent parallel rods through supramolecular interactions of the naphthalimide rings. Each of the strontium cations is 8-coordinate. Six of the eight coordination sites are occupied by bridging μ-κ^1:κ^2 carboxylates from four different ligands. While the two nonequivalent ligands share the same coordination mode, they are distinct in that one has a coordinated naphthalimide carbonyl oxygen that forms a 7-membered chelate ring while the other does not. The ligand without the second mode of coordination is disordered over two positions; only one is shown. The last coordinate site is occupied by a water molecule that is involved in hydrogen bonds to the carboxylate O8A and to the naphthalimide carbonyl O6A from a different ligand (Figure 2.7). The P helix created by edge-shared strontium polyhedra has a pitch of 14.98 Å (Figure 2.8, left). Each of the helical rods interacts with four adjacent rods through strong π···π stacking interactions generating rectangular-shaped channels with a pore size of 1.9 x 7.7 Å that are occupied by disordered water molecules (Figure 2.9). The π···π stacking metrics for compound **3** are listed in Table 2.2.

The structure of compound **3***, formed with the ligand R-isomer, $\mathbf{L_{ala}}^{*-}$, is the same as **3,** but in the enantiomeric space group. As shown in Figure 2.8 (right), the helical rod has the opposite, *M*-helicity.

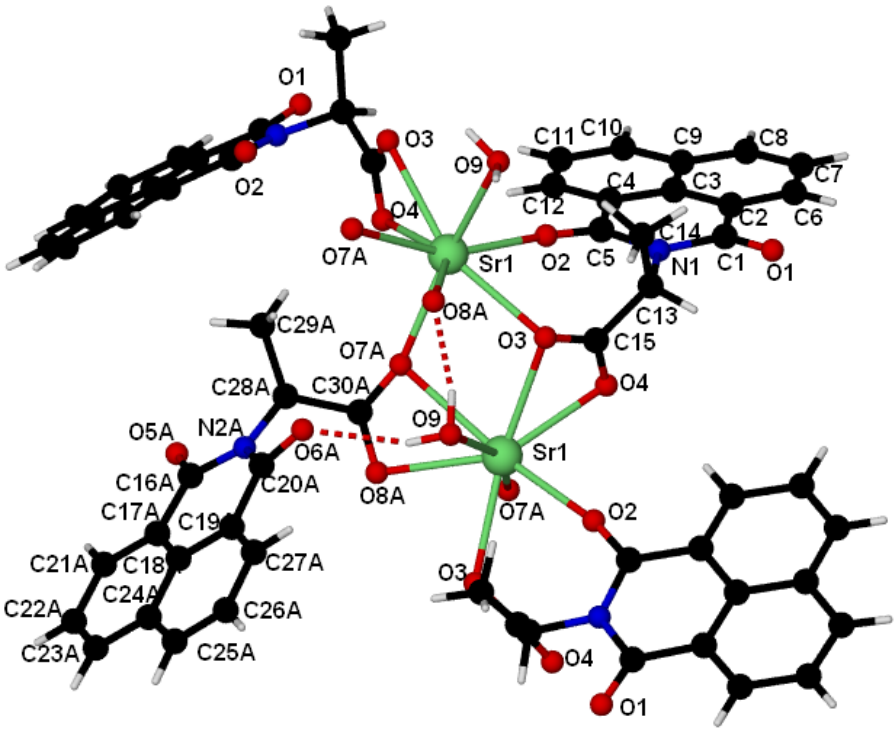

Figure 2.7 The Sr^{2+} coordination environment of $[Sr(\mathbf{L_{ala}})_2(H_2O)]\cdot(H_2O)_3$ (**3**)

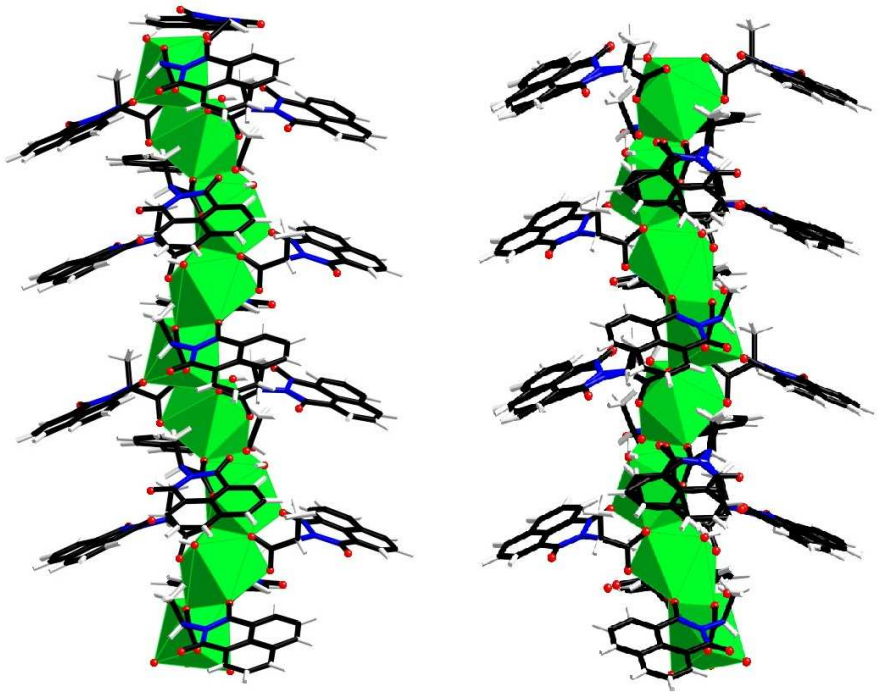

Figure 2.8 Chiral rods in **3** (left) and **3*** (right) formed by edge shared strontium polyhedra generating *P* and *M* helices, respectively.

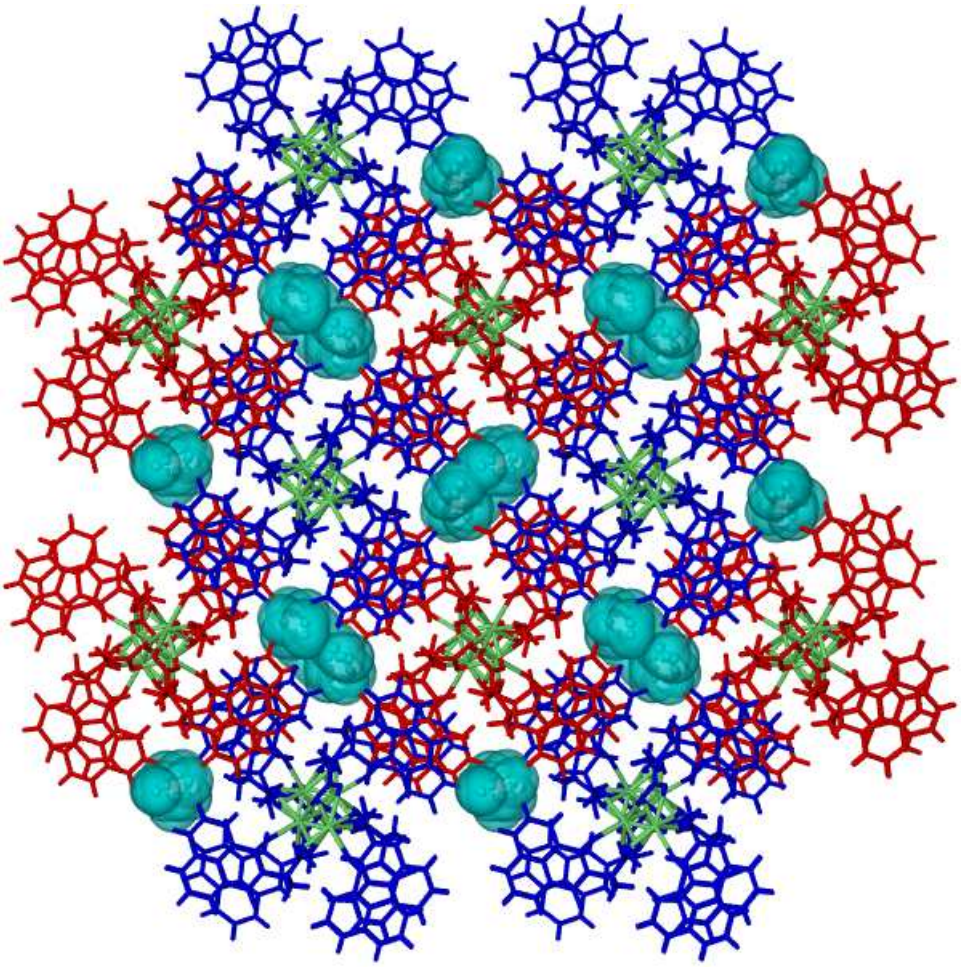

Figure 2.9 A top down view of the 3D supramolecular structure of compound **3** where strontium cations are highlighted in green, adjacent helices are either red or blue and the disordered interstitial water molecules are colored teal.

Compound **3** undergoes a single-crystal to single-crystal transformation when **3** is left under vacuum to form [Sr($\mathbf{L_{ala}}$)$_2$(H_2O)] (**4**), where all of the interstitial water is removed. The overall structure about strontium and the SBU rods for compound **4** are similar to **3** (Figure 2.10), but the unit cell volume has been reduced by about 9%, mostly along the crystallographic *a*- and *b*-axis. Figure 2.11 shows that the once open channels of **3** are now gone generating a closed form. There are surprisingly large differences in the $\pi^{\cdots}\pi$ stacking metrics as listed in Table 2.2.

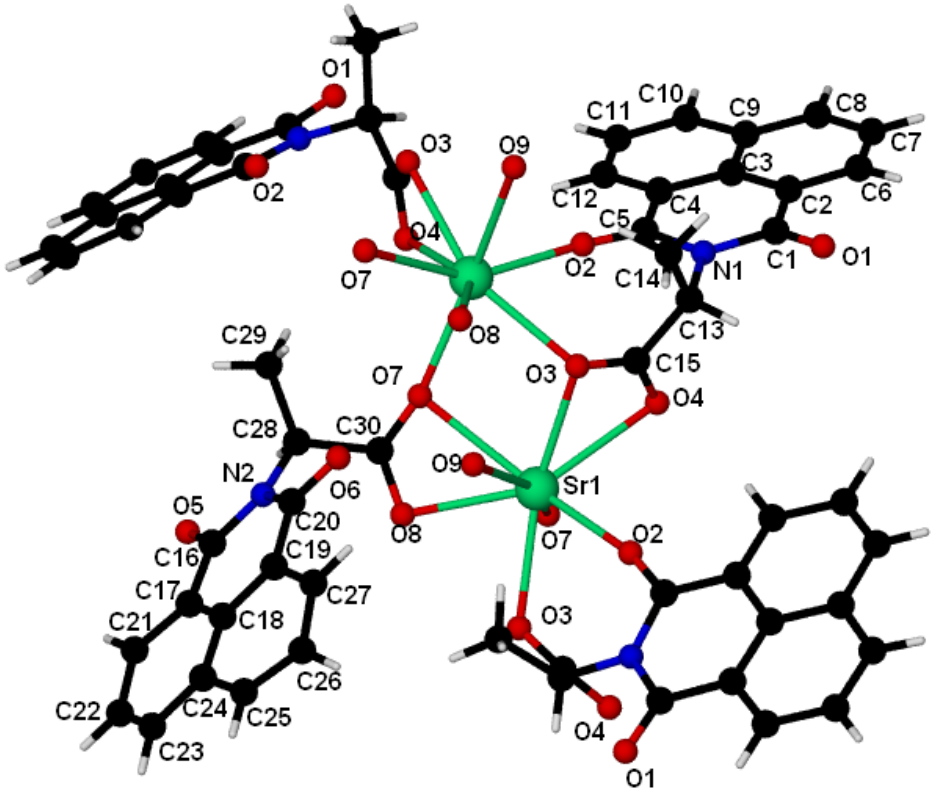

Figure 2.10 The Sr^{2+} coordination environment of $Sr(\mathbf{L_{ala}})_2(H_2O)$ (**4**)

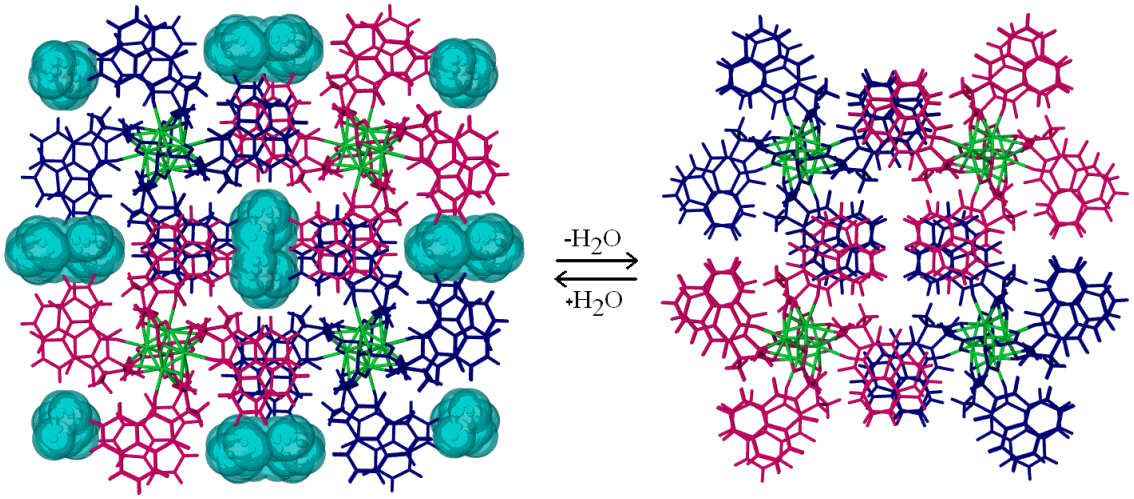

Figure 2.11 View showing how the channels of compound **3** (left) close in **4** (right) along the crystallographic *c* axis. Strontium cations are highlighted in green, adjacent helices are pink or blue and the disordered interstitial water molecules are teal.

Compound **5**, $[Sr(\mathbf{L_{ser}})_2(H_2O)]$, contains strontium cations bridged by $\mathbf{L_{ser}}^-$ ligands into a homochiral rod SBU that interacts with adjacent parallel rods through

supramolecular interactions of the naphthalimide rings. The strontium cations are 9-coordinate and bridged by μ-κ^2 carboxylates from four different ligands. This monodentate carboxylate coordination mode leaves room for the alcohol group of both ligands to coordinate forming 6-membered chelate rings. In addition, for one of the two ligands a naphthalimide carbonyl oxygen bonds forming a [3.2.2] bicycle with the strontium cation through the carboxylate, the alcohol and one of the carbonyls of the naphthalimide ring (Figure 2.12). Another difference from compound **3** is the water molecule bridges strontium cations. Because there are now three bridging oxygen atoms between each cation, this chiral rod SBU is composed of face-sharing strontium polyhedra (Figure 2.13). The M helix created by the bridged strontium cations has a pitch of 7.09 Å. Each of the rods interacts with four adjacent rods through π···π stacking of the naphthalimide rings, but no channels form in this compound due to the offset packing (Figure 2.14). The π···π stacking metrics for compound **5** are listed in Table 2.2.

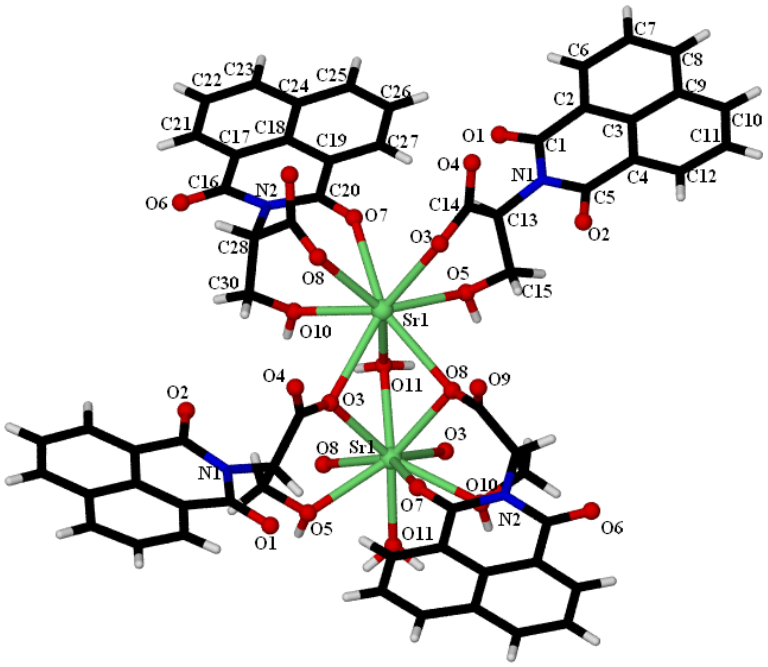

Figure 2.12 The Sr^{2+} coordination environment of [Sr(**L**$_{ser}$)$_2$(H_2O)] (**5**)

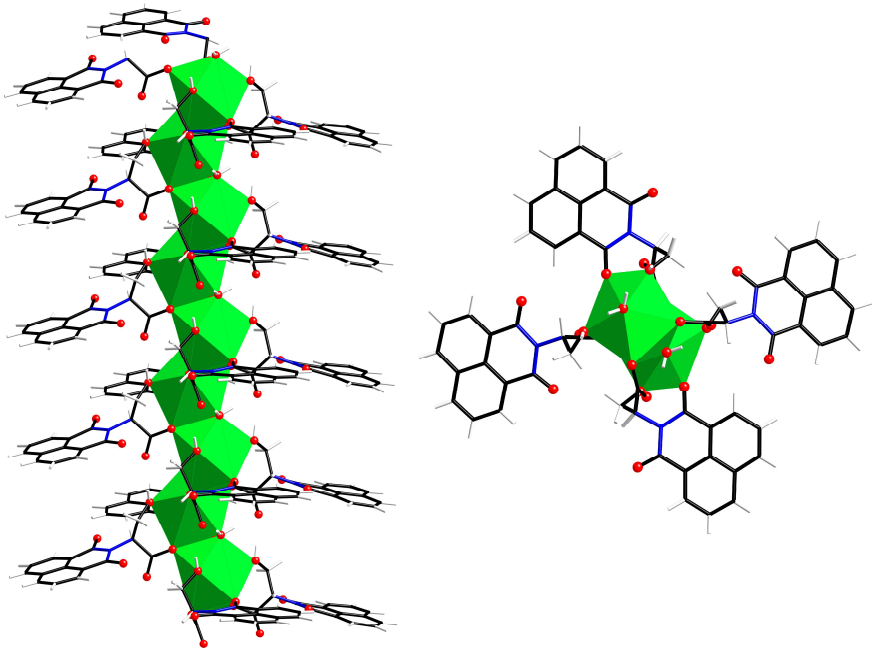

Figure 2.13 Side view for **5** of the chiral rod formed by face-shared strontium polyhedra (left) and a top-down view of the rod (right).

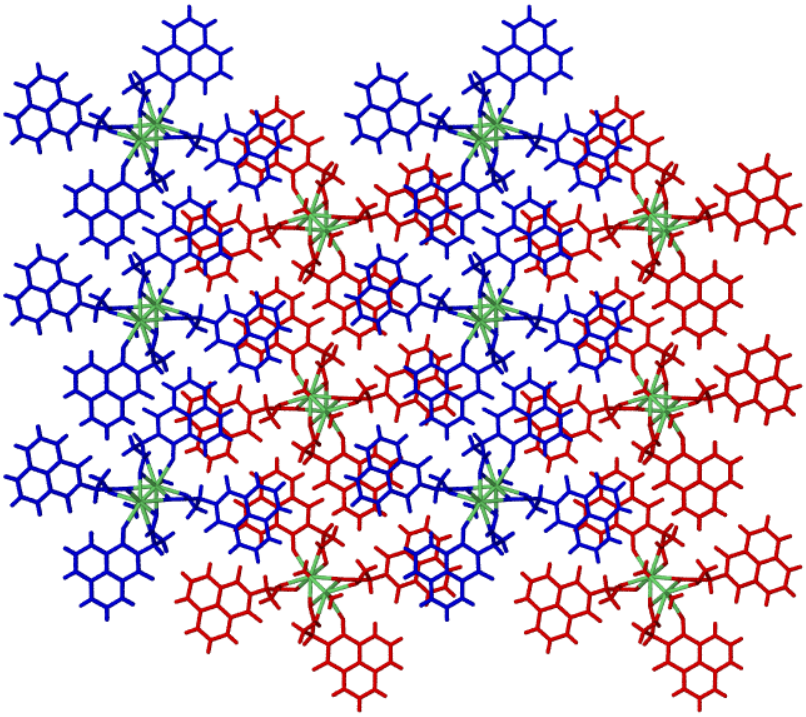

Figure 2.14 A top down view along the crystallographic *a*-axis of the 3D supramolecular structure of compound **5** where strontium cations are highlighted in green and adjacent helices are red or blue.

Table 2.2 $\pi^{\cdots}\pi$ Stacking Parameters

	Compound	Type of Stacking	Cen-Cen(Å)	dipole ∠ (°)[a]	plane ∠ (°)	avg dist (Å)	χ (Å)[b]
1	$[Ca(\mathbf{L_{ala}})_2(H_2O)]\cdot(H_2O)$	intra-rod	3.77	53	1.7	3.50	1.42
		inter-rod	3.62	129	0.5	3.48	0.99
		inter-rod	3.67	115	3.8	3.51	1.06
2	$[Ca(\mathbf{L_{ser}})_2]\cdot(H_2O)_2$	inter-rod	4.37	137	27	4.04	1.69
		inter-rod	4.17	130	26	3.93	1.39
3	$[Sr(\mathbf{L_{ala}})_2(H_2O)](H_2O)_3$	inter-rod	4.46	91	8.6	3.48	2.79
		inter-rod	3.57	127	9.7	3.48	0.73
		inter-rod	3.54	64	9.3	3.51	0.47
4	$[Sr(\mathbf{L_{ala}})_2(H_2O)]$	inter-rod	4.46	71	1.2	3.31	2.98
		inter-rod	3.51	70	6.9	3.50	0.23
		inter-rod	4.00	52	10.7	3.55	1.84
5	$[Sr(\mathbf{L_{ser}})_2(H_2O)]$	inter-rod	4.00	160	19.8	3.46	1.96
		inter-rod	4.42	176	19.8	3.48	2.68

[a]relative rotation of the rings (180° is the head to tail arrangement) [b]slippage parameter, the third side of the right triangle formed with the average perpendicular distance between the two rings and the line between the two central carbon atoms of the rings.

Infrared Spectroscopy. Infrared spectroscopy, coupled with the preparation of isotopomers, were employed to better understand the role of both the interstitial and coordinated waters during the "breathing mechanism" of the inter-conversion of $[Sr(\mathbf{L_{ala}})_2(H_2O)]\cdot(H_2O)_3$ (**3**) and $[Sr(\mathbf{L_{ala}})_2(H_2O)]$ (**4**). In order to eliminate the impact of atmospheric moisture, samples were ground in a drybox with nujol oil and the sample chamber of the FT-IR instrument had a continuous flow of nitrogen. The spectra for compound **3** and $[Sr(\mathbf{L_{ala}})_2(D_2O)]\cdot(D_2O)_3$, $\mathbf{3d_8}$ (prepared using D_2O as the solvent in the reaction), are shown at the top of Figure 2.15. For **3** (a), an O-H stretching vibration is located at 3520 cm^{-1} and for $\mathbf{3d_8}$ (d) an O-D stretching vibration is located at 2600 cm^{-1}. The broad peak and 2 small humps just below 3000 cm^{-1} and the two sharp peaks below 2400 cm^{-1} are due to the nujol oil. Spectra run on crystals of both compounds exposed to vacuum, now the dehydrated forms **4** (b) and $\mathbf{4d_2}$ (e), show similar H_2O and D_2O peaks, respectively. When **4** is rehydrated with D_2O vapor for 24 hours, *compound* $\boldsymbol{3d_8}$ *forms*; the IR spectrum (c) shows only a D_2O peak and little or none of the H_2O peak. When $\mathbf{4d_2}$

is introduced to H_2O vapor, *compound **3** forms*; the IR spectrum (f) shows only the H_2O peak and little or none of the D_2O peak. The coordinated water cannot be distinguished from the interstitial water in any of these spectra.

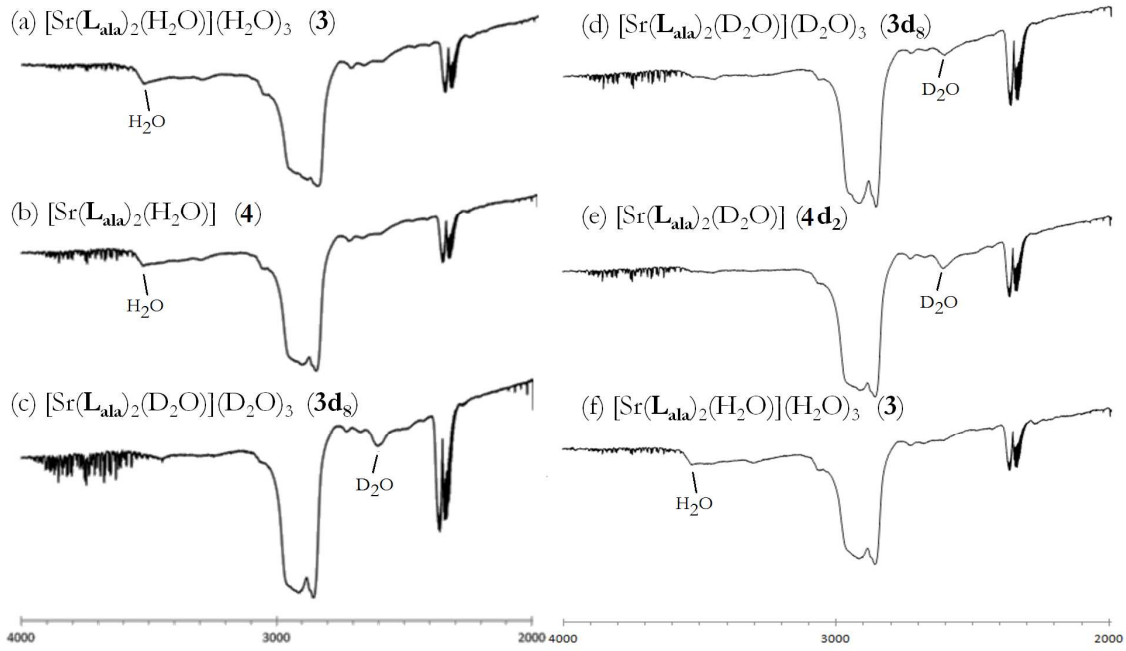

Figure 2.15 Infrared spectra of Nujol mull of compound **3** (a) which was dehydrated (b) then rehydrated with D_2O (c). The opposite was done with the perdeutero **3d$_8$** (d) which was dehydrated (e) then rehydrated with H_2O (f).

Nuclear Magnetic Resonance. Solid-state nuclear magnetic resonance experiments were performed on compounds **3** and **4** to investigate the use of these methods on the single-crystal to single-crystal transformation. The ^{1}H NMR experiments had poor resolution, but some information could still be learned. Fortunately, the ^{13}C NMR spectra have well-resolved resonances and assignments can be made when coupled with FSLG HETCOR (Figure 2.16). The resonances at 15 ppm in the ^{13}C NMR spectra are assigned to the methyl group and correlate strongly with the resonance at 1.5 ppm in the ^{1}H NMR spectra. The methine carbon has a distinguishing resonance at 60 ppm in the ^{13}C NMR spectra that correlates strongly with the resonance at 4.5 ppm in the ^{1}H NMR spectra. The

large resonances around 140 ppm are assigned to the aromatic carbons, which correlate to the 7 ppm range in the ^{1}H NMR spectra. The naphthalimide carbonyl resonances are located at 160 ppm and the carboxylate carbonyl resonances are at 175 ppm. Even though **3** and **4** share the same assignments, they can be clearly differentiated by their ^{13}C NMR spectra. ^{1}H NMR experiments on compounds **3** and **4** show nearly identical spectra, but with **3** having a much larger integration at 4.5 ppm than **4**. The resonance at 4.5 ppm has two components; one from the methine hydrogen of the ligand, as confirmed by HETCOR experiments, and the other comes from the water contribution, which has much less integration for compound **4**.

This assignment of the water resonance was confirmed by ^{2}H NMR experiments. The ^{2}H NMR experiments were carried out on crystals prepared using deuterated solvents, D_2O and D_3COD, to yield the compound **3d$_8$**. Initial ^{2}H NMR experiments were measured on as-prepared crystals that were not vacuum dried because drying also removes the interstitial waters of **3**. The fast spinning spectra showed a sharp resonance and a small broad resonance that was apparent after deconvolution (Figure 2.17a). By slowing down the spin rate the two components split more and it is more obvious (Figure 2.7b) that there is a sharp and weaker broad component (pake pattern). Because of the sharpness of the dominant resonance, indicating that this species is in the *fast motion limit* in the solid-state,[14] the sharp component was attributed to adsorbed water on the crystals and the broad component to compound **3**. In order to confirm this assignment, the adsorbed water was removed by drying, thus dehydrating compound **3d$_8$**, and rehydrating the resulting **4d$_2$** in the presence of D_2O vapor restoring compound **3d$_8$**, but now with no adsorbed water. Spectra of this sample (Figure 2.17c, d) show only the broad peak that

had been deconvoluted from the original spectrum of the as-prepared crystals; confirmed by chemical shift and similar half height widths of 140 Hz. Due to the broadness of the resonance, the interstitial water was found to be indistinguishable from the coordinated water by ^{2}H NMR spectroscopy, but the chemical shift assignment made from the ^{1}H spectra around 4.5 ppm was confirmed.

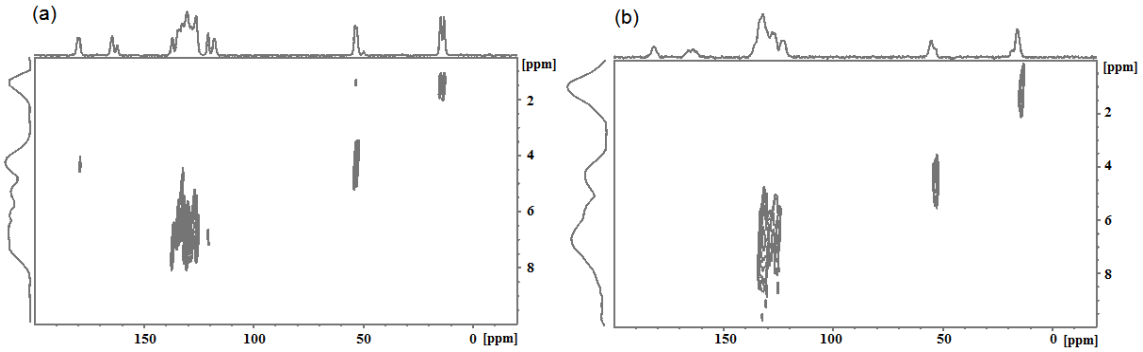

Figure 2.16 FSLG HETCOR spectra of compound **3** (a) and **4** (b).

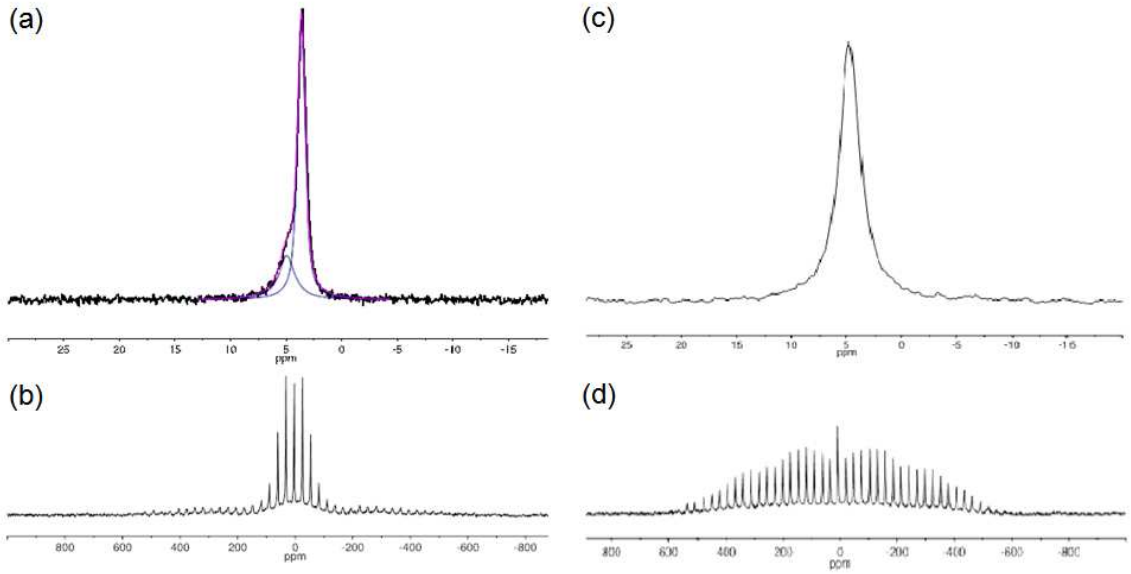

Figure 2.17 ^{2}H NMR of as prepared **3d$_8$**: fast spin (a) and slow spin (b). ^{2}H NMR of **3d$_8$** after dehydrating and rehydrating in the presence of D_2O: fast spin (c) and slow spin (d).

Thermal Analysis. Thermal gravimetric analyses of compounds **1-5** under a steady stream of dry air are shown in Figure 2.18. Upon heating, compound **1** experiences a weight loss between 51 and 181 °C corresponding to the loss of coordinated and interstitial water from the compound (7.5%, calcd. 5.6%). Compound **1** remains stable upon further heating until reaching the decomposition point of 357 °C, well beyond the decomposition point of the protonated ligand, H$\mathbf{L}_{\mathbf{ala}}$. At this temperature the solid begins to froth so the experiment was terminated. Compound **2** undergoes a similar weight loss between 64 and 139 °C corresponding to the loss of interstitial water (6.4%, calcd. 5.6%). Compound **2** remains stable until the decomposition point of 249 °C. Compound **3** shows a gradual weight loss between 35 and 197 °C corresponding to the loss of coordinated and interstitial water (9.0%, calcd. 10.3%) and remains stable until decomposition at 305 °C. Thermal analysis of compound **5** shows the loss of coordinated water between 104 and 186 °C (2.6%, calcd. 2.6%) and remains stable until decomposition at 247 °C. Rehydration experiments were performed with all compounds by switching to ambient air; in the cases of compounds **2** and **5**, when crystals were heated well above the dehydration point followed by cooling in air, water is reincorporated over a period of ca 18 hr into the compounds regaining the lost weight (Figure 2.19). These solids have lost single crystallinity in this process, but were shown to retain crystallinity at the end of the rehydration by PXRD (see Supporting Information). In similar experiments, compound **3** does not rehydrate for a week. In this case, PXRD experiments on this heated and dehydrated solid of **3** show loss of crystallinity.

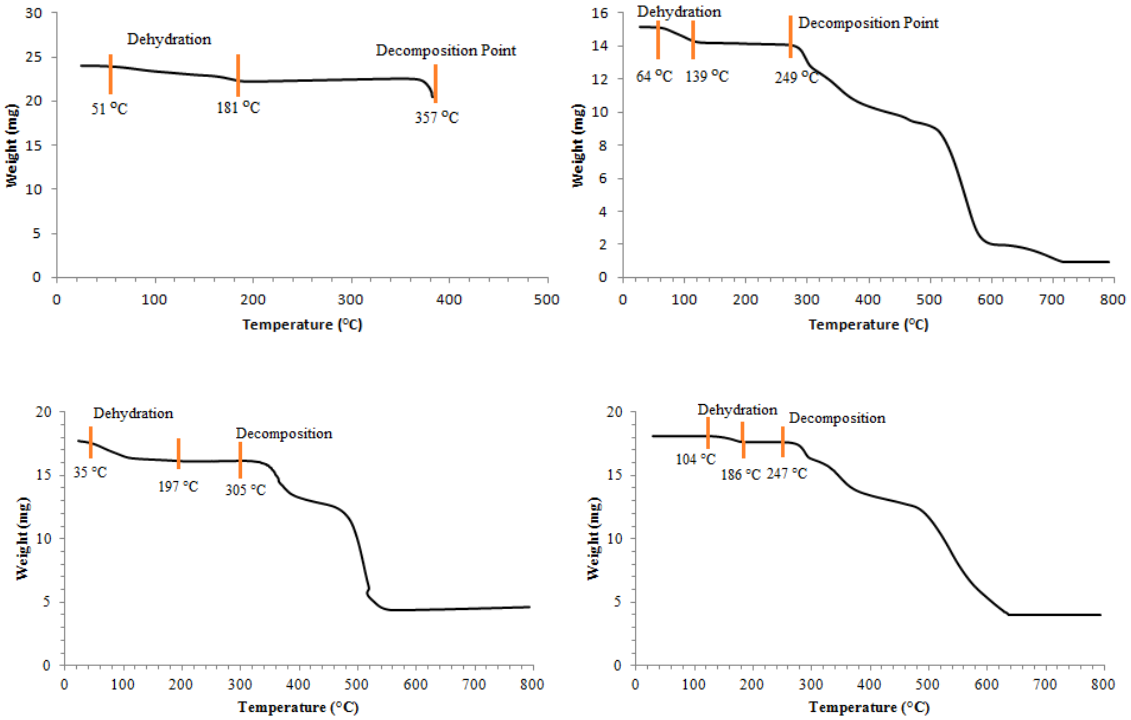

Figure 2.18 TGA for compounds **1**, [Ca($\mathbf{L_{ala}}$)$_2$(H_2O)]·(H_2O) (top left), **2**, [Ca($\mathbf{L_{ser}}$)$_2$]·(H_2O)$_2$ (top right), **3**, [Sr($\mathbf{L_{ala}}$)$_2$(H_2O)]·(H_2O)$_3$ (bottom left) and **5,** [Sr($\mathbf{L_{ser}}$)$_2$(H_2O)] (bottom right).

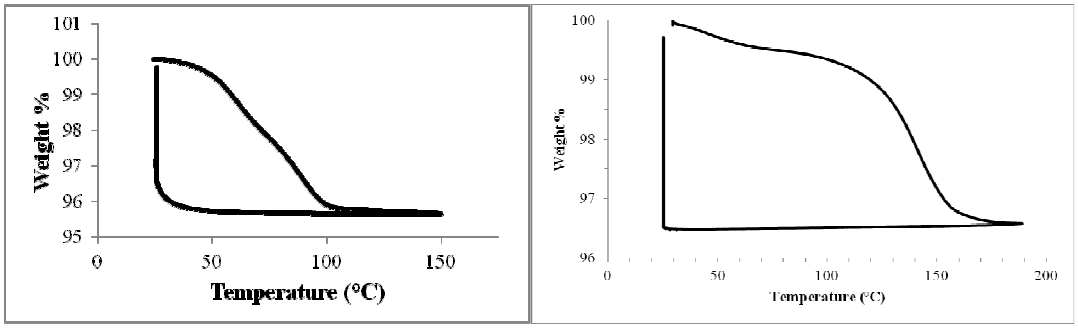

Figure 2.19 Removal and reuptake of water from compound **2** (left) and compound **5** (right).

As outlined in the NMR section, ^{2}H NMR experiments indicated that the as-prepared crystals of **3** contained some adsorbed water. To test for the presence of this adsorbed water, TGA analyses were carried out on the as-prepared compound **3d$_8$** that had undergone the brief air drying protocol used in the initial NMR experiment and

another batch of crystals that had been dried and rehydrated with D_2O (**3d$_8$**→**4d$_2$**→**3d$_8$**). As shown in Figure 2.20, the weight loss of the two samples was different with the weight difference between the two of 0.56% (about 0.3 water molecules per strontium cation).

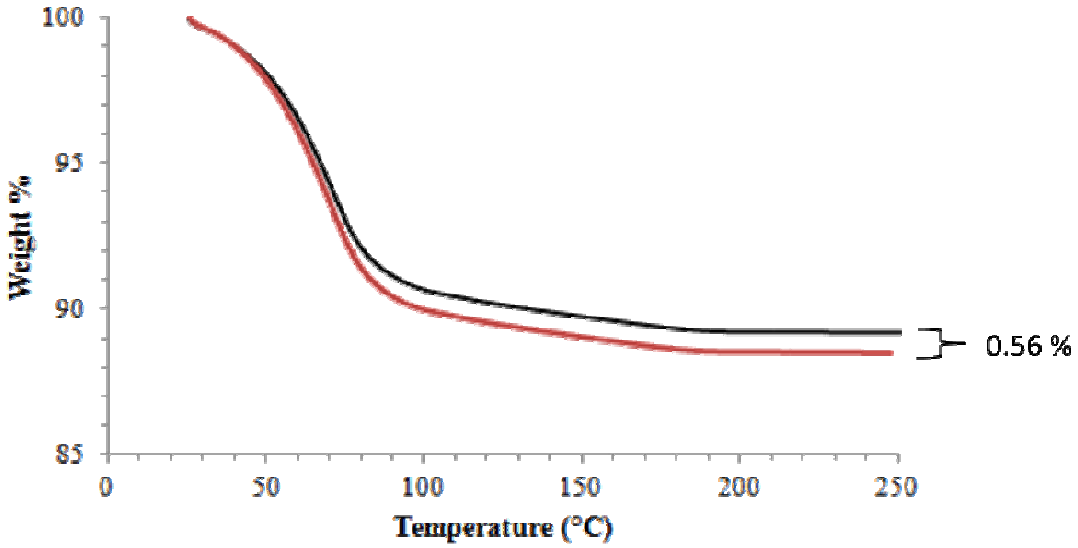

Figure 2.20 TGA of as prepared compound **3d$_8$** (red) and **3d$_8$** after being dehydrated and rehydrated in the presence of D_2O vapor (black).

Fluorescence Analysis. Compounds **1**-**3** and **5** exhibit substantial solid-state fluorescence originating from the naphthalimide chromophore in the ligand and their spectra are shown in Figure 21. In the case of the **L$_{ala}^-$** adducts of the group 2 metals (**1** and **3**), the fluorescence maximum is red-shifted with respect to the ligand and in the case of **L$_{ser}^-$** adducts of the group 2 metals (**2** and **5**), the fluorescence maximum is blue-shifted with respect to the ligand.

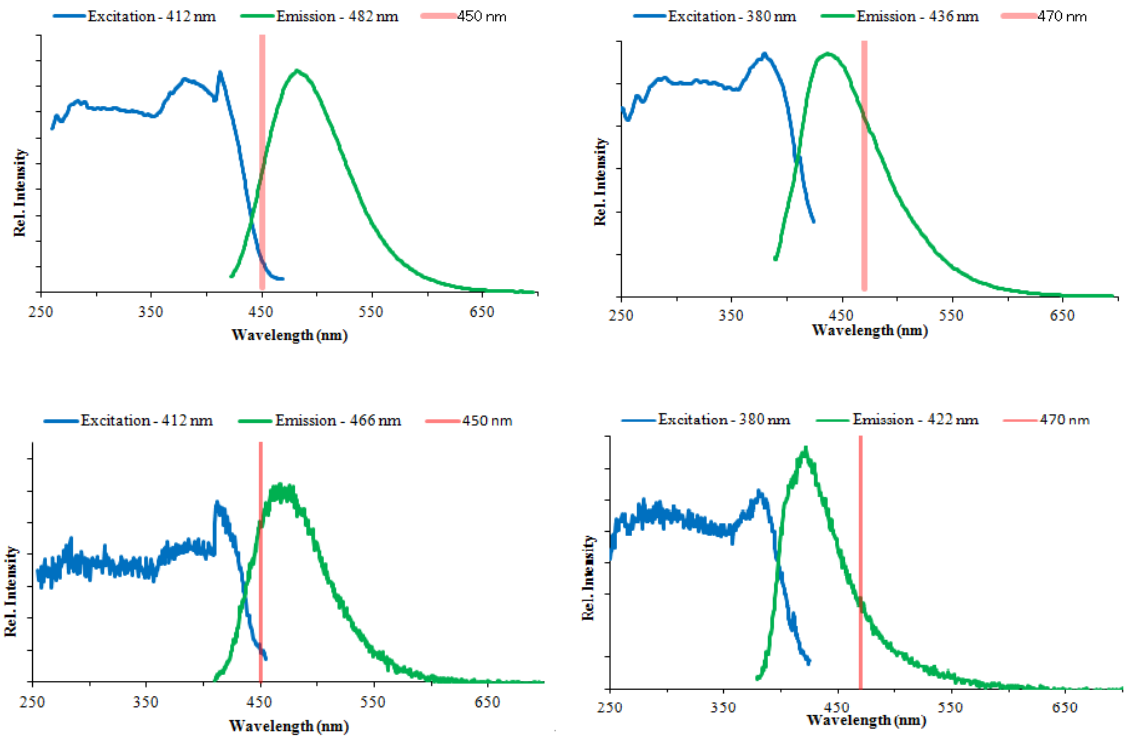

Figure 2.21 Solid-state fluorescence spectra for compound **1** (top left), **2** (top right), **3** (bottom left) and **5** (bottom right). The blue lines illustrate the excitation spectrum, the green lines represent the emission spectrum, and the red lines signify the fluorescence maximum of the protonated form of the ligand from each complex H$\mathbf{L_{ala}}$ (**1, 3**) and H$\mathbf{L_{ser}}$ (**2, 5**), respectively.

Discussion

We have prepared a series of compounds from two alkaline earth metals (Ca^{2+} and Sr^{2+}) and $\mathbf{L_{ala}}^-$ ($\mathbf{L_{ala}}^{*-}$) and $\mathbf{L_{ser}}^-$ (Scheme 1) ligands, designed for the preparation of enantiopure, chiral supramolecular MOFs (SMOFs). Similarly to complexes of these ligands with group 1 metals, a consistent structural motif is formed where homochiral rod-shaped SBUs dominate the topology and π···π stacking between 1,8-naphthalimide rings link adjacent rod SBUs with supramolecular interactions. While the rod structural motif is the same in all compounds, there are important differences, including how the cations are bridged by carboxylate groups and solvent, the orientation and overlap of the naphthalimide rings and whether or not the compounds are porous. The coordination

number of the cations that make up the rod-shaped SBU range from seven-coordinate (**1**) to nine-coordinate (**5**) where the other compounds (**2**, **3**, **3***) are eight-coordinate. All of the SBUs rods are homochiral and consist of either edge-shared polyhedra (**1**-**4**) or the unusual face-shared polyhedra (**5**). Very few MOFs containing homochiral rod SBUs have been reported previously.[15] As expected, the structures of **3** and **3***, formed from enantiomeric forms of the same ligand, are the same but the rods have opposite helicity.

The most prominent structural feature of this work, especially when coupled with our previous paper on group 1 metals with the same ligands, is the consistent formation of rod SBUs, rods that are necessarily homochiral because of building the ligands from enantiopure amino acids. The s-block metals generally lack the formation of consistent SBUs as one varies the metals,[12] although it has been pointed out recently that the larger metals of group 1 are likely to form rod structures with anionic oxygen donor ligands.[16] With our ligands containing the large, $\pi\cdot\cdot\pi$ stacking naphthalimide group, we consistently observe rods with both group 1 and 2 metals even though the rods are built from a variety of bridging oxygen donor motifs, including cases where the only bridge comes from the solvent. Nevertheless, the rods consistently form. In contrast, transition metal complexes of these ligands do not form rod SBUs.[6,9,10]

In four of the five compounds (**1**, **3**, **4** & **5**), each of the rod-shaped SBUs is interlocked with four adjacent rods through $\pi\cdots\pi$ stacking in a motif similar to the uninodal 4*c* net if they were covalent connections. In **2**, the naphthalimide rings for one rod are oriented in a position where two pairs of naphthalimide rings interdigitate with two pairs on two adjacent rods resulting in 2D sheets instead of a 3D network. In the case of compounds **1** and **3,** which are complexes with the $\mathbf{L_{ala}^-}$ ligand, there are open 1D

channels along the crystallographic *c* axis that are occupied by disordered solvent. In the $\mathbf{L_{ser}^-}$ ligand compounds **2** and **5**, the introduced alcohol functional group bonds the metal decreasing ligand flexibility and impacting the structures. In the calcium complex **2**, the alcohol in the ligand occupies the coordination sites occupied by the coordinated solvent in its analogous alanine analog **1**, whereas in the strontium complexes the presence of an additional oxygen donor serves to increase the coordination number of the cation when compared to the alanine analog **3**. In both complexes with the $\mathbf{L_{ser}^-}$ ligand there are no channels present. Finally, of the eight group 1 complexes reported previously and the group 2 complexes reported here, only compound **1** exhibits intrarod $\pi\cdots\pi$ stacking. While compound **1** is unstable in air, compounds **2-5** are robust. When compounds **2** and **5** were heated in a dry environment they lost water as well as single crystallinity, but upon cooling and exposure to atmosphere the lost water was reincorporated into the structures, as confirmed by TGA and PXRD. The role of the water is different in both compounds, interstitial in **2** and coordinated in **5**. The removal of coordinated and interstitial water could not be differentiated in the TGA of **1**.

In a similar way, compound **3** loses bonded and interstitial waters between 64-139 °C (again not differentiated in the TGA), but in this case the dehydrated solid does not readily rehydrate. In contrast, when exposed to a vacuum, compound **3** loses only interstitial waters while holding coordinated waters, and retains single crystallinity to form **4**. In this reversible transformation, the pores in compound **3**, which are oriented along the crystallographic *c*-axis, are closed by a contraction along the other two crystallographic axes leaving the unit cell volume of **4** reduced by 9%.The flexibility needed for this process to take place without loss of single crystallinity is imparted into

these solids by the inherent flexibility of the π···π stacking interactions of the naphthalimide rings. As we have discussed before[9a,17] and again emphasized by the data in Table 2.2, the rings can rotate and/or slip in the solid-state with respect to each other (as measured by the dipole angle and slippage parameter χ, respectively) *without any large change in the energy associated with the supramolecular forces*. For example, as shown in Figure 2.22 for two of the interactions, in the transformation of **3** to **4** the rings rotate (91, 127, 64° in **3** versus 71, 70, 52° in **4**) and slip (2.79, 0.73, 0.47 Å in **3** versus 2.98, 0.23, 1.84 Å in **4**) to accommodate the reversible loss or gain of water. By combining the strong covalent forces of the rod-shaped SBUs with the flexible π···π stacking of the naphthalimide supramolecular synthon, the structures of the resulting solids can readily adapt to opening or closing of the pores while maintaining single crystallinity. This type of "dynamic breathing" for our SMOFs is thus *an expected consequence of the design of the system*. We note that others have reported the use of hydrogen bonding interactions to prepare complex structures with mixed covalent/ supramolecular interactions with interesting properties.[18]

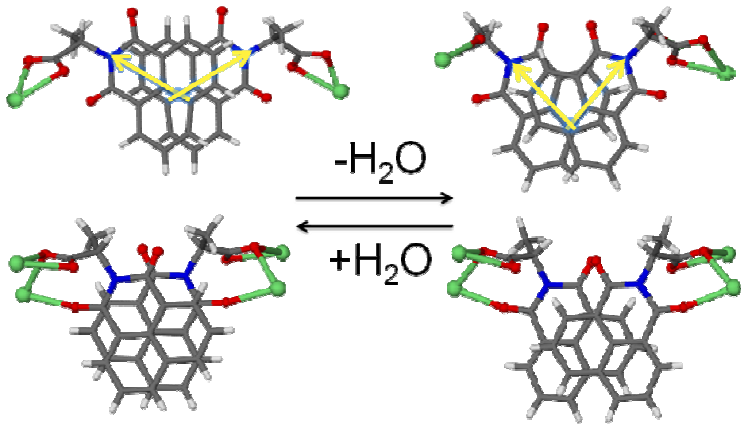

Figure 2.22 View of two of the π···π stacking interactions of the naphthalimide rings found in compound **3** (left) and **4** (right). Top: the dipole vectors between the rings decrease from 127° to 70° accompanied by a slippage parameter decrease of 0.73° to 0.23°. Bottom: the slippage parameters between the rings increase from 0.47° to 1.84°.

We used the preparation of isotopomers (exchanging D_2O for H_2O) and X-ray crystallography, solid-state IR and ^1H, ^2H and ^{13}C NMR to more closely investigate the breathing mechanism of compound **3**. Single crystal X-ray diffraction shows that after exposing dehydrated **4** to D_2O for 24 hours the channels reopen and fill with disordered solvent, analogous to the experiments described above with rehydration with H_2O. The IR spectrum of this compound shows a peak at 2600 cm^{-1} correlating to the D-O stretching and *no peak at 3500 cm^{-1}* correlating to H_2O, indicating the formation of **$3d_8$**. This isotopomer can also be made directly by using D_2O in the original preparation. This cycling of **3→4 →$3d_8$** and also **$3d_8$→$4d_2$→3** showed conclusively there is an exchange between the coordinated water and the interstitial waters of **3** during the breathing, even though the compound that forms upon dehydration, **4**, retains the coordinated water. The ^1H NMR spectrum of both of **3** and of **4** are similar, with the only difference the integration of the resonance around 4.5 ppm, which is attributed to the water. This resonance assignment was confirmed by the ^2H NMR spectra of **$3d_8$**. In contrast, the ^{13}C NMR spectra of the two compounds are very different and clearly identify the compounds. We note an interesting and potentially confusing observation while obtaining the ^2H NMR spectra of **$3d_8$**. The initial spectrum of the as prepared sample of **$3d_8$**, synthesized from deuterated solvents but not vacuum dried to prevent the formation of **4**, was unexpected as it showed a sharp component nearly drowning out the broader signal from the compound. The sharp component was determined to arise from adsorbed water on the crystals from the solvothermal synthesis. After vacuum/hydration cycling the crystals, **$3d_8$→$4d_2$→$3d_8$**, the adsorbed water was absent and the ^2H NMR spectra had only one resonance, showing that the sharp resonance was indeed the adsorbed water.

These experiments also show that the coordinated water could not be distinguished from the interstitial waters by either IR or ^{2}H NMR.

Like most compounds with a 1,8-naphthalimide moiety, compounds **1**-**5** all exhibit significant solid-state luminescence. The fluorescence maxima for compounds **1** and **3** are red-shifted by 32 and 16 nm, respectively, when compared to the protonated ligand, as expected for a typical ligand to metal charge transfer. Interestingly the fluorescence maxima for compounds **2** and **5** are blue-shifted by 34 and 48 nm respectively. All alkali metal complexes with these same two ligands exhibit the same trend of red-shifted fluorescence maxima for $\mathbf{L_{ala}}^-$ and blue-shifted for $\mathbf{L_{ser}}^-$ complexes. Compound **5**, the only compound containing face-shared polyhedra, exhibits the most blue-shifted maximum of all our compounds to date.[7]

References.

(1) (a) Qiu, S.; Zhu, G. *Coord. Chem. Rev.* **2009**, *253*, 2891. (b) Fan, J.; Zhu, H.-F.; Okamura, T.-a.; Sun, W.-Y.; Tang, W.-X.; Ueyama, N. *Inorg. Chem,* **2003**, *42*, 158. (c) de Lill, D. T.; Bozzuto, D. J.; Cahill, C. L. *Dalton Trans.* **2005**, *12*, 2111.

(2) (a) Tranchemontagne, D. J.; Mendoza-Cortés, J. L.; O'Keefe, M.; Yachi, O. M. *Chem. Soc. Rev.* **2009**, *38*, 1257. (b) Rosi, N. L.; Kim, J.; Eddaoudi, M.; Chem. B.; O'Keeffe, M.; Yaghi, O. M. *J. Am. Chem. Soc.* **2005**, *127*, 1504. (c) O'Keeffe, M.; Yaghi, O. M. *Chem. Rev.* **2012**, *112*, 675.

(3) (a) *Design of Organic Solids*; Weber, E., Ed. *Topics in Current Chemistry*; Springer: Berlin, **1998**; Vol. 198. (b) Pidcock, E.; Motherwell, W. D. S. *Cryst. Growth Des.* **2005**, *5*, 2232. (c) Du, M.; Zhang, Z. H.; Zhao, X. J. *Cryst. Growth Des.* **2005**, *5*, 1199. (d) Takahashi, S.; Katagiri, T.; Uneyama, K. *Chem. Commun.* **2005**, 3658. (e) Weatherhead-Kloster, R. A.; Selby, H. D.; Miller, W. B.; Mash, E. A. *J. Org. Chem.* **2005**, *70*, 8693. (f) Zhang, J. P.; Lin, Y.-Y.; Huang, X. C.; Chen, X.-M. *Chem. Commun.* **2005**, 1258. (g) Vangala, V. R.; Bhogala, B. R.; Dey, A.; Desiraju, G. R.; Broder, C. K.; Smith, P. S.; Mondal, R.; Howard, J. A. K.; Wilson, C. C. *J. Am. Chem. Soc.* **2003**, *125*, 14495.

(4) (a) Murdock, C. R.; McNutt, N. W.; Keffer, D. J.; Jenkins, D. M. *J. Am. Chem. Soc.* **2014**, *136*, 671. (b) Li, G.; Zhu, C.; Xi, X.; Cui, Y. *Chem. Commun.* **2009**, *16*, 2118. (c) Wu, H.n; Reali, R. S.; Smith, D. A.; Trachtenberg, M. C.; Li, J. *Chem. Eur. J.* **2010**, *16*, 13951.

(5) (a) Sutrisno, A.; Huang, Y. *Solid State Nucl. Magn. Reson.* **2013**, *49*, 2013. (b) Hoffman, H. C.; Debowski, M.; Müller, P.; Paasch, S.; Senkovska, I.; Kaskel, S.; Brunner, E. *Materials*, **2012**, *5*, 2537.

(6) (a) Reger, D. L.; Horger, J. J.; Smith. M. D.; Long, G. J.; Grandjean. F. *Inorg. Chem.* **2011**, *50*, 686. (b) Reger, D. L.; Horger, J. J.; Smith, M. D. *Chem. Commun.* **2011**, *47*, 2805. (c) Reger, D. L.; Horger, J. J.; Debreczeni, A.; Smith, M. D. *Inorg. Chem.* **2011**, *50*, 10225.

(7) (a) Reger, D. L.; Leitner, A. P.; Smith, M. D. *Inorg. Chem.* **2012**, *51*, 10071. (b) Reger, D. L.; Leitner, A.; Smith, M. D.; Tran, T. T.; Halasyamani, P. S. *Inorg. Chem.* **2014**, *52*, 10041.

(8) (a) Rombach, M.; Gelinsky, M.; Vahrenkamp, H. *Inorg. Chim. Acta.* **2002**, *334*, 25. (b) Fox, S.; Buesching, I.; Barklage, W.; Strasdeit, H. *Inorg. Chem.* **2007**, *46*, 818.

(9) (a) Reger, D. L.; Debreczeni, A.; Smith, M. D. *Inorg. Chem.* **2011**, *50*, 11754-11764. (b) Reger, D. L.; Debreczeni, A.; Smith, M. D..; Jezierska, J.; Ozarowski, A. *Inorg. Chem.* **2012**, *51*, 1068-1083. (c) Reger, D. L.; Debreczeni, A.; Reinecke, B.; Rassolov, V.; Smith, M. D.; Semeniuc, R. F. *Inorg. Chem.* **2009**, *48*, 8911-8924.

(10) Reger, D. L.; Debreczeni, A.; Horger, J. J.; Smith, M. D. *Cryst. Growth Des.* **2011**, *11*, 4068-4079.

(11) Banerjee, S.; Veale, E. B.; Phelan, C. M.; Murphy, S. A.; Tocci, G. M.; Gillespie, L. J.; Frimannsson, D. O.; Kelly, J. M.; Gunnlaugsson, T. *Chem. Soc. Rev.* **2013**, *42*, 1601.

(12) (a) Fromm, K. M. *Coord. Chem. Rev.* **2008**, *252*, 856. (b) Banerjee, D.; Parise, J. B. *Cryst. Growth. Des.* **2011**, *11*, 4704.

(13) Appelhans, L. N.; Kosa, M.; Radha, A. V.; Simoncic, P.; Navrotsky, A.; Parrinello, M.; Cheetham, A. K. *J. Am. Chem. Soc.* **2009**, *131*, 15375.

(14) Duer, M. J. *Introduction to Soild-State NMR Spectroscopy*, Blackwell Publishing Inc., Oxford, UK, **2004**.

(15) (a) Mallick, A.; Saha, S.; Pachfule, P.; Roy, S.; Banerjee, R. *J. Mater. Chem.* **2010**, *20*, 9073. (b) Appelhans, L. N.; Kosa, M.; Radha, A. V.; Simoncic, P.; Navrotsky, A.; Parrinello, M.; Cheetham, A. K. *J. Am. Chem. Soc.* **2009**, *131*, 15375. (c) Yeung, H. H.-M.; Kosa, M.; Parrinello, M.; Forster, P. M.; Cheetham, A. K. *Cryst. Growth Des.* **2011**, *11*, 221. (d) Rood, J. A.; Noll, B. C.; Henderson, K. W. *J. Solid State Chem.* **2010**, *183*, 270. (e) Gao, Q.; Wang, X.; Conato, M. T.; Makerenko, T.; Jacobson, A. *J. Cryst. Growth Des.* **2011**, *11*, 4632.

(16) Bertke, J. A.; Oliver, A. G.; Henderson, K. W. *Inorg. Chem.* **2012**, *51*, 1020.

(17) Reger, D. L.; Debreczeni, A.; Reinecke, B.; Rassolov, V.; Smith, M. D.; Semeniuc, R. F. *Inorg. Chem.* **2009**, *48*, 8911.

(18) (a)Thomas-Gipson, J.; Beobide, G.; Castillo, O.; Cepeda, J.; Luque, A.; Pérez-Yáñez, S.; Aguayo, A. T.; Román, P. *Cryst. Eng. Comm.* **2011**, *13*, 3301. (b) Nugent, P. S.; Rhodus, V. L.; Pham, T.; Forrest, K.; Wojitas, L.; Space, B.; Zaworotko, M. J. *J. Am. Chem. Soc.* **2013**, *135*, 10950.

Chapter III

Cesium complexes of naphthalimide substituted carboxylate ligands: Unusual geometries and extensive cation···π interactions [3]

[3]Adapted with permission from Reger, D. L.;Leitner, A.; Smith, M. D. *J. Mol. Struct.* **2015**, *1091*, 31-36. Copyright 2015 Elsevier.

Introduction

Coordination networks based on cesium cations are poorly understood and under-researched.[1-2] Such compounds generally have high coordination numbers for the large cesium cations, mainly with oxygen donors derived from solvents present during the synthesis.[3-5] When large aromatic groups are present in the ligands, some or all of the solvent donors can be excluded from the structures.[6-13] In these cases, the more normal cesium-oxygen bonds are replaced with interactions between the highly polarizable cesium cation and aromatic systems of the organic groups.

We have previously reported a series of ligands derived from amino acids containing the 1,8-naphthalimide group and studied their chemistry with transition.[14-16] and group 1 and 2 metals.[17, 18] An important goal of this work is to investigate the impact of the 1,8-naphthalimide supramolecular tecton, a group we have shown to enter into strong $\pi^{\cdots}\pi$ stacking interactions, on the formation of extended structures. Four of these ligands, differing in regards to the side-chain of the link between the carboxylate anion and a 1,8-naphthalimide functional groups, are pictured in Scheme 3.1. Of particular interest here was our reported structure of Cs$\mathbf{L_{ala}}$,[17] where the cesium cation is in an O_6 environment, and no solvent was present in the crystal despite a synthetic procedure that used both water and methanol. In the structure, the coordination environment of the highly distorted cesium cations appeared to be stabilized by interactions with the methyl groups and naphthalimide groups in the ligands. In contrast, the complex Cs$\mathbf{L_{ser}}$ has a

regular structure where the "designed ligand modification" of building into the ligand an additional alcohol donor group satisfies the cesium coordination sphere.[17]

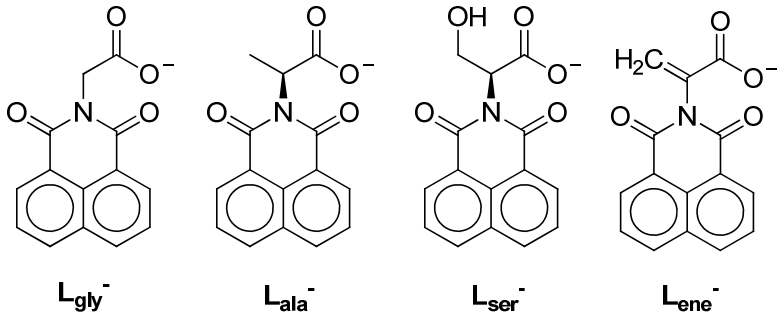

Scheme 3.1 Multifunctional Ligands

These results prompted additional efforts to prepare complexes of this family of ligands with cesium cations. Reported here are the syntheses, fluorescence and X-ray crystal structures of the cesium complexes Cs(**L**$_{gly}$) and Cs(**L**$_{ene}$), the latter forming from the dehydration of the ligand **L**$_{ser}^-$ during the synthesis. Both complexes show extensive interactions between the cesium cations and hydrocarbon groups in the ligands, as well as extensive supramolecular interactions between the strongly π···π stacking naphthalimide supramolecular tectons.

Experimental

All reactants and solvents were used as purchased from Aldrich and Strem. Elemental analyses were performed by Robertson Microlit Laboratories (Ledgewood, NJ). The fluorescence spectra were recorded on a Perkin-Elmer LS 55 fluorescence spectrometer. Single-crystal samples were ground into a 6 mm cell and a 1% attenuator was used for all measurements. The syntheses of H**L**$_{gly}$ and H**L**$_{ser}$ were reported previously.[19, 20]

*Synthesis of Cs(**L**$_{gly}$) (**1**)*

Cesium hydroxide hydrate (0.500 g, ca. 2.5 mmol) was dissolved in water (20 mL). H**L**$_{gly}$ (0.681 g, 2.67 mmol) was added and the reaction mixture stirred until homogeneous. The

solvent was removed and the remaining powder dried in vacuo to produce a yellow powder (0.984 g). A 9 mL thick walled glass tube with a Teflon stopcock was charged with the solid (0.10 g) and ethanol (2.0 mL) and heated at 120 °C overnight or until the solution became homogenous. The heat was removed and the system was allowed to slowly cool at a rate of about 1°C/min. Over the course of 3 hours needle crystals grew from the solution and were collected from the tubes and dried over filter paper to provide 0.080 g of light brown single crystals. Anal. Calcd. (Found) for $C_{14}H_8CsNO_4$: C 43.44 (43.58); H 2.08 (2.09); N 3.62 (3.47).

*Synthesis of Cs(**L**$_{ene}$) (**2**)*

H**L**$_{ser}$ (0.761 g, 3.5 mmol) was added to a solution of cesium hydroxide hydrate (0.500 g, ca. 2.5 mmol) in water (20 mL) and stirred for an hour until homogeneous. The solvent was removed and the precipitate dried in vacuo to produce a light yellow powder (1.017 g). A 9 mL thick walled glass tube with a Teflon stopcock was charged with the solid (0.10 g) and ethanol (2.0 mL) and heated at 120 °C. Over the course of heating for 6 hours, colorless platelike crystals grew on the walls of the tube above the solvent line. The heat was removed and the system was allowed to slowly cool at a rate of about 1°C/min. Crystals were collected from the walls of the tubes and dried over filter paper to provide 0.015 g of single crystals. Anal. Calcd. (Found) for $C_{15}H_8CsNO_4$: C 45.14 (44.80); H 2.02 (1.96); N 3.51 (3.45).

*Isolation of H**L**$_{ene}$*

Single crystals of **2** (0.050 g, 0.12 mmol) were added to water (10 mL) and mixed until homogeneous. The solution was acidified with 3*M* HCl and the resulting white precipitate was isolated via gravity filtration and washed with water and dried in vacuo to

yield 0.028 g (88%) of H**L**$_{\mathbf{ene}}$. HRMS: DP$^+$ (*m/z*): Calcd for $[C_{15}H_9NO_4]^+$ 267.0532; found 267.0528. ^{1}H NMR ($(D_3C)_2SO$, 300 MHz) δ 8.52 (dd, 4H, nphth), 7.91 (t, 2H, nphth), 5.71 (m, 1H, methylene), 4.90 (m, 1H, methylene).

Crystallographic Study

Crystal data and data collection and refinement parameters for **1** and **2** are given in Table 3.1. X-Ray intensity data were collected at 100(2) K using a Bruker SMART APEX diffractometer (Mo Kα radiation, λ = 0.71073 Å) [21, 22]. The raw area detector data frames were reduced and corrected for absorption effects with the SAINT+ and SADABS programs.[21, 22] Final unit cell parameters of **1** were determined by least-squares refinement of 8986 reflections from the data set. Final unit cell parameters of **2** were determined by least-squares refinement of 3216 reflections from the data set. Direct methods structure solution, difference Fourier calculations and full-matrix least-squares refinement against F^2 were performed with SHELXS/L^2 as implemented in OLEX2.[23]

Compound **1** crystallizes in the space group C2/c as determined by the pattern of systematic absences in the intensity data and by the successful solution and refinement of the structure. The asymmetric unit consists of two cesium atoms and one ligand. Both cesium atoms are located on special positions and therefore are each shared between two asymmetric units: Cs1 is located on an inversion center and Cs2 is located on a two-fold axis of rotation.

Compound **2** crystallizes in the space group $P2_1/n$ as determined by the pattern of systematic absences in the intensity data. The asymmetric unit consists of one cesium atom and one ligand. The largest electron density peak remaining in the final difference map (3.75 $e^-/Å^3$) is located 0.87 Å from the cesium atom. For both compounds non-

hydrogen atoms were refined with anisotropic displacement parameters. Hydrogen atoms were placed in geometrically idealized positions and included as riding atoms.

Table 3.1. Crystallography Data.

	1	**2**
Formula	$C_{14}H_8CsNO_4$	$C_{15}H_8CsNO_4$
Fw, g mol^{-1}	387.12	399.13
Cryst. Syst.	Monoclinic	Monoclinic
Space group	*C* 2/c	*P* 2_1/n
T, K	100(2) K	100(2) K
a , Å	30.430(7)	13.6049(15)
b , Å	4.9820(12)	6.8100(8)
c , Å	16.566(4)	14.4187(16)
α, deg	90	90
β , deg	101.951(4)	105.345(2)
γ, deg	90	90
V , Å^3	2457.0(10)	1288.3(3)
Z	8	4
Data/restraints/parameters	3067/0/183	2617/0/190
Final R indexes [I>=2σ (I)][a,b]	R_1=0.0224 wR_2=0.0549	R_1=0.0441 wR_2=0.0979
Final R indexes [all data]	R_1=0.0240 wR_2=0.0557	R_1=0.0529 wR_2=0.1021
Largest diff. peak/hole / e Å^{-3}	0.64/-0.42	3.75/-1.18

Mo Kα radiation, λ = 0.71073 Å. [a]$R1 = \Sigma \, ||F_o| - |F_c|| \, / \, \Sigma \, |F_o|$, [b]$wR2 = \{ \, \Sigma \, [\, w(F_o^2 - F_c^2)^2 \,] \, / \, \Sigma \, [\, w(F_o^2)^2 \,] \, \}^{1/2}$

Results

Syntheses. Mixing H$\mathbf{L_{gly}}$ and H$\mathbf{L_{ser}}$ with CsOH in water produced Cs($\mathbf{L_{gly}}$) and Cs($\mathbf{L_{ser}}$). Single crystals of Cs($\mathbf{L_{gly}}$) (**1**) were grown from heating the powder of Cs($\mathbf{L_{gly}}$) under solvothermal conditions in ethanol. Heating the powder of Cs($\mathbf{L_{ser}}$) in ethanol under solvothermal conditions resulted in the dehydration of the ligand forming single crystals of Cs($\mathbf{L_{ene}}$) (**2**) on the walls of the reaction vessel above the solvent line. We note that our previous preparation of crystalline Cs($\mathbf{L_{ser}}$) was the same as that reported here for Cs($\mathbf{L_{ene}}$), except methanol was used for the solvothermal step.[17] In determining the

structures of both **2** and Cs($\mathbf{L_{ser}}$), multiple crystals were mounted and the unit cell determined showing the sample was homogenous. We also isolated H$\mathbf{L_{ene}}$ in high yield from the decomposition of Cs($\mathbf{L_{ene}}$). The reasons for the dehydration of $\mathbf{L_{ser}}^-$ in ethanol are not clear, especially given that we have previously heated mixtures of other group 1 and 2 metals and $\mathbf{L_{ser}}^-$ under a variety of solvothermal conditions and observed no dehydration of the ligand.[17, 18, 20]

Solid State structure of 1. The coordination environments for both unique cesium cations are shown in Figure 3.1. The Cs2 cations are coordinated by six oxygen atoms from μ^3-κ^3:κ^2 carboxylates in an unusual O_6 planar arrangement. The carboxylate oxygen atoms (O3) from two $\mathbf{L_{gly}}^-$ ligands bridge Cs2 cations generating chains of edge-shared polyhedra extending along the crystallographic *b* axis. A second chain of edge-shared polyhedra (-Cs1-Cs2-Cs1-Cs2-) extends along the crystallographic *c* axis bridged by carboxylate oxygens (O3 and O4) to generate a two-dimensional sheet parallel to the crystallographic *bc* plane. The Cs1 cations are in an octahedral environment where O3 and O4 are in an equatorial belt and the axial sites are occupied carbonyls of the naphthalimide groups (O2), forming seven-member rings.

The hexagonal O_6-coordination geometry around the Cs2 cation is highly planar (Figure 3.2), where the least-squares plane has an average deviation of 0.019(3) Å, creating two open faces that are occupied by edges of the naphthalimide ring (C11, C12, H11, and H12) on either side. These interactions are identified as η^2-coordination because of the short bond Cs-C distances (3.22 - 3.78 Å). Similar reported cesium carbon interactions are between 3.20 and 4.17 Å.[6-13]

In addition to these cation-π interactions, the 1,8-naphthalimide rings are involved in a unique form of π···π stacking. As we have outlined previously,[24] these relatively strong interactions are defined by a series of metrics: the angle made by the planes of the two rings and the separation; the overlap of the rings as measured by the "slippage" parameter χ, which is the third side of the right triangle formed with the average perpendicular distance between the rings and the line joining the central fused ring carbon atoms of the two rings; and the rotation angle made by the two naphthalimide dipole vectors, which run through the central ring carbon atoms, pointing toward the nitrogen. As can be seen in Figure 3.3a, the orientation of the naphthalimide rings that results from the coordination of one of the carbonyl oxygen atoms with Cs1 and the η^2-interaction with Cs2 leads to intra-sheet π···π stacking interactions where the average distance between the parallel rings is 3.30 Å, an indication of a relatively strong interaction, but the slippage parameter is fairly large at 3.73 Å (stronger interactions are below 3.0 Å).[14-16]

The unusual feature of the interaction is that the rings are oriented head to head with a dipole vector rotation angle of zero. We have previously shown that the strength of the interaction is not very sensitive to this rotation angle unless it is very small – our previous low value is 35°.[24] This potentially negative force is negated in compound **1** by the large slippage parameter, where all of the slippage is along the aligned dipole vectors, such that the nitrogen atoms are oriented over the aromatic rings and not the nitrogen from adjacent rings, Figure 3.3b. Because of the intra-sheet π···π stacking of the naphthalimide rings, there is no strong interaction between sheets.

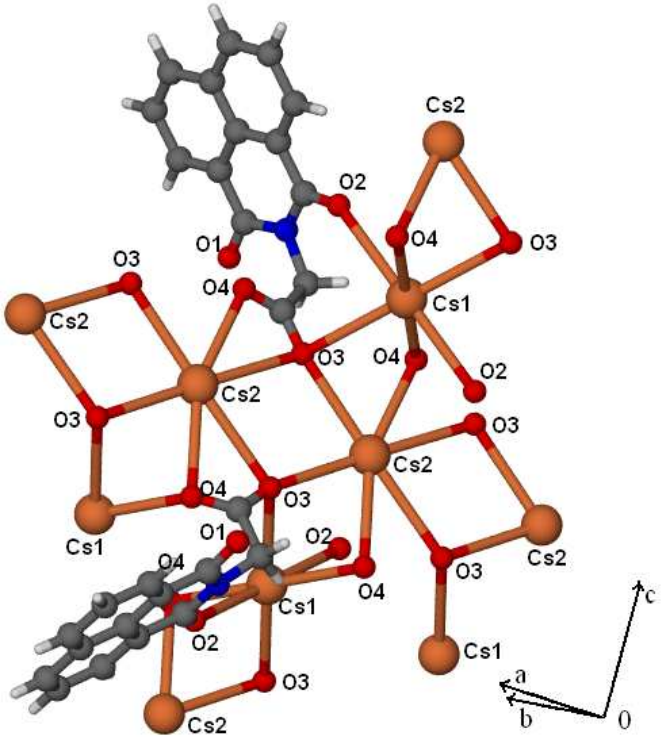

Figure 3.1. Coordination environment for cesium in Cs($\mathbf{L_{gly}}$) (**1**).

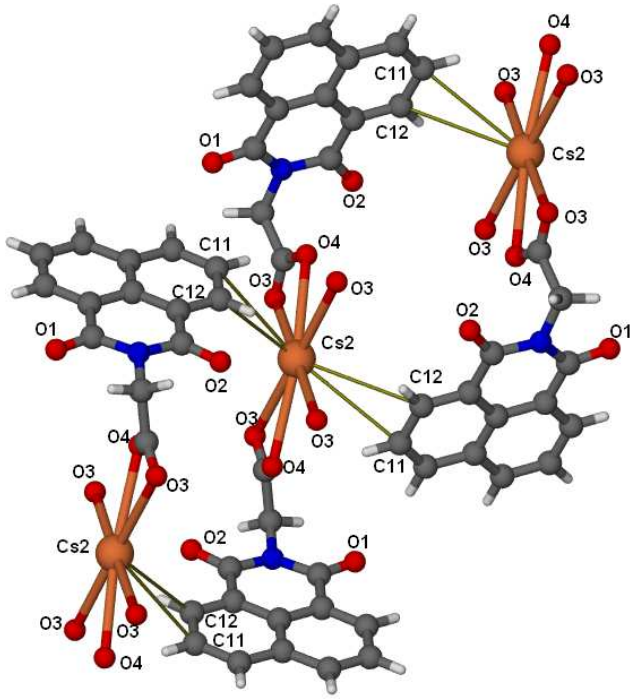

Figure 3.2. Coordination environment of Cs2 from Cs($\mathbf{L_{gly}}$) (**1**) with thin gold lines highlighting η^2 interactions with 1,8-naphthalimide rings.

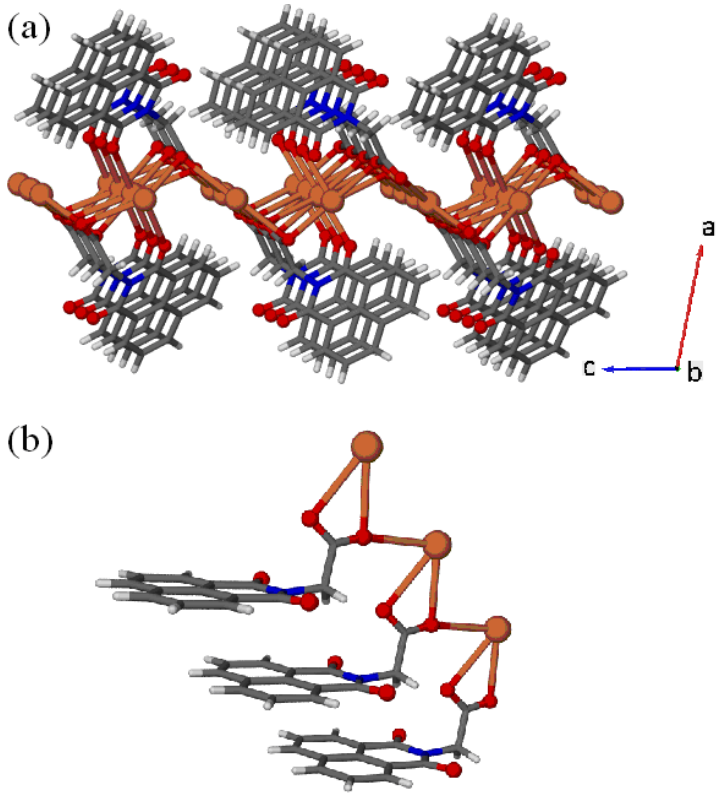

Figure 3.3. (a) View along the crystallographic *b* axis of a sheet of Cs(**L**$_{gly}$) (**1**). (b) View showing intra-sheet head to head $\pi\cdots\pi$ stacking and slippage of the naphthalimide rings.

Solid State structure of 2. The irregular coordination environment for the cesium cations in Cs(**L**$_{ene}$) (**2**) is shown in Figure 3.4. Each cation is 6-coordinate, bonded by four different ligands, three of which are involved in bridging the cations into rods through μ-κ^2:κ^2 carboxylates extending along the crystallographic *b* axis. The **L**$_{ene}^-$ ligand that is chelated to a given cesium cation also bonds to that cesium through a naphthalimide carbonyl (O2) making seven membered rings. As shown in Figure 3.5, the sixth site on each cesium cation is filled by a naphthalimide carbonyl (O1) from an adjacent rod. These interactions bridge parallel rods into two-dimensional sheets along the (1 0-1) crystallographic plane.

Figure 5 also shows the most interesting feature of the structure. Each methylene group, which forms by elimination of water, is located between two cesium cations from

adjacent rods that are linked by the bridging naphthalimide carbonyl (O1). There are two types of interactions. In one case the C14-Cs1 distance is 3.58 Å and the C13-Cs1 distance is 3.81 Å; this interaction is best described as η^2-coordination. A second Cs1 from an adjacent rod interacts with the other face of the same methylene group, the C14-Cs1 distance is 3.67 Å, but the C13-Cs1 distances is long at 4.34 Å, indicative of an η^1-interaction.[25-27] Each of the highly distorted cesium cations makes an interaction of each type from its open face to two different methylene groups, one intra-rod and one inter-rod. These bridging μ-η^2:η^1 interactions with each methylene group support the O1-linkage of the rods into sheets.

The 2D sheets are held together into a 3D supramolecular structure by interdigitated 1,8-naphthalimide rings involved in strong $\pi\cdots\pi$ interactions, Figure 3.6a. The rings in any stack are parallel with an average distance of 3.32 Å and the dipole angle between the rings is 180°. As seen in Figure 3.6b, there is a moderately large slippage parameter of 2.62 Å.

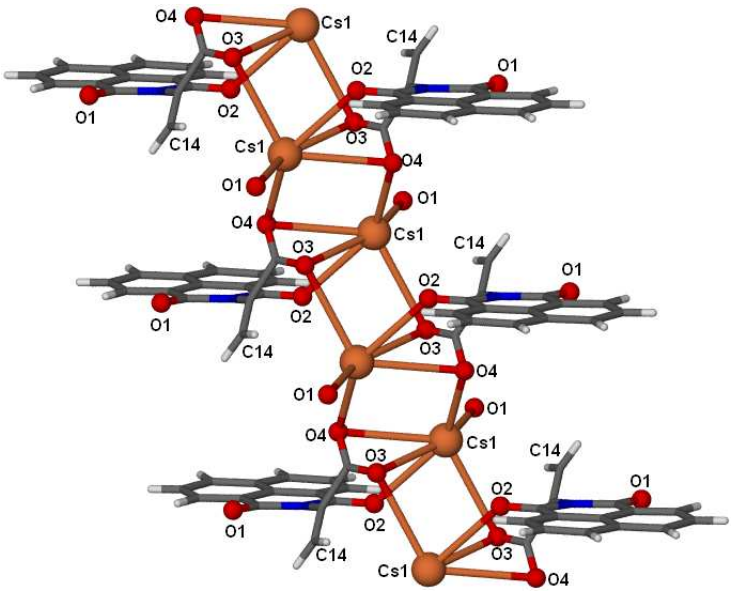

Figure 3.4. Rods of Cs($\mathbf{L_{ene}}$) (**2**).

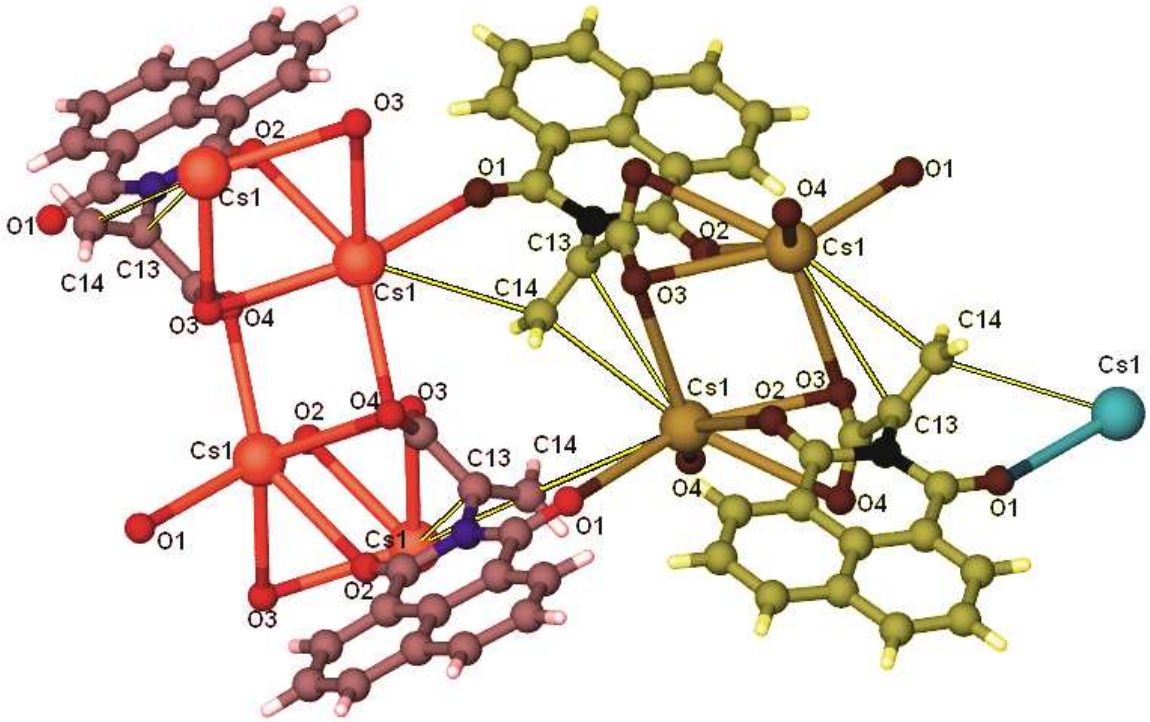

Figure 3.5. Coordination environment in Cs(**L**$_{ene}$) (**2**) showing the linkage of the rods into sheets by interactions of naphthalimide carbonyl groups with cesium cations in adjacent rods and the η^2:η^1-interactions between cesium cations and the methylene groups. Adjacent rods are tinted red, yellow and blue respectively.

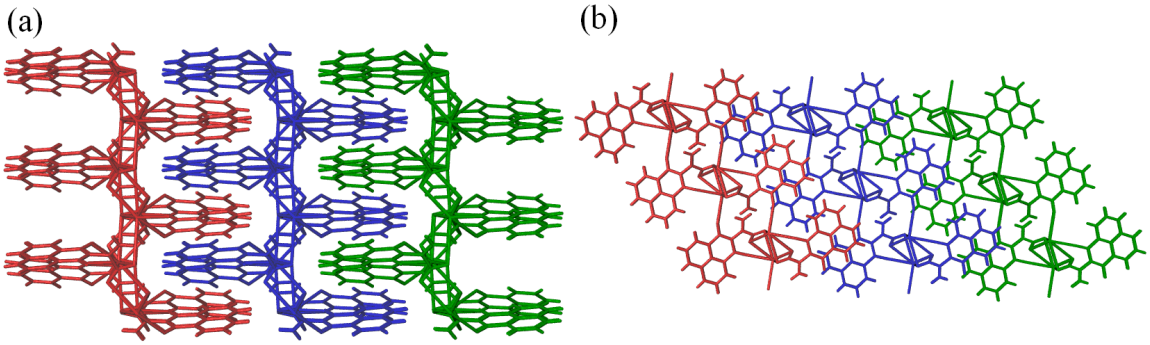

Figure 3.6. (a) View parallel to the crystallographic (1 0 -1) plane of Cs(**L**$_{ene}$) (**2**) showing the "zipper-like" π···π stacking interactions between differently colored sheets. (b) View along the *b* axis showing the overlap of naphthalimide rings

Fluorescence

The fluorescence spectra for both compounds were compared to the protonated ligands of each complex, H**L**$_{gly}$ for **1** and H**L**$_{ene}$ for **2**. The protonated ligands have similar spectra with fluorescence emission maxima ($\lambda_{max,Fl}$) at 447 and 475 nm, respectively. The spectra

for compound **1** is slightly red-shifted ($\lambda_{max,Fl}$ = 453nm) and the spectra for compound **2** is slightly blue-shifted ($\lambda_{max,Fl}$ = 450nm).

Discussion

Both new compounds reported here form solid-state 2D sheet structures of cesium cations linked by oxygen donors, with naphthalimide rings located on each side of the sheets. Similar arrangements were observed in our previously reported compounds Cs(**L**$_{ala}$) and Cs(**L**$_{ser}$).[17, 18] An interesting feature is that none of the four compounds have solvent ligands originating from the polar, water/alcohol solvents used in the preparation/crystallization, a feature that appears common with ligands that contain the large "lipophilic" naphthalimide group.[17, 18, 20, 25]

In all cases, the cesium cations have a relatively low coordination number of six.[17, 18] Despite having the same coordination number, a variety of coordination geometries are observed. In Cs(**L**$_{ser}$), the cations are in a fairly regular trigonal prismatic coordination environment and the Cs1 sites in Cs(**L**$_{gly}$) are in a distorted octahedral environment. In contrast, the Cs(**L**$_{ene}$) and Cs(**L**$_{ala}$) cations have coordination spheres that are slightly over half-filled with oxygen atoms such that there is a large open face in each. The Cs2 sites in Cs(**L**$_{gly}$) are very unusual, where the geometry of the oxygen donor atoms is hexagonal planar and the cation has two open faces.

In these three cases of cesium cations with large open faces in the coordination sphere, the empty spaces are filled by interactions with hydrocarbon moieties in the ligands. Each type of interaction is different. In Cs(**L**$_{ala}$), there is an interaction with the edge of a naphthalimide group and there are also unusual agostic C-H interactions with

the methyl group of the ligand, having short Cs-C distances (3.66 Å) and small Cs···H-C angles (109-112°). We note agostic interactions between cesium cations and methyl groups have been suggested previously.[6-8] As outlined above, η^2-coordination from the edge of naphthalimide groups occupy the two faces of planar Cs2 and a combination of η^2- and η^1-interactions with methylene groups occupy the open faces in Cs(**L**$_{\mathbf{ene}}$). Overall, the distorted geometries observed for these cesium cations appear to be a result of the propensity of this polarizable cation to interact with π and even σ orbitals in the ligands; the former interactions have been termed "solvation."[6-13]

Finally, a driving force for the chemistry reported from our group using ligands such as pictured in Scheme 3.1 is a study of the consequences of the supramolecular organizing force of the strong π···π stacking of the naphthalimide groups. These forces do organize the 2D structure of Cs(**L**$_{\mathbf{ene}}$) (**2**) into a supramolecular 3D structure, as was observed in both Cs(**L**$_{\mathbf{ala}}$) and Cs(**L**$_{\mathbf{ser}}$). In contrast, the stacking interactions in Cs(**L**$_{\mathbf{gly}}$) are intra-sheet leaving the structure as 2D. The observed intra-sheet π···π stacking of naphthalimide rings with aligned dipole vectors present in compound **1** were predicted via ab initio calculations to be unfavorable, but those calculations had a slippage parameter of zero.[24] In Cs(**L**$_{\mathbf{gly}}$), these predicted unfavorable interactions are avoided by the large slippage value (3.73 Å) along the aligned dipole vectors.

The solid state fluorescence spectra for these solids were compared to the protonated forms of their respective ligands and show slightly red-shifted emission maxima for Cs(**L**$_{\mathbf{ala}}$) and Cs(**L**$_{\mathbf{gly}}$) and blue-shifted emission maxima for Cs(**L**$_{\mathbf{ser}}$) and Cs(**L**$_{\mathbf{ene}}$). This fluorescence is based on the naphthalimide group[28, 29] and is not greatly perturbed by the interactions this group has with the cesium cations.

References

(1) D. Banerjee, J. B. Parise, *Cryst. Growth Des*. **2011,** *11*, 4704-4720.

(2) K. M. Fromm, *Coord. Chem. Rev.* **2008**, *252* (2008) 856-885.

(3) J. A. Bertke, A. G. Oliver, K. W. Henderson, *Inorg. Chem.* **2012**, *51*, 1020-1027.

(4) B. Masci, S, Pasquale, P. Thuéry, *Cryst. Growth Des.* **2010**, *10*, 2004-2010.

(5) G. Smith, U. D. Wermuth, D. J. Young, J. M. White, *Polyhedron*, **2007**, *26*, 3645-3652.

(6) D. Hoffmann, W. Bauer, P. v. R. Schleyer, U. Pieper, D. Stalke, *Organometallics* **1993,** *12*, 1193-1200.

(7) M. Niemeyer, P. P. Power, *Inorg. Chem.* **1996,** *35*, 7264-7272.

(8) D. F.-J. Piesik, P. Haack, S. Harder, C. Limber, *Inorg. Chem.***2009,** *48*, 11259-11264.

(9) A. Steiner, D. Stalke, *Inorg. Chem.* **1993,** *32*, 1977-1981.

(10) G. W. Rabe, S. Kheradmandan, L. M. Liable-Sands, I. A. Guzei, A. L. Rheingold, *Angew. Chem. Int. Ed.* **1998**, 1404-1407.

(11) M. F. Zuniga, G. B. Deacon, K. Ruhlandt-Senge, *Inorg. Chem*.**2008,** *47*, 4669-4681.

(12) L. Orzechowski, G. Jansen, S. Harder, *Angew. Chem. Int. Ed.* **2009,** *48* 3825-3829.

(13) K. T. Quisenberry, C. K. Gren, R. E. White, T. P. Hanusa, W. W. Brennessel, *Organometallics*, **2007,** *26*, 4354-4356.

(14) D. L. Reger, A. Debreczeni, M. D. Smith, *Eur. J. Inorg. Chem*. **2012**, *2012*, 712-719.

(15) D. L. Reger, A. Debreczeni, M. D. Smith, J. Jezierska, A. Ozarowski, *Inorg. Chem.* **2012,** *51*, 1068-1083.

(16) D. L. Reger, A. Debreczeni, M. D. Smith, *Inorg. Chem*. **2011,** *50*, 11754-11764.

(17) D. L. Reger, A. Leitner, M. D. Smith, T. T. Tran, P. S. Halasyamani, *Inorg. Chem*. **2013,** *52*, 10041-10051.

(18) D. L. Reger, A. Leitner, P. J. Pellechia, M. D. Smith, *Inorg. Chem*. **2014,** *53*, 9932-9945.

(19) D. L. Reger, A. Debreczeni, J. J. Horger, M. D. Smith, *Cryst. Growth Des.* **2011,** *11*, 4068-4079.

(20) D. L. Reger, A. Leitner, M. D. Smith, *Inorg. Chem*. **2012,** *51*, 10071-10073.

(21) SMART Version 5.630, SAINT+ Version 6.45 and SADABS Version 2.10. Bruker Analytical X-ray Systems, Inc., Madison, Wisconsin, USA, 2003.

(22) G. M. Sheldrick, *Acta Cryst.* **2008,** *64*, 112-122.

(23) O. V. Dolomanov, L. J. Bourhis, R. J. Gildea, J. A. K. Howard, H. Puschmann, J. *Appl. Cryst.* **2009,** *42*, 339-341.

(24) D.L. Reger, A. Debreczeni, B. N. Reinecke, V. Rassalov, M. D. Smith, R. F. Semeniuc, *Inorg. Chem*. **2009,** *48*, 8911-8924.

(25) J. P. Tellam, G. Kociok-Köhn, D. R. Carbery, *Org. Lett.* **2008,** *10*, 5199-5205.

(26) H.-W. Lerner, I. Sänger, F. Schödel, A. Lorbach, M. Bolte, M. Wagner, *Dalton Trans*. **2008,** 787-792.

(27) M. Albrecht, O. Blau, R. Fröhlich, *Proc. Nat. Acad. Sci. USA*, **2002,** *99*, 4867-4872.

(28) V. Wintgens, P. Valat, J. Kossanyi, A. Demeter, L. Biczok, T. Berces, *New J. Chem*. **1996,** *20*, 1149-1158.

(29) A. P. de Silva, H. Q. N. Gunaratne, T. Gunnlaugsson, P. L. M. Lynch, *New J. Chem.* **1996,** *20*, 871-880.

Chapter IV

Homochiral, Helical Coordination Complexes of Lanthanides(III) and Mixed-Metal Lanthanides(III): Impact of the 1,8-Naphthalimide Supramolecular Tecton on Structure, Magnetic Properties and Luminescence [4]

[4]Adapted with permission from Reger, D. L.; Leitner, A.; Smith, M. D. *Cryst. Growth Des.* **2015**, *15*(11), 5637-5644. DOI: 10.1021/acs.cgd.5b01387 Copyright 2015 American Chemical Society.

Introduction

We have been developing the coordination chemistry of ligands functionalized with the naphthalimide π···π stacking supramolecular tecton.[1–10] In our initial studies with poly(pyrazolyl)methane ligands, we showed that the naphthalimide tecton is an effective functional group to organize supramolecular structures.[2] We then developed the chemistry of naphthalimide functionalized carboxylate ligands such as those pictured in Scheme 1 in order to take advantage of the well-established ability of the carboxylate donor group to build metal ions into secondary building units (SBUs), in order to form three-dimensional assemblies akin to metal-organic frameworks (MOFs).[5,11]

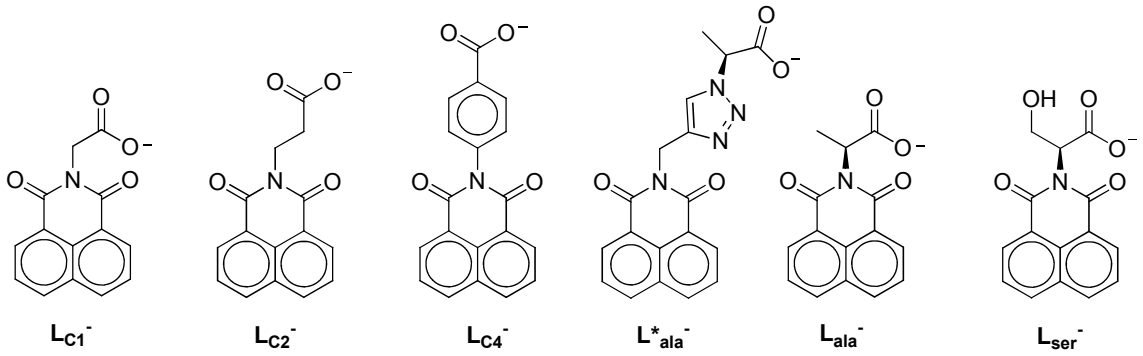

Scheme 4.1. Multifunctional Ligands

In the complexes formed with transition metal ions, most notably those with "paddlewheel" $M_2(O_2CR)_4$ central cores, complexes with 2-dimensional (2D) and mainly 3-dimensional (3D) structures were prepared that were similar in appearance to classical MOF complexes, but that were unique in that one or more of the dimensions of the structures were organized solely by strong π···π stacking, noncovalent forces.[1,3,5,7] We call

these structures supramolecular metal-organic frameworks (SMOFs). A unique feature of many of these complexes, clearly attributed to the versatility of the π···π stacking ability of the naphthalimide supramolecular synthon, was that many of them were able to undergo gas-solid, single-crystal to single-crystal transformations, both by removal and reabsorption of solvent molecules,[3–5,9] in some cases coordinated solvent,[3,8] and in phase changes when varying the temperature.[5] Our studies showed that in these transformations the metrics of the π···π stacking interactions could vary allowing the structures to "breath" while still maintaining crystallinity.[5,8,9]

More recently we have described the chemistry of these ligands, most notably those derived from enantiopure amino acids such as $\mathbf{L_{ala}}^-$ and $\mathbf{L_{ser}}^-$, with the oxophilic group 1 and 2 metals.[8–10] The structures of these complexes are dominated by the consistent formation of helical rod SBUs, rods that are homochiral due to their formation from enantiopure ligands. An interesting feature of these complexes was low coordination numbers for these large metal ions and the absence or near absence of solvent ligands, despite the fact that the preparations were carried out in water/alcohol solvents, an apparent general feature of ligands that contain bulky "lipophilic" groups,[10,12] such as 1,8-naphthalimide.[8–10]

These results prompted us to carry out analogous studies with lanthanide metals. We had two main goals. The first was quite simple; what type of structural changes would we observe with metals in the 3+ oxidation state interacting with our bulky π···π stacking, carboxylate ligands. The second relates to the spectral properties of the 1,8-naphthalimide chromophore. We have previously reported that the group 1 and 2 metal complexes of these ligands exhibit significant solid-state luminescence that was only

mildly influenced by these metals.[8–10] In contrast, we anticipated that the naphthalimide group could act as a sensitizer to enhance or diminish the photoluminescence of lanthanide metals.[13–16] Our earlier results showing the ability of these ligands to exclude solvent molecules was important because coordinated solvent molecules can quench lanthanide-based luminescence.[17,18] Interestingly, a recent paper published after the initiation of our studies has shown success of lanthanide complexes of our $\mathbf{L}_{C1}^-$ and $\mathbf{L}_{C2}^-$ ligands (Scheme 4.1) in "achieving white-light-emissions."[13]

Mixed-metal lanthanides are highly desirable for new photoluminescence lanthanide complexes because each metal has a different emission color which, when combined, can create a solid with a tunable emission spectrum.[14] Although desirable, solid state structures of mixed-metal complexes are somewhat rare because the syntheses generally lead to mixed phases rather than a pure phase of a mixed metal complex.[19] Two successful avenues for incorporating mixed metal lanthanides into MOF structures are: a known framework can act as a host to lanthanide cation guests or mixed metal lanthanides comprise the SBUs.[20,21]

Reported here are the syntheses and solid state structures of complexes of a series of lanthanide(III) metals (La, Ce, Sm, Eu, Gd, Tb and Dy) with the ligand $\mathbf{L}_{\mathbf{ser}}^-$. These complexes show a consistent structure type despite large differences in the cationic radii of the metals. The structures are so similar that single crystals of mixed lanthanide(III) metal complexes could be prepared and studied, where the stoichiometric ratios of metals in the final products are controlled somewhat by the relative molar ratios used in the reactions. The luminescence spectra for the pure-metal compounds were studied and compared to those of the protonated ligand, H$\mathbf{L}_{\mathbf{ser}}$. A series of mixed-metal compounds,

mainly with varying concentrations of cerium(III) and terbium(III), were studied to determine the effects of these changes on quantum yields. Representative compounds, including those of mixed-metals, are also characterized magnetically by SQUID measurements.

Experimental

All reactants and solvents were used as purchased from Aldrich and Strem. Samples of mixed lanthanide(III) metals were analyzed using a Finnigan ELEMENT XR double focusing magnetic sector field inductively coupled plasma-mass spectrometer (ICP-MS). The elemental composition of single crystals of mixed-metal complexes was verified using a TESCAN Vega-3 SBU SEM with EDS capabilities. Three single crystals from each reaction were mounted on carbon tape and analyzed using a 20 kV accelerating voltage and an accumulation time of 1 min. Excitation and emission spectra as well as Quantum Yield were collected and duplicated three times with an Edinburgh SpectroFluorometer FS5. Magnetic properties were collected on a Quantum Design Magnetic Properties Measurement System (QD-MPMS 3 SQUID Magnetometer). Molecular weights for the compounds in the yields and susceptibility calculations were based on the single crystal X-ray data and did not include the interstitial solvent removed by SQUEEZE. The synthesis of H$\mathbf{L}_{\mathbf{ser}}$ was reported previously.[8]

Synthesis of $[La_3(\mathbf{L}_{ser})_8(OH)(H_2O)]\bullet(H_2O, EtOH)_x$ ***(1)***

H$\mathbf{L}_{\mathbf{ser}}$ (1.0 g, 3.5 mmol) was added to a solution of lithium hydroxide hydrate (0.15 g, 3.5 mmol) in water (50 mL) and stirred for an hour until homogeneous. The solvent was

removed and the precipitate dried in vacuo to produce Li$\mathbf{L_{ser}}$ as a light yellow powder (0.868 g, 2.98 mmol). A 9 mL thick walled glass tube with a Teflon screw top was charged with lanthanum nitrate hexahydrate (0.030 g, 0.069 mmol), Li$\mathbf{L_{ser}}$ (0.050 g, 0.14 mmol), water (0.8 mL) and ethanol (0.2 mL) then heated in an oil bath at 120 °C. Yellow plate crystals grew over the course of 4 days on the walls of the reaction vessel above the solvent line. The heat was removed and the crystals were collected from the tube, washed with methanol and dried over filter paper to provide 0.060 g of single crystals of **1** in a 62% yield.

Synthesis of $[Ce_3(\mathbf{L_{ser}})_8(OH)(H_2O)]\bullet(H_2O, EtOH)_x$ ***(2)***

Compound **2** was synthesized in a similar manner to compound **1** but with cerium nitrate hexahydrate (0.030 g, 0.069 mmol). Yellow plate crystals grew overnight on the walls of the reaction vessel above the solvent line. The heat was removed and the crystals were collected from the tube, washed with methanol and dried over filter paper to provide 0.043 g of single crystals of **2** in a 67% yield.

Synthesis of $[Sm_3(\mathbf{L_{ser}})_8(OEt)]\bullet(H_2O, EtOH)_x$ ***(3)***

Compound **3** was synthesized in a similar manner to compound **1** but with samarium(III) chloride hexahydrate (0.030 g, 0.082 mmol). The resulting colorless block crystals were collected and washed with methanol to yield 0.036 g of **3** in a 60% yield.

Synthesis of $[Eu_3(\mathbf{L}_{ser})_8(OEt)]\bullet(H_2O, EtOH)_x$ ***(4)***

Compound **4** was synthesized in a similar manner to compound **1** but with europium nitrate pentahydrate (0.030 g, 0.070 mmol). The resulting colorless block crystals were collected and washed with methanol to yield 0.013 g of **4** in a 22% yield.

Synthesis of $[Gd_3(\mathbf{L}_{ser})_8(OEt)]\bullet(H_2O, EtOH)_x$ ***(5)***

Compound **5** was synthesized in a similar manner to compound **1** but with gadolinium nitrate hexahydrate (0.030 g, 0.066 mmol). The resulting colorless block crystals were collected and washed with methanol to yield 0.021 g of **5** in a 34% yield.

Synthesis of $[Tb_3(\mathbf{L}_{ser})_8(OEt)]\bullet(H_2O, EtOH)_x$ ***(6)***

Compound **6** was synthesized in a similar manner to compound **1** but with terbium nitrate hexahydrate (0.030 g, 0.066 mmol). The resulting colorless block crystals were collected and washed with methanol to yield 0.022 g of **6** in a 36% yield.

Synthesis of $[Dy_3(\mathbf{L}_{ser})_8(OEt)]\bullet(H_2O, EtOH)_x$ ***(7)***

Compound **7** was synthesized in a similar manner to compound **1** but with dysprosium nitrate hexahydrate (0.030 g, 0.066 mmol). The resulting yellow pyramidal crystals were collected and washed with methanol to yield 0.021 g of **7** in a 34% yield.

Synthesis of $[Ce_{2.3}Tb_{0.7}(\mathbf{L}_{ser})_8(OH)]\bullet(H_2O, EtOH)_x$ ***(8)***

Synthesis of the mixed metal species were the same as compound **1** but with cerium nitrate hexahydrate (0.024 g, 0.055 mmol) and terbium nitrate hexahydrate (0.006 g,

0.014 mmol). The resulting colorless block crystals were collected and washed with methanol to yield 0.022 g of **8** in a 37% yield.

Synthesis of $[Gd_{0.4}Tb_{2.6}(\mathbf{L_{ser}})_8(OEt)]\bullet(H_2O, EtOH)_x$ ***(9)***

Compound **9** was synthesized in a similar manner to compound **1** but with terbium nitrate hexahydrate (0.015 g, 0.033 mmol) and gadolinium nitrate hexahydrate (0.015 g, 0.033 mmol). The resulting colorless block crystals were collected and washed with methanol to yield 0.012 g of **9** in a 20% yield.

Synthesis of $[Ce_{1.4}Gd_{0.3}Tb_{1.3}(\mathbf{L_{ser}})_8(OH)]\bullet(H_2O, EtOH)_x$ ***(10)***

Compound **10** was synthesized in a similar manner to compound **1** but with cerium nitrate hexahydrate (0.010 g, 0.023 mmol), gadolinium nitrate hexahydrate (0.010 g, 0.022 mmol) and terbium nitrate hexahydrate (0.010 g, 0.022 mmol). The resulting colorless block crystals were collected and washed with methanol to yield 0.022 g of **10** in a 37% yield.

Powder X-Ray Diffraction

In order to test for phase purity of the crystalline products, samples of compounds **1**-**10** were collected from the walls of the solvothermal tubes, washed with acetone and ground in air. All measurements were performed on a Rigaku Ultima 4 instrument using Cu Kα radiation at a scan rate of 1 °/min between 4 and 30 °2θ with a step size of 0.02 °2θ. Powder patterns were analyzed using Microsoft Excel and were compared to the

powder patterns predicted by Mercury based on the single crystal data. These powder patterns demonstrate phase purity for **1-10**.

Crystallographic Study

Crystal data and data collection and refinement parameters for all compounds are given in Table 4.1. X-Ray structure determinations are discussed in detail in the Supporting Information.

Table 4.1. Crystallography Data.

	1	**2**	**3**	**4**
Formula	$C_{120}H_{91}La_3N_8O_{46}$	$C_{120}H_{91}Ce_3N_8O_{46}$	$C_{122}H_{93}N_8O_{45}Sm_3$	$C_{122}H_{93}Eu_3N_8O_{45}$
Fw, g mol^{-1}	2797.73	2801.36	2842.09	2846.92
Cryst. Syst.	Tetragonal	Tetragonal	Tetragonal	Tetragonal
Space group	$P4_32_12$	$P4_32_12$	$P4_32_12$	$P4_32_12$
T, K	100(2) K	100(2) K	100(2) K	100(2) K
a, Å	15.0506(6)	15.0749(10)	14.9573(9)	14.9044(10)
b, Å	15.0506(6)	15.0749(10)	14.9573(9)	14.9044(10)
c, Å	55.721(2)	55.646(7)	55.690(3)	55.800(4)
α, deg	90	90	90	90
β, deg	90	90	90	90
γ, deg	90	90	90	90
V, Å^3	12621.9(11)	12646(2)	12459.1(17)	12395.4(19)
Z	4	4	4	4
$R_1(I>2\sigma(I))$[a]	0.0502	0.0368	0.0326	0.0304
$wR_2(I>2\sigma(I))$[b]	0.0970	0.0894	0.0723	0.0657
Flack Parameter	-0.001(6)	-0.014(5)	-0.005(4)	-0.004(3)

	5	**6**	**7**
Formula	$C_{122}H_{93}Gd_3N_8O_{45}$	$C_{122}H_{93}N_8O_{45}Tb_3$	$C_{122}H_{93}Dy_3N_8O_{45}$
Fw, g mol^{-1}	2862.79	2867.80	2878.54
Cryst. Syst.	Tetragonal	Tetragonal	Tetragonal
Space group	$P4_32_12$	$P4_32_12$	$P4_32_12$
T, K	100(2) K	100(2) K	100(2) K
a, Å	14.9247(8)	14.9043(7)	14.9189(5)
b, Å	14.9247(8)	14.9043(7)	14.9189(5)
c, Å	55.654(6)	55.841(5)	55.485(4)
α, deg	90	90	90
β, deg	90	90	90
γ, deg	90	90	90
V, Å^3	12396.7(18)	12404.5(16)	12349.5(12)
Z	4	4	4
$R_1(I>2\sigma(I))$[a]	0.0424	0.0394	0.0539
$wR_2(I>2\sigma(I))$[b]	0.0938	0.0891	0.1223
Flack Parameter	0.009(4)	-0.001(4)	0.012(5)

	8	**9**	**10**
Formula	$C_{120}H_{89}Ce_{2.3}N_8O_{45}Tb_{0.7}$	$C_{122}H_{93}Gd_{0.4}N_8O_{45}Tb_{2.6}$	$C_{120}H_{89}Ce_{1.4}Gd_{0.3}N_8O_{45}Tb_{1.3}$
Fw, g mol^{-1}	2797.16	2867.20	2812.79
Cryst. Syst.	Tetragonal	Tetragonal	Tetragonal
Space group	$P4_32_12$	$P4_32_12$	$P4_32_12$
T, K	100(2) K	100(2) K	100(2) K
a, Å	14.8679(16)	14.9095(6)	14.9837(7)
b, Å	14.8679(16)	14.9095(6)	14.9837(7)
c, Å	55.353(6)	55.729(4)	55.753(5)
α, deg	90	90	90
β, deg	90	90	90
γ, deg	90	90	90
V, Å^3	12236(3)	12388.3(13)	12517.3(17)
Z	4	4	4
$R_1(I>2\sigma(I))$[a]	0.0548	0.0378	0.0411
$wR_2(I>2\sigma(I))$[b]	0.1137	0.0748	0.0975
Flack Parameter	-0.007(11)	-0.009(5)	-0.007(4)

[a] $R1 = \Sigma \, ||F_o| - |F_c|| \, / \, \Sigma |F_o|$ [b] $wR2 = \{ \Sigma [w(F_o^2 - F_c^2)^2] / \Sigma [w(F_o^2)^2] \}^{1/2}$

Results

Syntheses of complexes. Mixing H$\mathbf{L_{ser}}$ with LiOH in water produced Li$\mathbf{L_{ser}}$. Heating mixtures of Li$\mathbf{L_{ser}}$ in ethanol/water with $La(NO_3)_3$•$6H_2O$, $Ce(NO_3)_3$•$6H_2O$, $SmCl_3$•$6H_2O$, $Eu(NO_3)_3$•$5H_2O$, $Gd(NO_3)_3$•$6H_2O$, $Tb(NO_3)_3$•$6H_2O$ and $Dy(NO_3)_3$•$6H_2O$ under solvothermal conditions produced single crystals of $[La_3(\mathbf{L_{ser}})_8(OH)(H_2O)]$•$(H_2O, EtOH)_x$ (**1**), $[Ce_3(\mathbf{L_{ser}})_8(OH)(H_2O)]$•$(H_2O, EtOH)_x$ (**2**), $[Sm_3(\mathbf{L_{ser}})_8(OEt)]$•$(H_2O, EtOH)_x$ (**3**), $[Eu_3(\mathbf{L_{ser}})_8(OEt)]$•$(H_2O, EtOH)_x$ (**4**), $[Gd_3(\mathbf{L_{ser}})_8(OEt)]$•$(H_2O, EtOH)_x$ (**5**), $[Tb_3(\mathbf{L_{ser}})_8(OEt)]$•$(H_2O, EtOH)_x$ (**6**) and $[Dy_3(\mathbf{L_{ser}})_8(OEt)]$•$(H_2O, EtOH)_x$ (**7**), respectively. An interesting observation of our synthetic method is that the crystals grow above the solvent line in the solvothermal tubes.

The mixed-metal compounds $[Ce_{2.3}Tb_{0.7}(\mathbf{L_{ser}})_8(OH)]$•$(H_2O, EtOH)_x$ (**8**), $[Gd_{0.4}Tb_{2.6}$ $(\mathbf{L_{ser}})_8(OEt)]$•$(H_2O, EtOH)_x$ (**9**) and $[Ce_{1.4}Gd_{0.3}Tb_{1.3}(\mathbf{L_{ser}})_8(OH)]$•$(H_2O, EtOH)_x$ (**10**) were grown under the same conditions as **1**-**7**, and characterized by single crystal X-ray crystallography, ICP-MS and EDS. A variety of additional reactions were carried out using different molar ratios of the lanthanide(III) metals and the formulas of the crystalline products determined by ICP-MS. Table 4.2 compares the percentages used in the syntheses to the actual percentages determined in the products in all of these experiments. EDS measurements showed a consistent distribution of the metals at different locations in the crystals.

Table 4.2. Formulas of products and percentages of metals used in the syntheses (R) and measured in the products per helicate (P).

Compound	Ce		Sm		Eu		Gd		Tb	
	R	**P**	**R**	**P**	**R**	**P**	**R**	**P**	**R**	**P**
$Ce_{1.4}Gd_{0.3}Tb_{1.3}$	33%	47%	-	-	-	-	33%	10%	33%	43%
$Gd_{0.4}Tb_{2.6}$	-	-	-	-	-	-	50%	13%	50%	87%
$Ce_{0.3}Tb_{2.7}$	21%	10%	-	-	-	-	-	-	79%	90%
$Ce_{0.8}Tb_{2.2}$	34%	27%	-	-	-	-	-	-	66%	73%
$Ce_{1.6}Tb_{1.4}$	57%	53%	-	-	-	-	-	-	43%	47%
$Ce_{1.9}Tb_{1.1}$	68%	63%	-	-	-	-	-	-	32%	37%
$Ce_{2.4}Tb_{0.6}$	81%	80%	-	-	-	-	-	-	19%	20%
$Eu_{1.5}Tb_{1.5}$	-	-	-	-	51%	50%	-	-	49%	50%
$Eu_{2.6}Gd_{0.4}$	-	-	-	-	51%	87%	49%	13%	-	-
$Ce_{1.6}Eu_{1.4}$	50%	53%	-	-	50%	47%	-	-	-	-
$Sm_{1.8}Eu_{1.2}$	-	-	54%	60%	46%	40%	-	-	-	-
$Sm_{1.5}Tb_{1.5}$	-	-	55%	50%	-	-	-	-	45%	50%
$Ce_{1.4}Sm_{1.6}$	46%	47%	54%	53%	-	-	-	-	-	-

Solid state structure of $[Sm_3(L_{ser})_8(OEt)]\bullet(H_2O, EtOH)_x$ (3). The solid state structure of compound **3** is a supramolecular framework of trinuclear, carboxylate bonded helicates that crystallizes in the chiral space group $P4_32_12$. The 1,8-naphthalimide π···π stacking synthons organize the helicates into a 3D, supramolecular structure. There is a crystallographically imposed two-fold axis of rotation about the central samarium(III) cation (Sm2). The C_2 axis in the center of the helicate renders the two terminal

samarium(III) cations equivalent and creates two symmetrical sets of four ligands, A-D and A*-D*, totaling eight ligands per helicate (Figure 4.1). The homochiral helicates consist of three edge-shared samarium(III) cations with six bridging $\mathbf{L_{ser}}^-$ ligands (A, A*, B, B*, D, D*) and two capping κ^1, κ^1-carboxylate $\mathbf{L_{ser}}^-$ ligands (C, C*). The A ligand bridges Sm1 with Sm2 via μ^2-κ^1:κ^2 carboxylate and the alcohol chelates to Sm1 generating a 6-membered ring. The B ligand similarly bridges Sm1 and Sm2 but through a μ-κ^1:κ^1 carboxylate while the alcohol does not coordinate to a metal. The D ligand bridges all three metals Sm1, Sm1* and Sm2 through a μ^3-κ^1:κ^2 carboxylate while chelating with Sm1 via the alcohol and a carbonyl from the 1,8-naphthalimide forming a [3.2.2] bicyclic system. The nine-coordinate Sm1 cations are each bonded to five ligands (A, B, C, D & D*), while the central nine-coordinate Sm2 cation is bonded to six ligands (A, A*, B, B*, D & D*). The nine-coordinate Sm1* is symmetry equivalent to Sm1 and is bonded to five ligands (A*, B*, C*, D* & D). The final coordination site for Sm2 is occupied by an ethoxide ligand disordered over two positions (O6) related by the C_2 symmetry.

Each of the four types of naphthalimide groups is involved in two types of $\pi\cdots\pi$ stacking interactions, one per face. The $\pi\cdots\pi$ stacking interactions between 1,8-naphthalimide rings are defined by the following series of metrics: the angle between the planes of each ring and their average distance; the angle between the dipole vectors of each ring, which run through the central carbon atoms toward the nitrogen atoms; and the slippage parameter (χ), which gives the overlap of the two rings defined by the third side of the right triangle formed between the average perpendicular distance between the two rings and the line between the two central carbon atoms of each ring.

In **3**, the order of stacking goes …C, A, D, B, C, A… The C···A stacking is between helicates along the crystallographic *c* axis forming a *supramolecular helix* with a pitch of 56 Å, Figure 4.2. Because there are two of types of each ligand per helicate, two supramolecular helices branch from each helicate (Figure 4.2, right) with each helix of the pair rejoining after the repeating unit of four helicate units along each chain, the pitch. The *M* helices are tightly wound and nestled together through additional π···π stacking interactions. The A···D, D···B and B···C stacking are between adjacent helicates lying in the crystallographic *ab* plane; these interactions create 2D sheets of helicates (Figure 4.3). In these sheets, each helicate interacts with four other helicates. When combined with the π···π stacking in the *c*-direction, the supramolecular structure is three dimensional. The metrics for these interactions are listed in Table 4.3.

There is a large amount of featureless interstitial electron density peaks observed in difference maps located in cavities between helicates (Figure 4.3); this mixture of the crystallization solvents water and ethanol could not be sensibly modeled and were removed by SQUEEZE.

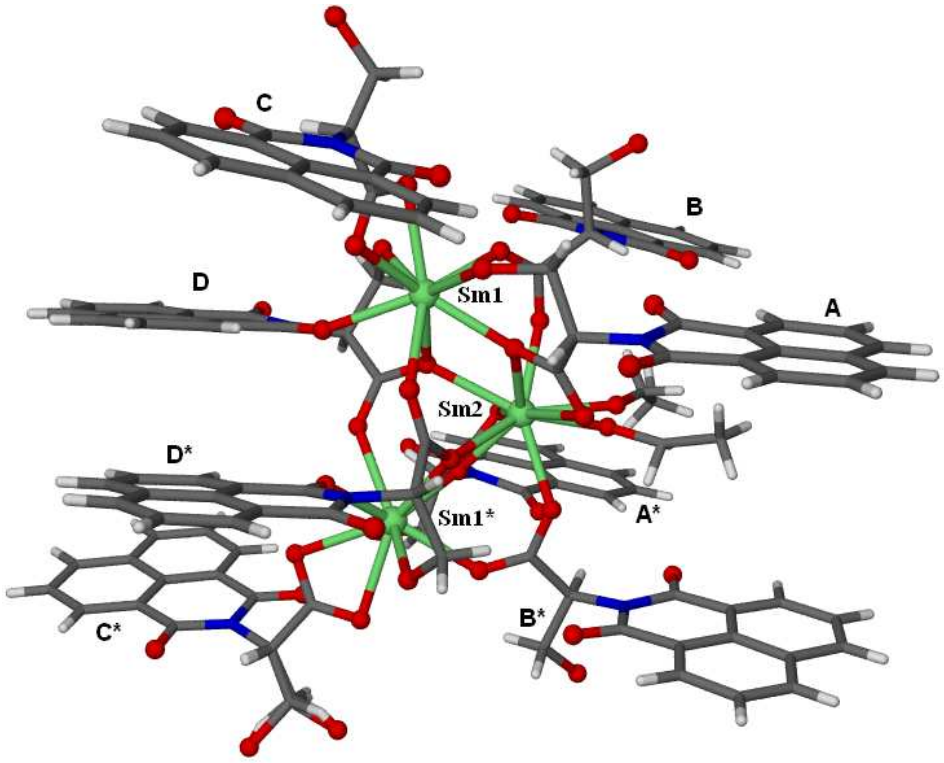

Figure 4.1. Coordination environment for samarium(III) cations of $[Sm_3(\mathbf{L_{ser}})_8(OEt)]\bullet(H_2O, EtOH)_x$ (**3**).

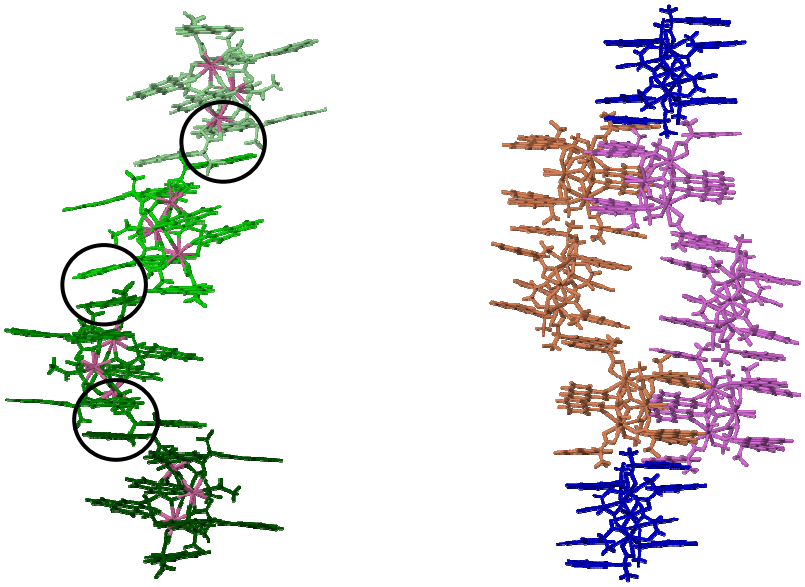

Figure 4.2. (left) Side view of the supramolecular *M* helices of **3** formed by A···C stacking along the crystallographic *c* axis. Samarium cations are in pink and the circles highlight the A···C stacking. (right) Two *M* helices built from A···C stacking (orange and pink) branch from a single helicate (blue) and rejoin after the repeating unit of four helicates.

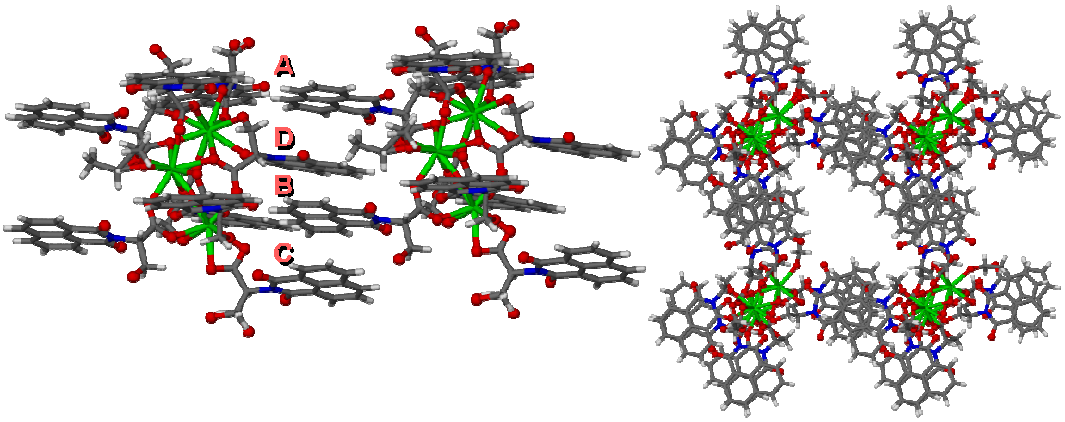

Figure 4.3. (left) Structure of **3** showing how adjacent helices are nestled and held together by A···D, D···B and B···C stacking to create a 2D sheet of helicates in the *ab*-plane. (right) View down the crystallographic *c*-axis illustrating the cavities, which are filled with disordered solvent.

The compounds **3**-**7** are isostructural, despite the changes in the sizes of the metals. The La and Ce compounds, **1** and **2,** are slightly different in that the coordinated disordered ethoxide in **3**-**7**, which occupies a single coordination site, is replaced by a water and a hydroxide anion, occupying two coordination sites and making the central Ln2 cation ten-coordinate. The extended structure and all π-stacking interactions remain the same with slight variations in the parameters due to differences in cation size (Table 4.3). Based on single crystal X-ray data for compounds **8**-**10**, the mixed-metal compounds adopt solid state structures identical to those of **3** with a single disordered ethoxide ligand in the case of **9** and a hydroxide disordered over three positions in the cases of **8** and **10**. The different metals are disordered evenly throughout the structure with a preference for the larger cation at the central position of the helicate, as indicated by the crystallographic U_{eq} values for Ln1 site compared to Ln2 from single crystal data.

Magnetism. The magnetic susceptibility data for selected pure and mixed-metal compounds were measured with a SQUID magnetometer and the results shown in Table

Table 4.3. $\pi^{\cdots}\pi$ Stacking Parameters

	Compound	Type of Stacking	Cen-Cen(Å)	dipole ∠ (°)	plane ∠ (°)	avg dist (Å)	χ (Å)
1	$[La_3(\mathbf{L_{ser}})_8(OH)(H_2O)]\cdot(H_2O, EtOH)_x$	C - A	3.60	58.8	5.6	3.54	0.66
		A - D	3.89	148.5	9.1	3.55	1.56
		D - B	4.70	135.0	9.0	3.42	3.21
		B - C	3.79	175.2	5.9	3.44	1.58
2	$[Ce_3(\mathbf{L_{ser}})_8(OH)(H_2O)]\cdot(H_2O, EtOH)_x$	C - A	3.57	58.7	6.0	3.52	0.61
		A - D	3.89	148.8	8.6	3.54	1.61
		D - B	4.73	136.2	9.7	3.35	3.32
		B - C	3.81	175.2	6.4	3.46	1.58
3	$[Sm_3(\mathbf{L_{ser}})_8(OEt)]\cdot(H_2O, EtOH)_x$	C - A	3.56	58.5	7.1	3.53	0.44
		A - D	3.95	146.6	8.9	3.54	1.73
		D - B	4.85	138.3	9.2	3.30	3.53
		B - C	3.87	174.0	7.6	3.48	1.68
4	$[Eu_3(\mathbf{L_{ser}})_8(OEt)]\cdot(H_2O, EtOH)_x$	C - A	3.56	58.1	6.3	3.53	0.47
		A - D	3.95	146.4	9.0	3.54	1.74
		D - B	4.89	139.3	10.5	3.28	3.60
		B - C	3.93	174.0	8.4	3.49	1.78
5	$[Gd_3(\mathbf{L_{ser}})_8(OEt)]\cdot(H_2O, EtOH)_x$	C - A	3.55	58.4	6.5	3.52	0.43
		A - D	3.94	146.3	8.4	3.52	1.73
		D - B	4.89	138.8	10.6	3.30	3.58
		B - C	3.90	173.9	7.5	3.48	1.74
6	$[Tb_3(\mathbf{L_{ser}})_8(OEt)]\cdot(H_2O, EtOH)_x$	C - A	3.56	57.9	6.7	3.53	0.47
		A - D	3.96	145.9	9.2	3.52	1.77
		D - B	4.92	139.2	11.0	3.30	3.62
		B - C	3.93	173.1	7.7	3.49	1.78
7	$[Dy_3(\mathbf{L_{ser}})_8(OEt)]\cdot(H_2O, EtOH)_x$	C - A	3.55	57.9	7.1	3.52	0.35
		A - D	3.93	146.3	7.4	3.50	1.77
		D - B	4.89	139.2	9.8	3.29	3.60
		B - C	3.90	172.8	7.3	3.49	1.71
8	$[Ce_{2.3}Tb_{0.7}(\mathbf{L_{ser}})_8(OH)]\cdot(H_2O, EtOH)_x$	C - A	3.51	58.4	5.7	3.48	0.40
		A - D	3.92	147.2	9.3	3.52	1.70
		D - B	4.84	139.4	12.1	3.35	3.46
		B - C	3.85	173.9	7.2	3.40	1.80
9	$[Gd_{0.4}Tb_{2.6}(\mathbf{L_{ser}})_8(OEt)]\cdot(H_2O, EtOH)_x$	C - A	3.56	57.8	6.6	3.53	0.45
		A - D	3.95	146.1	9.7	3.53	1.75
		D - B	4.89	138.9	11.2	3.28	0.65
		B - C	3.91	173.6	7.8	3.49	1.75
10	$[Ce_{1.4}Gd_{0.3}Tb_{1.3}(\mathbf{L_{ser}})_8(OH)]\cdot(H_2O, EtOH)_x$	C - A	3.56	58.7	6.1	3.53	0.47
		A - D	3.90	146.5	9.5	3.56	1.58
		D - B	4.85	138.1	10.5	3.36	3.48
		B - C	3.86	173.5	6.4	3.47	1.69

4.4. The experimental susceptibilities obtained by zero-field cooling at 1000 Oe (Figure 4.4, Table 4.4) were as expected for each of the metals in an isolated environment. Fitting the data to the Curie-Weiss law yields effective magnetic moments of 2.26, 7.62, 9.22, 6.67, 8.16 and 6.90 μ_B, respectively, which are in good agreement with the expected values of 2.54, 7.94, 9.72, 6.89, 9.50 and 7.09 μ_B.[22] There are no indications of interactions between the metals despite the extensive oxygen bridging groups in the structures. Compound **2** shows deviation from simple paramagnetic behavior in the form

of antiferromagnetic ordering below 50 K. For the mixed-metal lanthanides, the total susceptibilities are equal to that expected for the sum of each of the metals present, taking into account the make-up of the mixture, as determined via ICP-MS. Only $[Gd_{0.4}Tb_{2.6}(\mathbf{L_{ser}})_8(OEt)]\bullet(H_2O, EtOH)_x$ deviates somewhat, but in this measurement there was only a small amount of sample available, lowering the accuracy of the result.

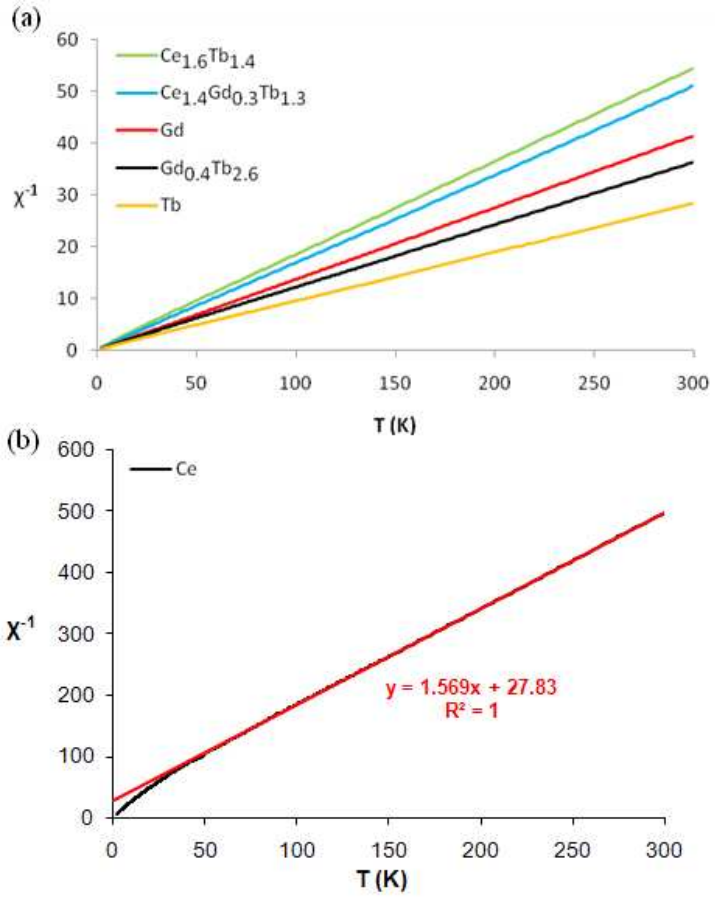

Figure 4.4. (a) Inverse susceptibilities, χ_m^{-1}, measured in an applied field of 1000 Oe. (b) Inverse susceptibility data for the Ce complex with a nonlinear deviation below 50 K.

Table 4.4. Magnetic moments (μ_{exp}) of all the compounds calculated from the inverse susceptibility, expected theoretical moment ($\mu_{calc,}$ calculated for the mixed-metal complexes using the molar ratios based on the ICP-MS measurements), and paramagnetic Curie-Weiss temperature, θ (K).

Compound	$\mu_{exp}(\mu_B/F.U.)$	$\mu_{calc}(\mu_B/F.U.)$	θ (K)
$[Ce_3(\mathbf{L_{ser}})_8(OH)(H_2O)]\bullet(H_2O, EtOH)_x$	2.26	2.54	-17.7
$[Gd_3(\mathbf{L_{ser}})_8(OEt)]\bullet(H_2O, EtOH)_x$	7.62	7.94	0.0
$[Tb_3(\mathbf{L_{ser}})_8(OEt)]\bullet(H_2O, EtOH)_x$	9.22	9.72	-2.1
$[Ce_{1.6}Tb_{1.4}(\mathbf{L_{ser}})_8(OH)]\bullet(H_2O, EtOH)_x$	6.67	6.89	-2.6
$[Gd_{0.4}Tb_{2.6}(\mathbf{L_{ser}})_8(OEt)]\bullet(H_2O, EtOH)_x$	8.16	9.50	-1.3
$[Ce_{1.4}Gd_{0.3}Tb_{1.3}(\mathbf{L_{ser}})_8(OH)]\bullet(H_2O, EtOH)_x$	6.90	7.09	-1.0

Luminescence. With one exception, all of the compounds exhibit solid-state luminescence dominated by the naphthalimide chromophore in the ligand. For all cases, a blue-green emission is observed where the maximum is red-shifted with respect to the ligand which is typical for ligand to metal charge transfer (LMCT). Surprisingly, these results are different from all of the group 1 and 2 complexes prepared with the $\mathbf{L_{ser}}^-$ ligand, where the maxima are blue-shifted with respect to the ligand. The emission spectra for all of the pure metal compounds (**1**-**7**) are identical ($[Gd_3(\mathbf{L_{ser}})_8(OEt)]\bullet(H_2O, EtOH)_x$ shown in Figure 4.5) with the exception of the cerium(III) and europium(III) compounds (**2** and **4**). Compound **4** has an additional peak at ~615 nm originating from a sensitized europium(III) emission as seen in Figure 4.8.

The cerium(III) compound **2** has no solid state emission. To investigate the impact of cerium(III) doping on the naphthalimide emission of the other complexes, a series of mixed-metal compounds with varying ratios of cerium(III) and terbium(III)

were synthesized and fully characterized. Figure 4.6 shows how the characteristic solid-state naphthalimide emission spectra is quenched upon doping with cerium(III). To quantitate these observations, *absolute quantum yields* in the solid-state of these mixed-metal and the pure metal complexes were measured on an Edinburgh SpectroFluorometer FS5 (Table 4.5). The pure Tb compound has the greatest quantum yield of 13.3 ± 1.0%, while the Ce compound excited at the same wavelength (300 nm) has a quantum yield of 0.2 ± 0.2 %. All of the compounds containing a mixture of these two metals have a quantum yield of less than 1.7 % except for one which has 90% Tb and a quantum yield of 4.5 ± 0.2 %.

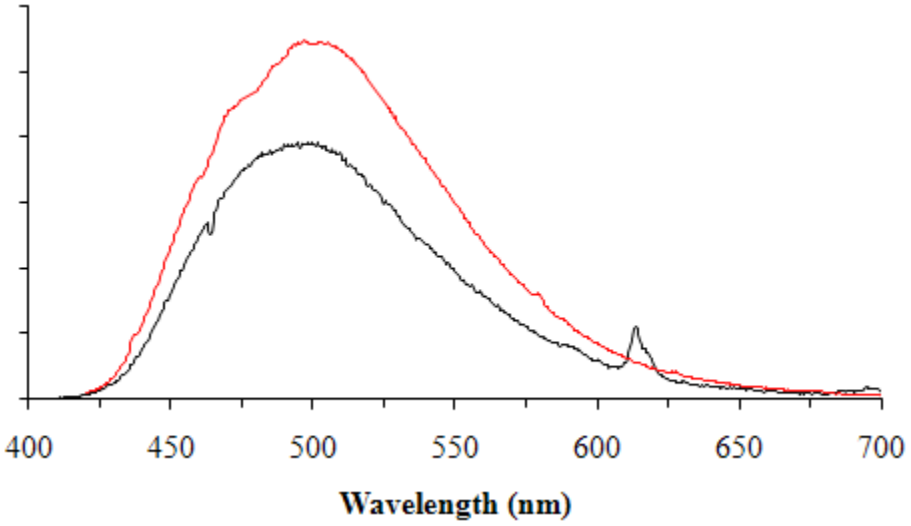

Figure 4.5. Emission spectrum for $[Gd_3(\mathbf{L_{ser}})_8(OEt)]\bullet(H_2O, EtOH)_x$ (**5**, red) and $[Eu_3(\mathbf{L_{ser}})_8(OEt)]\bullet(H_2O, EtOH)_x$ (**4**, black).

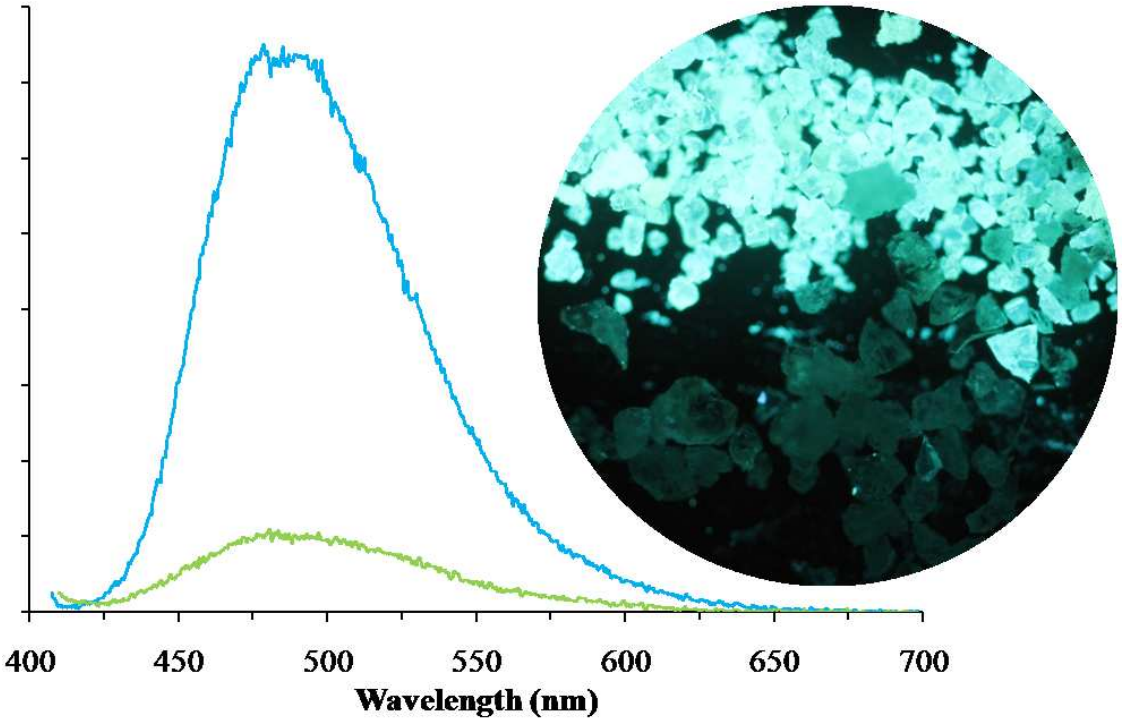

Figure 4.6. Emission spectra for $[Tb_3(\mathbf{L_{ser}})_8(OEt)]\bullet(H_2O, EtOH)_x$ (blue) and $[Ce_{0.7}Tb_{2.3}(\mathbf{L_{ser}})_8(OH)]\bullet(H_2O, EtOH)_x$ (green), The inset is the emission of crystals of $[Tb_3(\mathbf{L_{ser}})_8(OEt)]\bullet(H_2O, EtOH)_x$ on top and $[Ce_{0.7}Tb_{2.3}(\mathbf{L_{ser}})_8(OH)]\bullet(H_2O, EtOH)_x$ on the bottom.

Table 4.5. Absolute Quantum Yield Data.

Metal Ratios	QY (%)
Tb_3	13.3 ± 1.02
$Ce_{0.3}Tb_{2.7}$	4.5 ± 0.21
$Ce_{0.7}Tb_{2.3}$	1.7 ± 0.18
$Ce_{1.6}Tb_{1.4}$	1.6 ± 0.18
$Ce_{1.9}Tb_{1.1}$	0.9 ± 0.10
$Ce_{2.4}Tb_{0.6}$	0.3 ± 0.11
Ce_3	0.2 ± 0.29

Discussion

We have prepared a series of compounds from several lanthanide(III) metals (La, Ce, Sm, Eu, Gd, Tb, Dy) and the $\mathbf{L_{ser}}^-$ ligand (Scheme 4.1). Complexes containing two or more metals were also prepared. In our previous work with group 1 and 2 compounds, 1D homochiral helical rod-shaped SBUs dominated the covalently bonded part of the structures, but with the lanthanide metals discrete homochiral helicate SBUs are formed. All of the complexes with group 1 and 2 metals had at least one dimension of the structure held together by covalent interactions, whereas the lanthanide(III) solid state extended structures are held together solely by $\pi^{\cdots}\pi$ stacking. All of the lanthanides studied form a single structural type: trinuclear helicates held together by the $\mathbf{L_{ser}}^-$ ligands, which interact with adjacent helicates through π-stacking interactions. In this case, the helicates are organized along the *c*-axis into *homochiral helices* with an average pitch of 56 Å, *exclusively by $\pi^{\cdots}\pi$ stacking interactions.* We have observed a similar structural arrangement once previously in $[Zn(L^*_{ala})_2(bipyridine)(H_2O)_2]\bullet 4.74H_2O$,[4] although the structures are more complex with the lanthanide complexes. These lanthanide structures are very unusual because each helicate is part of two helices creating multiple pairs of *intertwined helices*.

The chirality from the ligands is expressed through the supramolecular arrangement of helicates into homochiral *M* helices. It is interesting that despite the oxophilic nature of lanthanide(III) metals, not all of the alcohol moieties present in the ligands are bonded to the metals. The complexes with lanthanides are the first cases where there is deprotonated solvent as part of the SBU with the class of ligands shown in Scheme 4.1: OH^- in **1**, **2**, **8** and **10,** and EtO^- for the rest of the complexes. We attribute

these latter two results to the bulkiness of the ligands coupled with the higher charge of the metals that increases the ligand/metal ratio. All of the structures have cavities occupied by disordered solvent molecules.

Very recently, lanthanides complexes of our achiral $\mathbf{L_{C1}}^-$ and $\mathbf{L_{C2}}^-$ ligands (Scheme 4.1), $[Ln(\mathbf{L}_{C1})_3(CH_3OH)(H_2O)]_n$ and $[Ln(\mathbf{L}_{C2})_3(H_2O)]_n \bullet H_2O_x$ (Ln = Eu & Gd), have been prepared and structurally characterized by Yan et al.[13] The structures of these complexes are built on rod-shaped SBUs similar to our compounds with group 1 and 2 metals,[8,9] but very different from compounds **1**-**10**. The presence of the alcohol moiety in the ligand side-chain, an additional potential donor group, leads to discrete trinuclear helicate SBUs in the compounds reported here.

ICP-MS, single crystal XRD and EDS confirm that the mixed-metal crystals contain a disordered mixture of the metals across all positions in the same structure type as the pure metal complexes. Although a breadth of Ln^{3+} ratios for the mixed-metal complexes were observed, there appears to be a preference for some metals over others in the crystallization process. No mixed-metal complexes were synthesized for dysprosium(III) despite attempted syntheses containing dysprosium and other lanthanides (Ce, Tb, & Eu), possibly due to crystallization problems (only crystalline products were analyzed in these studies). In the three examples of mixed metal gadolinium(III) compounds, the percentage of that metal in the resulting products is much lower than in the reactants used. Thus, Gd was found to be more difficult to incorporate into the structure despite other cations of similar size and charge easily forming mixed complexes. Ce and Tb readily formed mixed metal species, with a slight preference for Tb. The other metals preferences are about equal. For all of the mixed-metal species there

is a slight preference for the larger of the cations to be located at the central M2 site of the trinuclear helicate.

The flexible nature of the π-stacking interactions likely contributes to the wide range of metals that can be incorporated into the same structure type for **1-7** and the mixed-metal complexes **8-10**. Several trends can be observed across the trinuclear lanthanide complexes. As the size of the cation changes, from 1.03 Å in the case of La^{3+} to 0.91 Å in the case of Dy^{3+}, the pi stacking parameters change, most notably the slippage parameter and the dipole angle. The two types of stacking are along the crystallographic *c* axis (C – A stacking) and across the *ab*-plane (A – D, D – B and B – C). The slippage parameters of the C ligand (Table 4.3) are the most affected by change in cation size while the rest of the parameters remain relatively unchanged. The slippage parameters of the C ligand change from 0.35 Å and 1.71 Å in the case of the smallest cation, Dy^{3+}, to 0.66 Å and 1.58 Å in the case of the largest cation, La^{3+}. The C ligand is likely more flexible because it serves only as a capping ligand to the helicates, the carboxylate is κ^1, κ^1 chelating to a single lanthanum(III) cation. The movement of the other ligands is more restricted because they bridge two or three metals.

Magnetic measurements of several compounds were collected and found to display the expected paramagnetic properties. No significant interactions between metals within the helicates or between helicates were observed. The magnetic susceptibilities very closely match those predicted based on the metals used for the homo-metallic compounds. For the hetero-metallic compounds, the total magnetic susceptibility is equal to the sum of each individual metal's susceptibilities and these metal ratios match those from the ICP-MS. The only deviation from normal Curie paramagnetic behavior is

observed in the Ce compound **2**, where, below 50 K, there is antiferromagnetic ordering most likely arising from intramolecular magnetic coupling.

Previous complexes with group 1 and 2 metals yielded solids that exhibited luminescence most closely resembling that of the protonated naphthalimide ligand. Complexes with $\mathbf{L_{ser}^-}$ were consistently blue shifted with respect to the ligand whereas the complexes with $\mathbf{L_{ala}^-}$ were red shifted; red shifting is typical for ligand to metal charge transfer (LMCT). The $\mathbf{L_{ser}^-}$ complexes with lanthanide metals are also red shifted. Despite the 1,8-naphthalimide group being a good sensitizer for white light emission in some cases,[13,15] the lanthanide luminescence was completely overwhelmed by the organic luminescence in our complexes. The europium(III) complex is an outlier with a sensitized europium emission peak, resolved at 613 nm, which was far enough away from the blue-green emission of the ligand to be observed.

The Ce complex **2** is non-emissive and heterometallic complexes containing cerium(III) were found to have a much lower quantum yield than others without it. In order to study the effect of cerium(III) on naphthalimide emission, a series of complexes with different concentrations of Ce/Tb were prepared and the resulting ratios determined from ICP-MS. The absolute quantum yield (solid state) for the pure terbium(III) complex is 13.3 ± 1.0 %, but once 10% cerium(III) was incorporated the quantum yield dropped to 4.5 ± 0.2 %. As more cerium(III) is doped into the complex and the statistical likelihood of there being at least one cerium(III) cation per helicate increases, the quantum yield drops significantly until reaching 0.2 ± 0.2 %. The fluorescence quenching mechanism is most likely due to a charge transfer relaxation similar to those observed with transition metals.[23,24]

References

(1) Reger, D. L.; Debreczeni, A.; Reinecke, B.; Rassolov, V.; Smith, M. D.; Semeniuc, R. F. *Inorg. Chem.* **2009**, *48* (18), 8911–8924.

(2) Reger, D. L.; Sirianni, E.; Horger, J. J.; Smith, M. D.; Semeniuc, R. F. *Cryst. Growth Des.* **2010**, *10* (1), 386–393.

(3) Reger, D. L.; Horger, J. J.; Debreczeni, A.; Smith, M. D. *Inorg. Chem.* **2011**, *50* (20), 10225–10240.

(4) Reger, D. L.; Horger, J. J.; Smith, M. D.; Long, G. J.; Grandjean, F. *Inorg. Chem.* **2011**, *50* (2), 686–704.

(5) Reger, D. L.; Debreczeni, A.; Smith, M. D. *Inorg. Chem.* **2011**, *50* (22), 11754–11764.

(6) Reger, D. L.; Debreczeni, A.; Horger, J. J.; Smith, M. D. *Cryst. Growth Des.* **2011**, *11* (9), 4068–4079.

(7) Reger, D. L.; Debreczeni, A.; Smith, M. D.; Jezierska, J.; Ozarowski, A. *Inorg. Chem.* **2012**, *51* (2), 1068–1083.

(8) Reger, D. L.; Leitner, A.; Smith, M. D.; Tran, T. T.; Halasyamani, P. S. *Inorg. Chem.* **2013**, *52* (17), 10041–10051.

(9) Reger, D. L.; Leitner, A.; Pellechia, P. J.; Smith, M. D. *Inorg. Chem.* **2014**, *53* (18), 9932–9945.

(10) Reger, D. L.; Leitner, A.; Smith, M. D. *J. Mol. Struct.* **2015**, *1091*, 31–36.

(11) Eddaoudi, M.; Moler, D. B.; Li, H.; Chen, B.; Reineke, T. M.; Keeffe, M. O.; Yaghi, O. M. *Acc. Chem. Res.* **2001**, *34* (4), 319–330.

(12) Abuo-Rahma, G. E. D. A. A.; Sarhan, H. A.; Gad, G. F. M. *Bioorganic Med. Chem.* **2009**, *17* (11), 3879–3886.

(13) Zhang, J.; Li, H.; Chen, P.; Sun, W.; Gao, T.; Yan, P. *J. Mater. Chem. C* **2015**, *3* (8), 1799–1806.

(14) Zhang, H.; Shan, X.; Zhou, L.; Lin, P.; Li, R.; Ma, E.; Guo, X.; Du, S. *J. Mater. Chem. C* **2013**, *1* (5), 888–891.

(15) Bonnet, C. S.; Devocelle, M.; Gunnlaugsson, T. *Org. Biomol. Chem.* **2012**, *10* (1), 126.

(16) Shelton, A. H.; Sazanovich, I. V.; Weinstein, J. A.; Ward, M. D. *Chem. Commun.* **2012**, *48* (22), 2749.

(17) Lam, A. W.-H.; Wong, W.-T.; Gao, S.; Wen, G.; Zhang, X.-X. *Eur. J. Inorg. Chem.* **2003**, *2003* (1), 149–163.

(18) Yang, X.; Jones, R. A.; Huang, S. *Coord. Chem. Rev.* **2014**, *273-274*, 63–75.

(19) Wang, L. J.; Deng, H.; Furukawa, H.; Ga, F.; Cordova, K. E.; Peri, D.; Yaghi, O. M. *Inorg. Chem.* **2014**, *53*, 5881–5883.

(20) White, K. A.; Chengelis, D. A.; Gogick, K. A.; Stehman, J.; Rosi, N. L.; Petoud, S. *J. Am. Chem. Soc.* **2009**, *131* (50), 18069–18071.

(21) An, J.; Shade, C. M.; Chengelis-Czegan, D. A.; Petoud, S.; Rosi, N. L. *J. Am. Chem. Soc.* **2011**, *133* (5), 1220–1223.

(22) Greenwood, N. N.; Earnshaw, A. *Chemistry of the Elements*, 2nd ed.; Butterworth-Heinemann, 1997.

(23) Setlur, A. A; Shiang, Joseph, J. *J. Phys. Chem. C* **2010**, *114*, 2792–2798.

(24) Shakhverdov, T. A. *Opt. Spectrosc.* **2003**, *95* (4), 571–580.

Chapter V

Supramolecular Metal-Organic Frameworks of s- and f-Block Metals: Impact of 1,8-Naphthalimide Functional Group

Introduction

Metal-Organic Frameworks (MOFs), highly organized networks of organic ligands coordinated to metal secondary building units (SBUs) to create multidimensional structures, provide an excellent system for examining the coordination environments of the "hard" group 2 and "inner" transition metals interacting with bulky polytopic ligands.[1–7] The organic bridging ligands can be ornamented with functional groups that impart new properties on the materials.[8–10] The bulky 1,8-naphthalimide functional group is both an excellent chromophore and flexible supramolecular tecton.[3,4,11–14] MOFs prepared from ligands containing this group (Scheme 5.1) provide an excellent strategy to arrange organic photosensitizers in proximity to metal cations in an effort to create sensitized luminescent materials.[5–7,15,16]

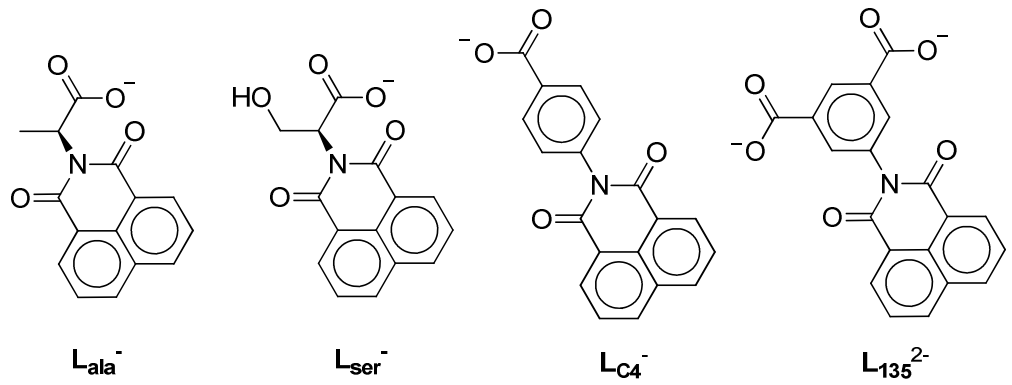

Scheme 5.1. Multifunctional Ligands

We have previously synthesized a series of ligands (for example, $\mathbf{L_{ala}^-}$, $\mathbf{L_{ser}^-}$ and $\mathbf{L_{C4}^-}$ in Scheme 1) derived from amino acids containing the 1,8-naphthalimide supramolecular tecton and several points of connectivity including a single

carboxylate.[3,11,15,17,18] When combined with group 1, 2 and transition metals, a variety of structural types were formed ranging from completely covalent three-dimensional (3D) structures[11] to those that are partially[3] or completely[15] organized by π···π stacking supramolecular interactions. We have referred to structures organized in one or more dimension by noncovalent forces as Supramolecular Metal-Organic Frameworks (SMOFs).[12–14,19,20] When the ligand $\mathbf{L_{ser}}^-$ is combined with group 1 and 2 metals, 1D helical rods of corner, edge, and/or face-shared cations are formed where the naphthalimide supramolecular synthon organizes the rods into SMOFs.[3,11,18] In one case, [Cs($\mathbf{L_{ser}}$)], the ligand excludes coordinating solvent (ethanol and water) from the oxophilic cesium cations. This exclusion of solvent is of particular interest because solvent molecules coordinated to lanthanide cations can quench fluorescence.[21,22] For a series of complexes with the formula $[Ln_3(OR)(\mathbf{L_{ser}})_8]\bullet(H_2O, EtOH)_x$ (Ln = Sm, Eu, Gd, Tb and Dy), a single structure type was formed and mixed metals complexes could be prepared with some degree of control of the mixture. The luminescence properties of these compounds were studied and in most cases the naphthalimide emission completely dominated the spectrum, but in the case of Eu^{3+} some sensitization occurs. Interestingly, the Ce^{3+} complex quenches luminescence, so a quantum yield study on mixed metal species was conducted that elucidated a charge transfer mechanism between Ce^{3+} and the naphthalimide ring.[15]

Actinide usage in MOF materials has been seldom studied due to the diverse topologies and coordination environments.[23–29] The coordination environments of actinide metals are of particular interest because of the applications in designing extracting agents and novel fuel precursors.[30] The uranyl cation (UO_2^{2+}) is an excellent fluorophore with

well resolved emission peaks and has a consistent linear O=U=O moiety, but is rare as an SBU in MOF materials.[30,31] The thorium cation (Th^{4+}) is even more rare than uranyl in the study of MOF architectures and the comparison of the different coordination environments can help with separations studies.[23,26,29]

Reported here are the syntheses and the solid state crystal structures of a series of complexes of a new ligand, containing the naphthalimide group and two carboxylate groups ($\mathbf{L_{135}}^{2-}$), with a series of oxophilic metals (Ca^{2+}, Ba^{2+}, La^{3+}, Ce^{3+}, Eu^{3+}, Tb^{3+} UO_2^{2+} and Th^{4+}). Structural similarities and differences arise among the different metals. All of the compounds have at least one dimension organized by the 1,8-naphthalimide supramolecular synthon. The fluorescence spectra for all compounds were studied and compared to those of the protonated ligand, $H_2\mathbf{L_{135}}$. No fluorescence was observed for $Ce_2(\mathbf{L_{135}})_3(DMF)_4$ and $[UO_2(\mathbf{L_{135}})(DMF)]\cdot(py)_{0.5}(EtOH)_{0.5}$, despite the presence of multiple fluorophores.

Experimental

General Considerations

All reactants were used as purchased from Aldrich and Strem. Elemental analyses were performed by Robertson Microlit Laboratories (Ledgewood, NJ) on samples dried to constant weight. ^{1}H NMR spectra were recorded on a Bruker 300 MHz spectrometer. The fluorescence measurements were carried out on an Edinburgh Spectrofluorometer FS5. The emission spectra were measured with a 400 nm excitation wavelength in all cases except for compound **6**, $Tb_2(\mathbf{L_{135}})_3(DMF)_4$, which used a 507 nm wavelength. Caution: Uranyl nitrate hexahydrate and thorium nitrate hydrate are radioactive materials. All

standard precautions for handling radioactive and highly toxic substances should be followed.

Synthesis of $H_2\mathbf{L_{135}}$

1,8-Naphthalic anhydride (1.98 g, 10.0 mmol) and 3-aminoisophthalic acid (2.18 g, 12.0 mmol) were stirred in dimethylformamide (120 mL) and heated under reflux conditions overnight. The hot reaction mixture was added to ice and the resulting precipitate gravity filtered and dried in vacuo. The cream colored solid was added to a solution of methanol (100 mL) containing triethylamine (1.50 g, 14.8 mmol) and stirred for 1 hour. Impurities were separated via gravity filtration and the remaining homogeneous brown solution acidified with 3 *M* HCl and let rest overnight. The precipitate was collected and washed with methylene chloride (2 x 50 mL) to provide a white solid that was dried in vacuo to yield 2.84 g (7.86 mmol, 79 % yield) of product. HRMS: ES^+ (*m*/*z*): Calcd. for $[C_{20}H_{12}NO_6]^+$ 362.0665; found 362.0662. ^{1}H NMR (DMSO-d_6, 300 MHz) δ 7.92 (t, 2H, napht), 8.25 (d, 2H, phen), 8.508 (s, 1H, phen), 8.53 (d, 2H, napht), 8.56 (t, 2H, napht), 9.90 (s, 2H, -COOH). Anal. Calcd. (Found) for $C_{20}H_{11}NO_6$: C 66.49 (66.05); H 3.07 (3.58); N 3.88 (4.15).

*Synthesis of $[Ca_4(\mathbf{L_{135}})_4(H_2O)_8]\cdot(H_2O)_{9.5}(DMF)_{2.6}$ **(1)***

$H_2\mathbf{L_{135}}$ (0.520 g, 1.44 mmol) was added to a solution of calcium hydroxide (0.120 g, 1.60 mmol) in a 1:1 mixture of water and methanol (100 mL) and heated under refluxing conditions for 1 hour. The heat was removed and the yellow solid was collected and washed with water and dried in vacuo to collect 0.487 g of product. A 9 mL thick walled

glass tube with a Teflon screw top was charged with a sample of this solid (0.050 g), dimethylformamide (1.5 mL) and water (1.5 mL) and heated in an oil bath at 120 °C. Over the course of 1 day colorless block crystals grew on the walls of the reaction vessel above the solvent line. The heat was removed and the crystals were collected from the tube and dried over filter paper to provide 0.043 g of **1** in a 55% yield. Anal. Calcd. (Found) for $C_{86}H_{54}Ca_4N_6O_{28}$: C 58.04 (57.55); H 3.06 (2.88); N 4.72 (5.39).

Synthesis of $Ba(\mathbf{L_{135}})(H_2O)_{1.5}(DMF)_{0.5}$ ***(2)***

Compound **2** was synthesized in a similar manner to compound **1** but with barium hydroxide (0.240 g, 1.40 mmol) and no water to give a white precipitate (0.320 g). The solid was heated under solvothermal conditions similar to compound **1** to yield colorless plate crystals (0.040 g) in a 33% yield. Anal. Calcd. (Found) for $C_{21.5}H_{15.5}BaN_{1.5}O_8$: C 46.10 (46.23); H 2.79 (2.75); N 3.75 (3.57).

Synthesis of $La_2(\mathbf{L_{135}})_3(DMF)_4$ ***(3)***

A 9 mL thick walled glass tube with a Teflon screw top was charged with lanthanum nitrate (0.090 g, 0.28 mmol), $H_2\mathbf{L_{135}}$ (0.037 g, 0.10 mmol), dimethylformamide (1.5 mL) and ethanol (0.5 mL) and heated in an oil bath at 100 °C. Colorless plate crystals grew overnight on the walls of the reaction vessel below the solvent line. The heat was removed and the crystals were collected from the tube, washed with methanol and dried over filter paper to provide 0.054 g of single crystals of **3** in a quantitative yield. Anal. Calcd. (Found) for $C_{72}H_{55}La_2N_7O_{22}$: C 52.47 (52.36); H 3.36 (3.35); N 5.95 (6.17).

*Synthesis of $Ce_2(\mathbf{L_{135}})_3(DMF)_4$ (**4**)*

Compound **4** was synthesized in a similar manner to compound **3** but with cerium(III) nitrate (0.096 g, 0.22 mmol). The resulting irregular yellow crystals were collected and washed with methanol to yield 0.040 g of **4** in a quantitative yield. Anal. Calcd. (Found) for $C_{72}H_{55}Ce_2N_7O_{22}$: C 52.40 (51.84); H 3.36 (3.05); N 5.94 (5.92).

*Synthesis of $Eu_2(\mathbf{L_{135}})_3(DMF)_4$ (**5**)*

Compound **5** was synthesized in a similar manner to compound **3** but with europium(III) nitrate (0.040 g, 0.093 mmol). The resulting colorless plate-like crystals were collected and washed with methanol to yield 0.040 g of **5** in a quantitative yield. Anal. Calcd. (Found) for $C_{72}H_{55}Eu_2N_7O_{22}$: C 51.66 (51.58); H 3.31 (3.11); N 5.86 (5.66).

*Synthesis of $Tb_2(\mathbf{L_{135}})_3(DMF)_4$ (**6**)*

Compound **6** was synthesized in a similar manner to compound **3** but with terbium(III) nitrate (0.040 g, 0.092 mmol). The resulting colorless plate-like crystals were collected and washed with methanol to yield 0.034 g of **6** in a quantitative yield. Anal. Calcd. (Found) for $C_{72}H_{55}Tb_2N_7O_{22}$: C 51.23 (51.08); H 3.28 (3.17); N 5.81 (5.76).

*Synthesis of $[UO_2(\mathbf{L_{135}})(DMF)]\cdot(py)_{0.5}(EtOH)_{0.5}$ (**7**)*

A 9 mL thick walled glass tube with a Teflon screw top was charged with uranyl nitrate (0.010 g, 0.025 mmol), $H_2\mathbf{L_{135}}$ (0.010 g, 0.028 mmol), dimethylformamide (1.5 mL), ethanol (0.5 mL) and pyridine (0.1 mL, 1.24 mmol) and heated in an oil bath at 120 °C. Over the course of 3 days yellow prism crystals grew on the walls of the reaction vessel

below the solvent line. The heat was removed and the crystals were collected from the tube, washed with methanol and dried over filter paper to provide 0.011 g of **7** in a 57% yield.

*Synthesis of [Th(**L**$_{135}$)(NO$_3$)$_2$(DMF)$_2$]·(DMF)$_2$ (**8**)*

A 9 mL thick walled glass tube with a Teflon screw top was charged with thorium nitrate (0.015 g, 0.031 mmol), H$_2$**L**$_{135}$ (0.020 g, 0.056 mmol), dimethylformamide (2 mL) and heated in an oil bath at 120 °C. Over the course of 3 days colorless plate crystals grew on the walls of the reaction vessel above the solvent line. The heat was removed and the crystals were collected from the tube, washed with methanol and dried over filter paper to provide 0.004 g of **8** in a 15% yield.

Table 5.1. Crystallography Data

	1	**2**	**3**	**4**
Formula	$C_{87.74}H_{89.1}Ca_4N_{6.58}O_{44.1}$	$C_{21.5}H_{15.5}BaN_{1.5}O_8$	$C_{72}H_{55}La_2N_7O_{22}$	$C_{72}H_{55}Ce_2N_7O_{22}$
Fw, g mol^{-1}	2101.75	560.19	1648.05	1650.47
Cryst. Syst.	triclinic	triclinic	orthorhombic	orthorhombic
Space group	*P*-1	*P*-1	*P*bcn	*P*bcn
T, K	100(2)	100(2)	100(2)	100(2)
a, Å	13.7978(8)	8.5215(16)	10.2418(8)	10.2277(10)
b, Å	18.3385(11)	8.6517(17)	34.742(3)	34.658(3)
c, Å	18.3572(11)	14.105(3)	19.1634(15)	19.1299(19)
α, deg	101.000(2)	97.693(4)	90	90
β, deg	91.968(2)	102.534(4)	90	90
γ, deg	92.246(2)	104.882(4)	90	90
V, Å^3	4552.0(5)	961.0(3)	6818.7(9)	6780.9(12)
Z	2	2	4	4
$R_1(I>2\sigma(I))$[a]	0.0523	0.0376	0.0596	0.0623
$wR_2(I>2\sigma(I))$[b]	0.1310	0.0740	0.1557	0.1648

	5	6	7	8
Formula	$C_{72}H_{55}Eu_2N_7O_{22}$	$C_{72}H_{55}Tb_2N_7O_{22}$	$C_{26.58}H_{21.47}N_{2.53}O_{9.47}U$	$C_{26}H_{23}N_5O_{14}Th$
Fw, g mol^{-1}	1674.15	1688.07	765.93	861.53
Cryst. Syst.	orthorhombic	Orthorhombic	monoclinic	triclinic
Space group	*P*bcn	*P*bcn	*I*2/a	*P*-1
T, K	100(2)	100(2)	100(2)	100(2)
a, Å	10.1619(5)	10.1594(7)	21.498(4)	9.0236(14)
b, Å	34.4601(16)	34.418(2)	16.531(4)	10.8046(17)
c, Å	19.0757(9)	18.9947(14)	16.688(3)	18.003(3)
α, deg	90	90	90	86.508(3)
β, deg	90	90	92.398(4)	87.408(3)
γ, deg	90	90	90	82.982(4)
V, $Å^3$	6679.9(6)	6641.9(8)	5925(2)	1737.6(5)
Z	4	4	8	2
$R_1(I>2\sigma(I))^a$	0.0567	0.0582	0.0501	0.0420
$wR_2(I>2\sigma(I))^b$	0.1371	0.1384	0.1429	0.0872

[a] $R1 = \Sigma ||F_o| - |F_c|| / \Sigma |F_o|$ [b] $wR2 = \{ \Sigma [w(F_o^2 - F_c^2)^2] / \Sigma [w(F_o^2)^2] \}^{1/2}$

Results and discussion

Synthesis. Naphthalic anhydride and 5-amino isophthalic acid were heated in DMF under reflux conditions to form the protonated ligand $H_2\mathbf{L_{135}}$. This compound when combined with $Ca(OH)_2$ and $Ba(OH)_2$ and heated under reflux conditions in 1:1, MeOH:H_2O or a pure MeOH solution precipitated salts of the ligand $Ca\mathbf{L_{135}}$ and $Ba\mathbf{L_{135}}$, respectively. After loading into high-pressure tubes partially submerged in an oil bath and heating under solvothermal conditions (DMF/water), single crystals of compounds $[Ca_4(\mathbf{L_{135}})_4(H_2O)_8]\cdot(H_2O)_{9.5}(DMF)_{2.6}$ (**1**) and $Ba(\mathbf{L_{135}})(H_2O)_{1.5}(DMF)_{0.5}$ (**2**) grew on the walls of the tubes. Heating mixtures of $H_2\mathbf{L_{135}}$ in DMF/ethanol with $La(NO_3)_3\cdot 6H_2O$, $Ce(NO_3)_3\cdot 6H_2O$, $Eu(NO_3)_3\cdot 5H_2O$ or $Tb(NO_3)_3\cdot 6H_2O$ produced single crystals of $La_2(\mathbf{L_{135}})_3(DMF)_4$ (**3**), $Ce_2(\mathbf{L_{135}})_3(DMF)_4$ (**4**), $Eu_2(\mathbf{L_{135}})_3(DMF)_4$ (**5**) and

$Tb_2(\mathbf{L_{135}})_3(DMF)_4$ (**6**), respectively, which grew on the walls of the solvothermal tubes below the solvent line. The reaction of uranyl nitrate with the protonated ligand $H_2\mathbf{L_{135}}$ under solvothermal conditions in a DMF/EtOH/pyridine solution yielded $[UO_2(\mathbf{L_{135}})(DMF)]\cdot(py)_{0.5}(EtOH)_{0.5}$ (**7**), which crystallized on the walls of the reaction vessel underneath the solvent line. Crystals of $Th(\mathbf{L_{135}})(NO_3)_2(DMF)_2]\cdot(DMF)_2$ (**8**) grew from the solvothermal reaction of thorium nitrate and $H_2\mathbf{L_{135}}$ in DMF.

Solid State structure of $[\mathbf{Ca_4(L_{135})_4(H_2O)_8}]\cdot\mathbf{(H_2O)_{9.5}(DMF)_{2.6}}$ (1). The irregular coordination environments for the calcium cations of compound **1** are shown in Figure 5.1. There are four unique ligands (A-D) and four unique calcium cations (Ca1-Ca4) per formula unit. The calcium cations are bridged into helical rods of edge-shared polyhedra through the carboxylates of the $\mathbf{L_{135}}^{2-}$ ligand (Figure 5.2). For each *P*-helical rod there is an adjacent *M*-helix generating a racemic mixture. All of the carboxylates are involved in μ-$\kappa^1\kappa^2$ bonding, with each ligand coordinating to four different metals along the same rod. Each of the calcium cations has an 8-coordinate geometry with 6 sites occupied by bridging carboxylates and the remaining two sites with water. The calcium cations differ in the disorder of the coordinated waters and the interactions with adjacent interstitial solvents. The two coordinated water molecules for Ca1 (O7 & O8) are ordered and the hydrogen atoms of the water molecules are modeled. The water O7 is a hydrogen bond donor to an interstitial water molecule and an interstitial DMF molecule. The water O8 is a hydrogen bond donor to a well ordered interstitial water molecule, which is locked in place by being a hydrogen bond donor to a carboxylate from ligand D and a carbonyl from ligand C coming from an adjacent rod. The two coordinated water molecules for Ca2 (O9 & O10) are both disordered over two positions and hydrogen atoms were not

modeled. The water O9 acts as a hydrogen bond acceptor with an interstitial DMF molecule. Of the two coordinated waters for Ca3, O11 is disordered over two positions and O12 is ordered and acts as a hydrogen bond donor to two different interstitial water molecules, one which is disordered and another that is locked in place by hydrogen bond interactions with a carboxylate from ligand B and a carbonyl from ligand A from an adjacent rod. Both of the coordinated waters (O13 & O14) for Ca4 are ordered and act as hydrogen bond donors for interstitial water molecules.

The four different naphthalimide rings of each rod are oriented in four directions perpendicular to the rod creating four nodes for supramolecular interactions with adjacent rods to build, along with the hydrogen bonding interactions, a 3D SMOF structure (Figure 5.3). The angles between each of the nodes from a given rod are as follows: ∠AD = 109º, ∠BC = 35º and ∠AB = ∠CD = 108º (Figure 2). Each of these nodes consists of an infinite stacking of naphthalimide rings contributed from four adjacent rods, two of which are *P*-helices and two of which are *M*-helices. The sequence of π···π stacking interactions is identical within each of the nodes, following the pattern ···D···A···B···C···D···A···. The parameters for each interaction in compound **1** are listed in Table 5.2. This three dimensional arrangement leaves four types of channels filled with solvent. Three of the channels are filled with slightly disordered interstitial solvent, an approximate 5:1 mixture of H_2O:DMF, and two water molecules coordinated to calcium cations. The second type of channel is filled with well ordered water hydrogen bonded to different coordinated ligands.

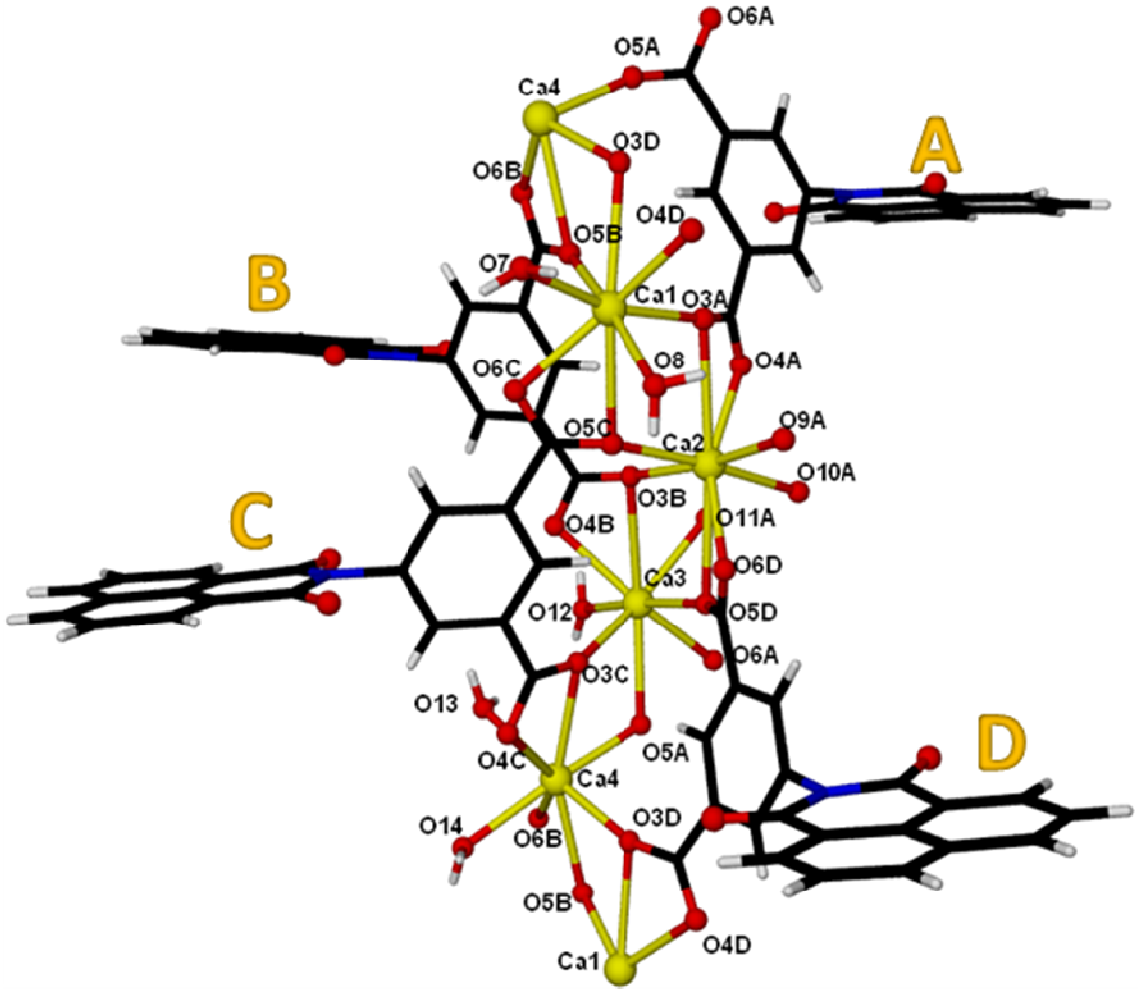

Figure 5.1. Coordination environment for the four unique calcium cations of $[Ca_4(\mathbf{L_{135}})_4(H_2O)_8]\cdot(H_2O)_{9.5}(DMF)_{2.6}$ **(1)**

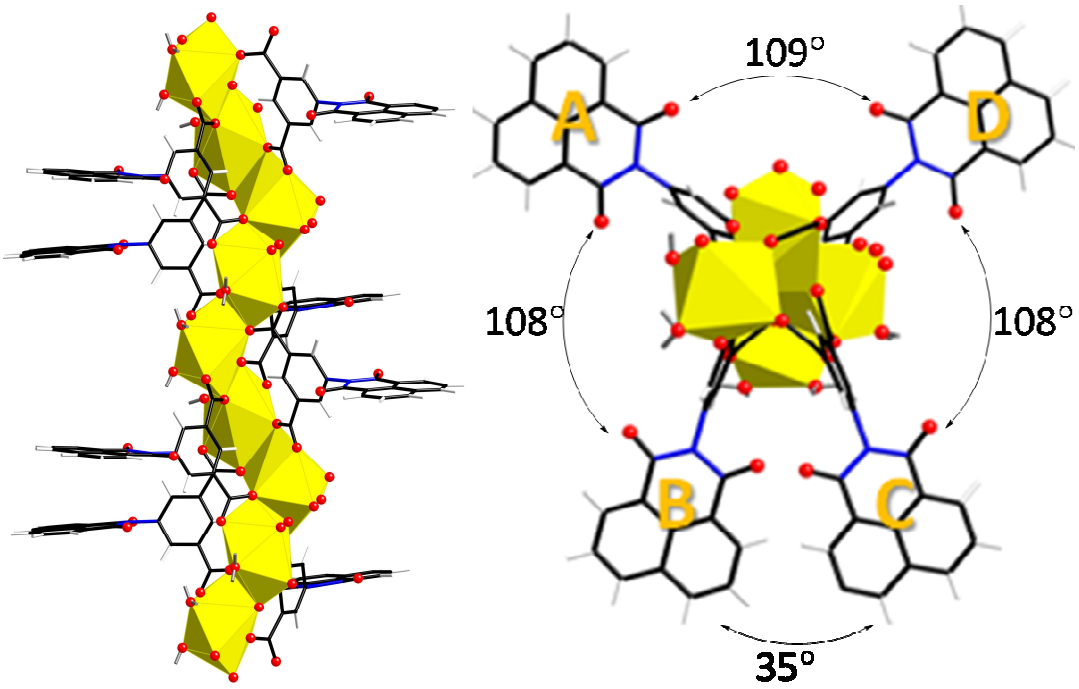

Figure 5.2. Two views of one-dimensional rods of compound **1.**

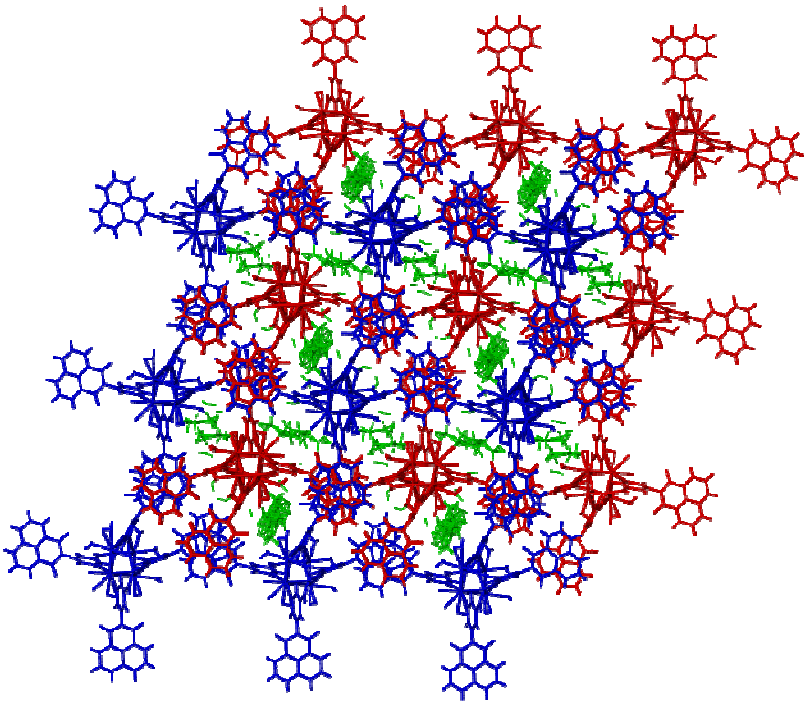

Figure 5.3. Three-dimensional structure of compound **1** where *P*-helices are red, *M*-helices are blue and uncoordinated interstitial solvent is green.

Solid State structure of Ba(L_{135})(H_2O)$_{1.5}$(DMF)$_{0.5}$ (2). The solid state structure of **2** consists of rod-shaped SBUs of edge-sharing 9-coordinate Ba^{2+} cations bridged by $\mathbf{L_{135}}^{2-}$ ligands into two dimensional sheets. Each barium cation is coordinated by 5 ligands, a water molecule and one site occupied by disordered water or dimethylformamide in a 50:50 ratio (Figure 5.4). The μ-$\kappa^1\kappa^2$ carboxylates bridge the cations into rod-shaped SBUs while the ligand connects adjacent rods on either side (Figure 5.5). The naphthalimide rings chelate the rods through the O2 carbonyl to a different Ba^{2+} cation along the chain. The naphthalimide rings on either side of the 2D sheets are able to engage in π···π stacking interactions with adjacent sheets to build a three-dimensional SMOF structure (Figure 5.6). The π···π stacking interactions for compound **2** are listed in Table 5.2. The coordinated DMF and water solvents are located between supramolecular synthons so that the sequence is …-ring-ring-solvent-ring-ring-solvent-….

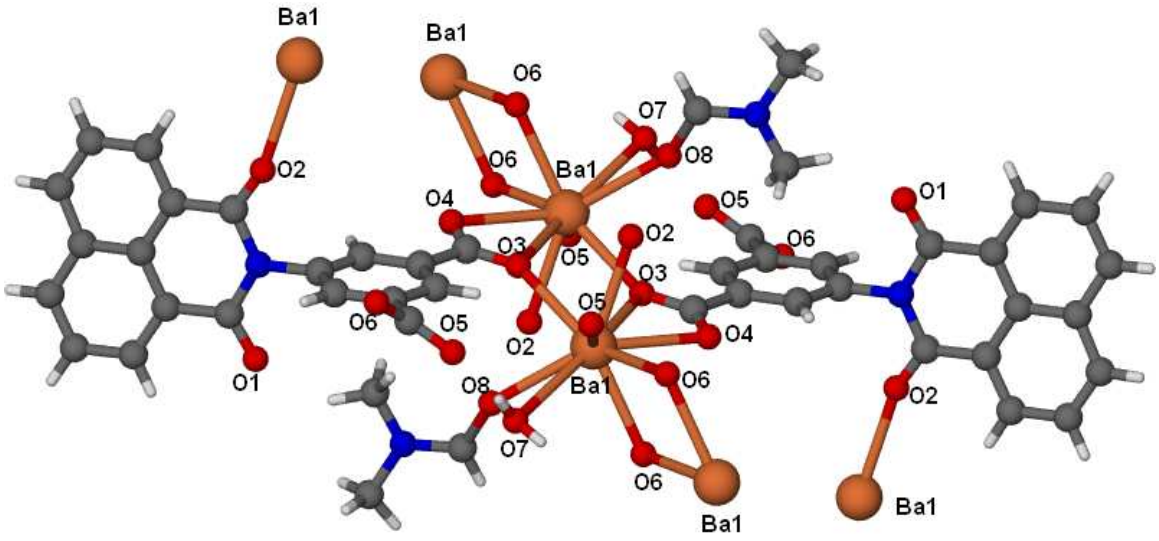

Figure 5.4. Coordination environment of Ba^{2+} and $\mathbf{L_{135}}^{2-}$ in Ba($\mathbf{L_{135}}$)(H_2O)$_{1.5}$(DMF)$_{0.5}$ (**2**)

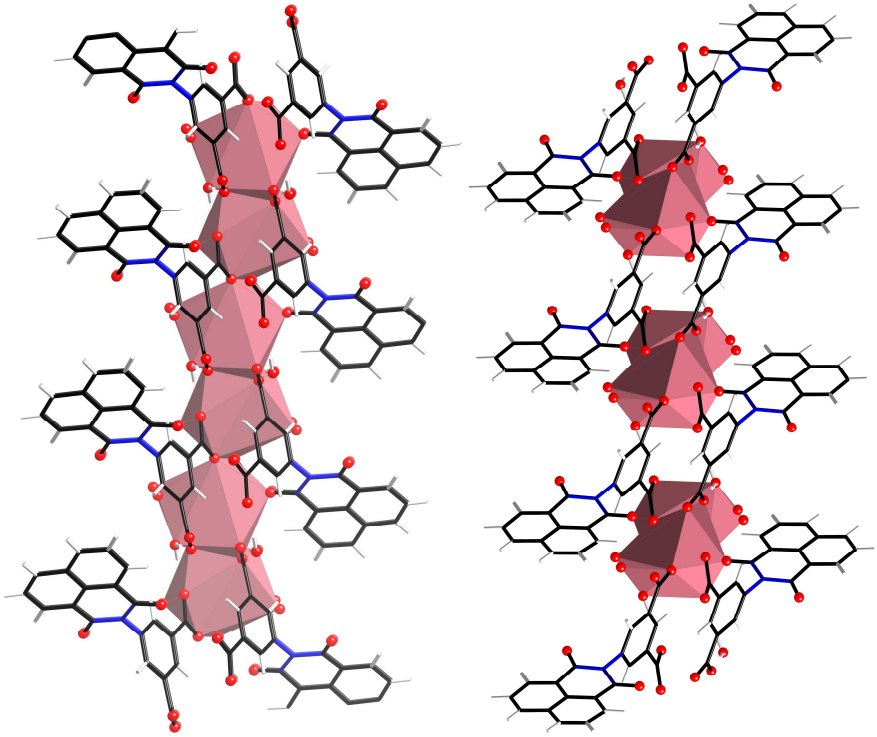

Figure 5.5. Views along edges of a sheet of compound **2** showing how ligand carboxylates bridge edge-shared barium polyhedra into 1D rod-shaped SBUs (left) and how rods are bridged into sheets with naphthalimide rings on either side (right).

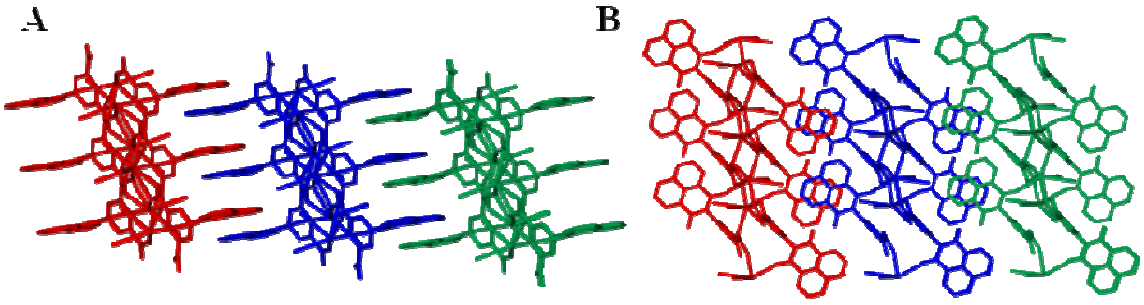

Figure 5.6. Views along [1 $\bar{1}$ 0] (**A**) and [1 1 0] (**B**) axis, showing the naphthalimide overlap between sheets of compound **2**. Adjacent sheets are colored differently.

Solid State structure of $La_2(L_{135})_3(DMF)_4$ (3). The solid state structure of **3** consists of dinuclear units of edge-sharing 9-coordinate La^{3+} cations that make up the SBU (Figure 5.7). The SBUs are connected in two dimensions by six bridging $\mathbf{L_{135}}^{2-}$ ligands to generate sheets in a square-shaped grid pattern, where the SBUs make up the nodes (Figure 5.8). Four of the ligands "di-bridge" SBUs along the crystallographic *a*-

axis while the other two ligands bridge SBUs along the crystallographic *c*-axis. This SBU is similar to others reported for lanthanide organic frameworks[21,32,33] and bares similarities to the paddlewheel SBU frequently observed with transition metals with four points of extension at 90° angles from one another.[19]

The 2D covalent sheets are engaged in π interactions with adjacent sheets on either side to generate a 3D SMOF (Figure 5.9). There are two types of π interactions that the naphthalimide is involved in: π···π interactions between naphthalimide rings of adjacent sheets and C-H···π interactions between rings within the same sheet (Figure 5.10). The π···π stacking interactions for compound **3** are listed in Table 5.2.

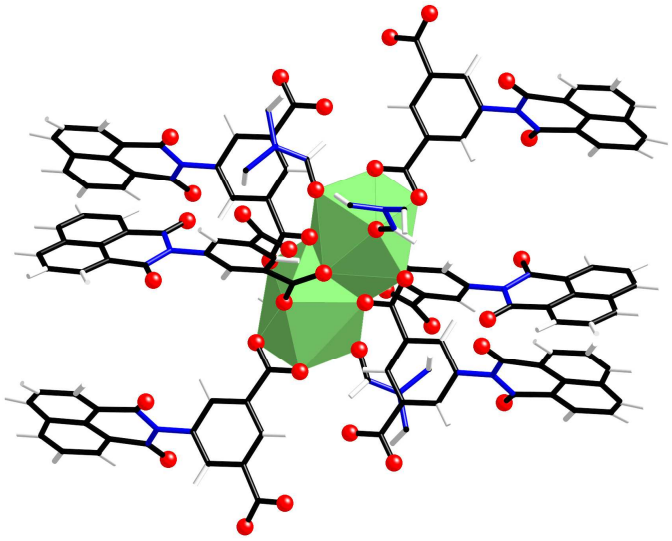

Figure 5.7. Secondary building unit (SBU) of compound $La_2(L_{135})_3(DMF)_4$ **(3)** consists of two edge shared La(III) cations.

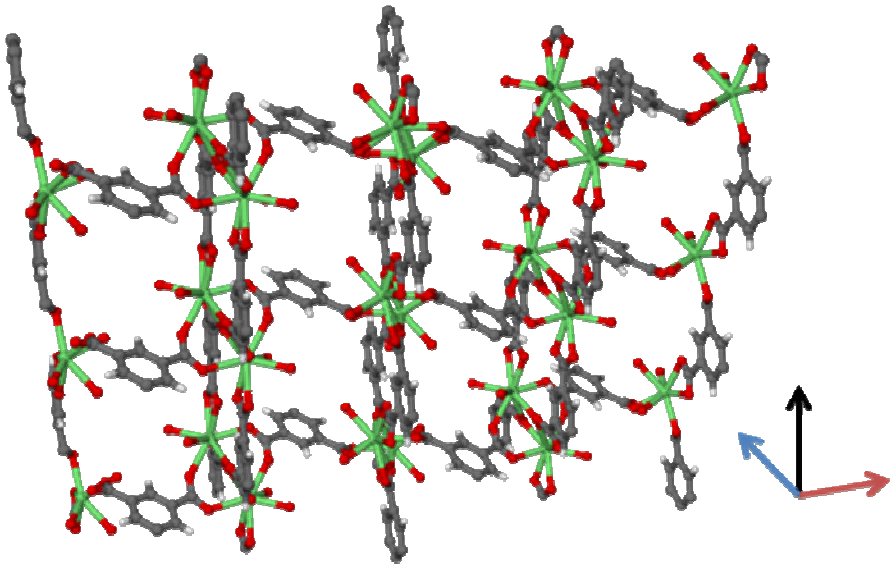

Figure 5.8. Covalent sheets (naphthalimide rings excluded) of compound **3** with di-bridging carboxylates along the *a*-axis (black) and singly-bridging carboxylates along the *c*-axis (red).

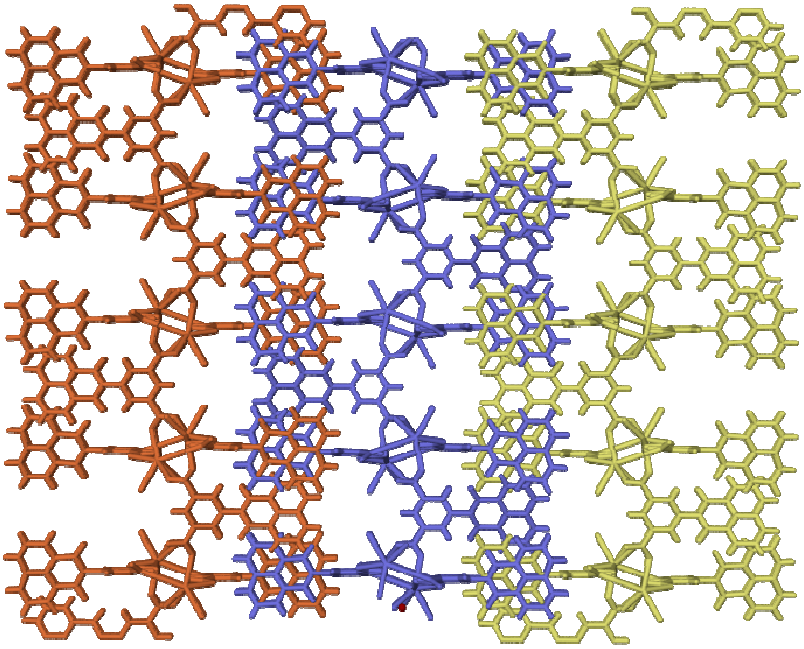

Figure 5.9. View showing interdigitation between covalent sheets of compound **3**.

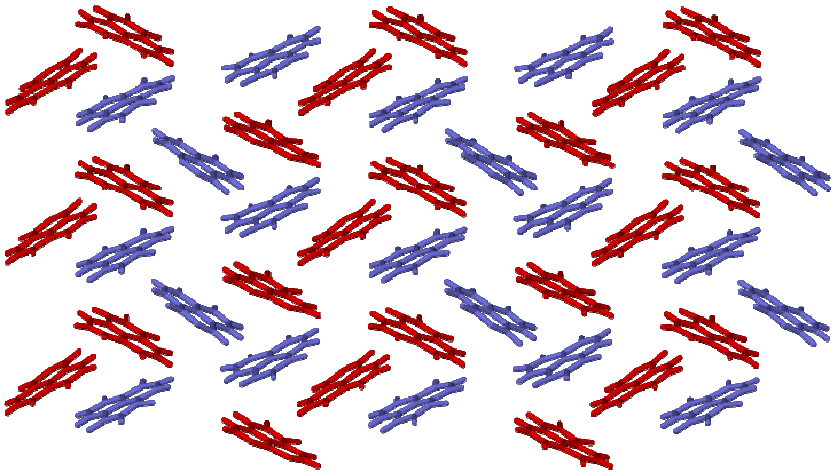

Figure 5.10. Orientation of naphthalimide rings between covalent sheets of compound **3** where rings from different sheets are different colors. There are C-H···π interactions within a sheet and π···π interactions between adjacent sheets.

The solid state structures of $La_2(\mathbf{L_{135}})_3(DMF)_4$ (**3**), $Ce_2(\mathbf{L_{135}})_3(DMF)_4$ (**4**), $Eu_2(\mathbf{L_{135}})_3(DMF)_4$ (**5**) and $Tb_2(\mathbf{L_{135}})_3(DMF)_4$ (**6**) are isostructural despite changes in the sizes of the metals. The extended structure and all π-stacking interactions remain the same with slight variations in the parameters due to differences in cation size (Table 5.2).

Solid State structure of $[UO_2(\mathbf{L_{135}})(DMF)]\cdot(py)_{0.5}(EtOH)_{0.5}$ (7). The solid state structure of **7** consists of 7-coordinate pentagonal bipyramid uranyl cations bridged by $\mathbf{L_{135}}^{2-}$ ligands into one dimensional ribbons. The coordination environment is typical for that of the uranyl cation (Figure 5.11) with the two axial sites occupied by oxide groups oriented at a 179° angle. Four of the five equatorial sites are occupied by carboxylates from three different ligands while the fifth is a dimethylformamide solvent molecule. For each ligand that bridges three uranyl cations, one of the carboxylates forms a κ^2 bond with one uranyl while the other forms a μ-$\kappa^1\kappa^1$ between two uranyl cations. Uranyl cations are dibridged by $\mathbf{L_{135}}^{2-}$ ligands to form a 1D ribbon (Figure 5.12). The naphthalimide rings end up on either side of the ribbon and interact with adjacent ribbons

to create a supramolecular 2D sheet (Figure 5.13). There are no interactions between the sheets of ribbons to generate a 3D SMOF structure (Figure 5.14).

There are uncoordinated solvent molecules, pyridine and ethanol, that occupy the space between pi stacking interactions so that the sequence is …-ring-ring-solvent-ring-ring-solvent-…. The pyridine molecule is engaged in pi stacking interactions on the outside of the naphthalimide ring sandwiches. The π···π stacking interactions for compound **7** are listed in Table 5.2.

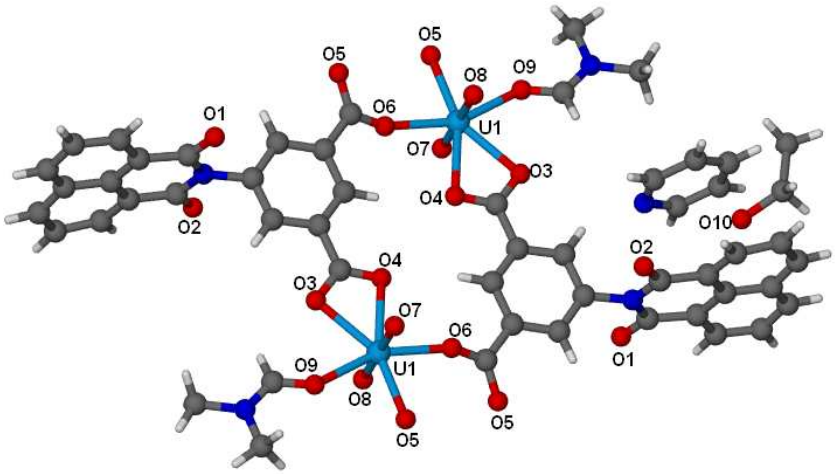

Figure 5.11. Building unit of a ribbon of $[UO_2(\mathbf{L_{135}})(DMF)]\cdot(py)_{0.5}(EtOH)_{0.5}$ (**7**)

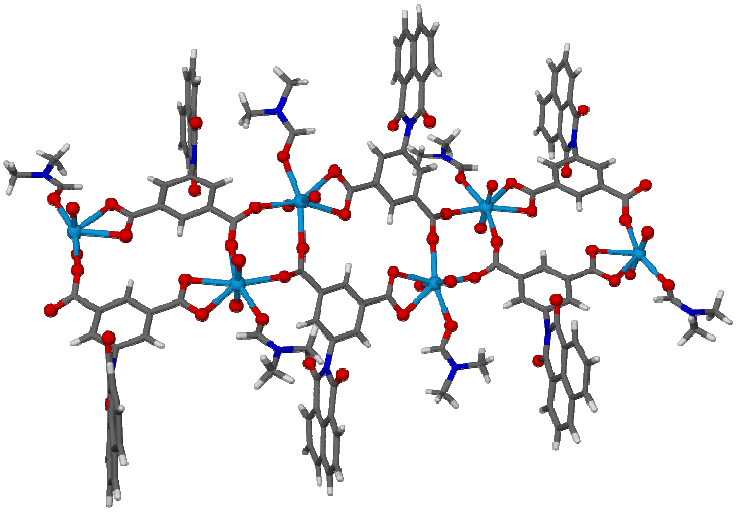

Figure 5.12. Ribbon of **7** extending along the crystallographic *a*-axis.

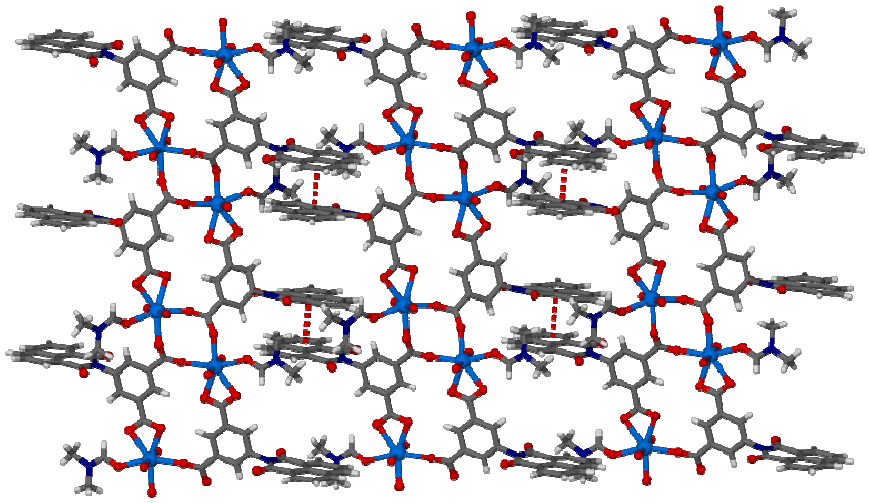

Figure 5.13. The π···π stacking between ribbons of **7** generating supramolecular 2D sheets along the *ac* plane

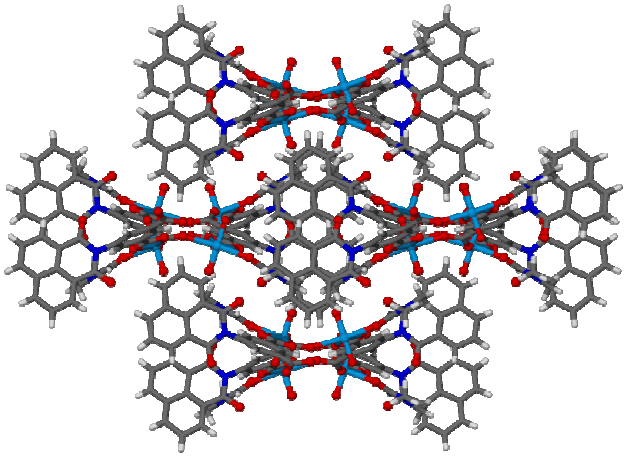

Figure 5.14. Four ribbons of **7** viewed down the *a*-axis with supramolecular sheets extending left and right and no interactions between ribbons above and below.

Solid State structure of [Th($\mathbf{L_{135}}$)$(NO_3)_2(DMF)_2$]·$(DMF)_2$ (8). The solid state structure of **8**, [Th($\mathbf{L_{135}}$)$(NO_3)_2(DMF)_2$]·$(DMF)_2$, consists of 10-coordinate thorium cations bridged by $\mathbf{L_{135}}^{2-}$ ligands in one dimensional ribbons. Of the ten coordination sites, four are occupied by oxygens from the carboxylates of $\mathbf{L_{135}}^{2-}$ originating from three distinct ligands, two are occupied by DMF solvent molecules (one of which is disordered over two positions) and the remaining four are occupied by two nitrate ligands chelating

through two oxygen atoms (Figure 5.15). The ligands coordinate to the thorium in a manner similar to that observed with the uranyl compound **7**, where one of the carboxylates forms a κ^2 bond with one thorium while the other forms a μ-$\kappa^1\kappa^1$ between two thorium cations. Figure 5.16 shows two side by side 1D ribbons where the ligands act to di-bridge thorium cations. There are $\pi^{\cdots}\pi$ stacking interactions (parameters listed in Table 5.2) between adjacent ribbons generating supramolecular 2D sheets along the *bc* plane. There are solvent-filled channels between the naphthalimide stacks that are occupied by disordered DMF molecules. As seen in Figure 5.17, there are no interactions between sheets making this a 2D SMOF structure.

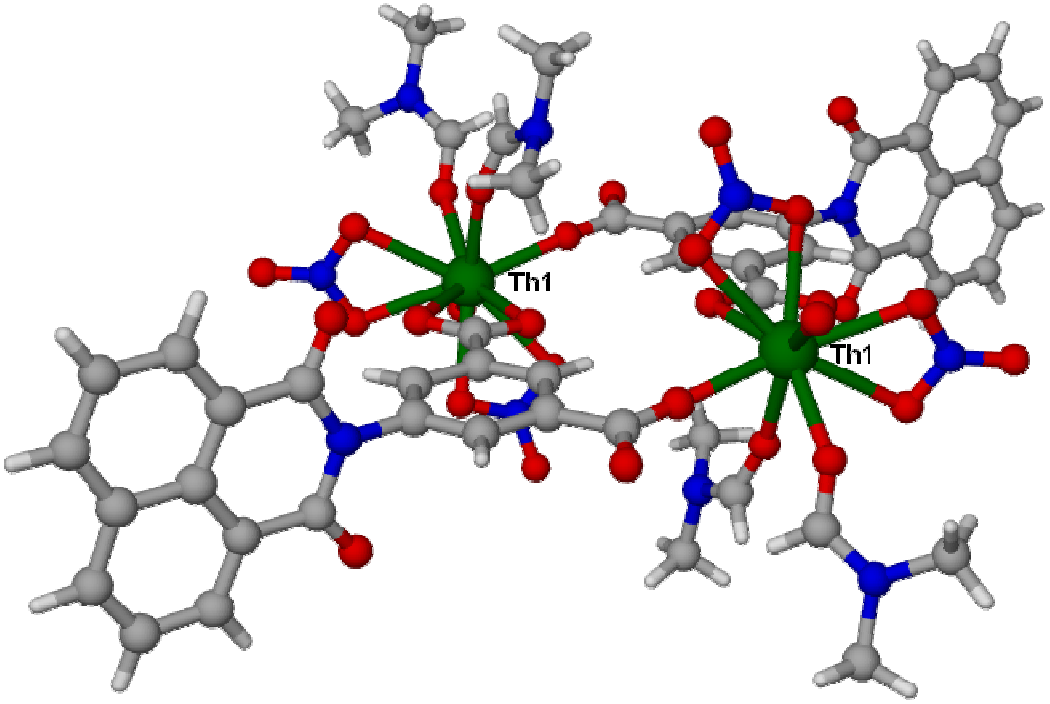

Figure 5.15. Building unit of a ribbon of [Th(**L$_{135}$**)$(NO_3)_2(DMF)_2]\cdot(DMF)_2$, (**8**).

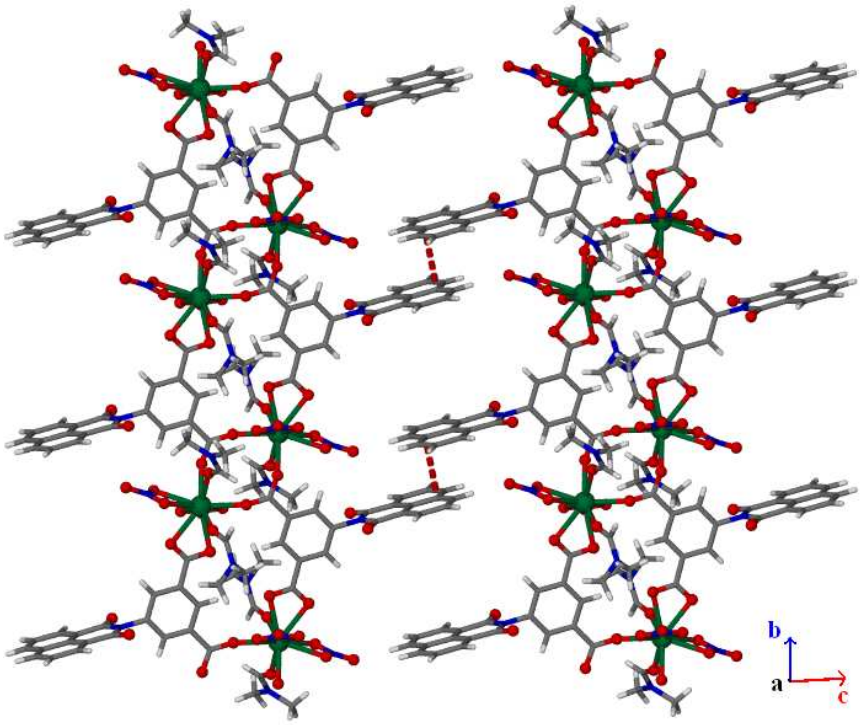

Figure 5.16. The π···π stacking of **8** between ribbons generating supramolecular 2D sheets along the *bc* plane.

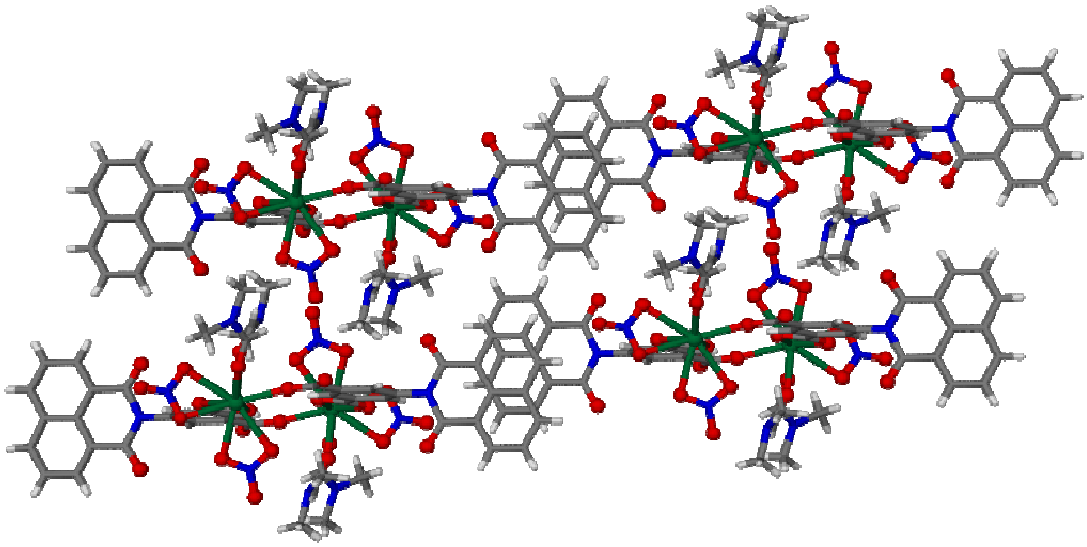

Figure 5.17. Four ribbons of **8** viewed down the *b*-axis with supramolecular sheets extending left and right and no interactions between ribbons above and below.

Table 5.2 Pi stacking parameters

	Compound	Type of Stacking	Cen-Cen (Å)[a]	dipole ∠ (°)[b]	plane ∠ (°)[c]	avg dist (Å)[d]	χ (Å)[e]
1	$[Ca_4(\mathbf{L_{135}})_4(H_2O)_8]\cdot(H_2O)_{9.5}(DMF)_{2.6}$	D-A	3.58	70.5	7.5	3.54	0.51
		A-B	3.54	69.9	7.4	3.50	0.52
		B-C	3.67	144.8	10.1	3.44	1.27
		C-D	3.59	70.1	1.4	3.38	1.22
2	$Ba(\mathbf{L_{135}})(H_2O)_{1.5}(DMF)_{0.5}$		3.71	180.0	0.0	3.38	1.53
3	$La_2(\mathbf{L_{135}})_3(DMF)_4$		4.99	179.1	5.2	3.47	3.57
			3.79	167.3	3.4	3.24	1.97
4	$Ce_2(\mathbf{L_{135}})_3(DMF)_5$		5.00	179.0	5.8	3.48	3.57
			3.81	167.7	4.2	3.24	2.00
5	$Eu_2(\mathbf{L_{135}})_3(DMF)_6$		4.86	179.9	5.6	3.48	3.39
			3.80	168.0	3.1	3.26	1.96
6	$Tb_2(\mathbf{L_{135}})_3(DMF)_7$		4.81	179.8	6.2	3.48	3.32
			3.81	168.1	3.9	3.27	1.96
7	$[UO_2(\mathbf{L_{135}})(DMF)]\cdot(py)_{0.5}(EtOH)_{0.5}$		3.64	133.4	6.3	3.63	0.31
8	$[Th(\mathbf{L_{135}})(NO_3)_2(DMF)_2]\cdot(DMF)_2$		4.70	180.0	0.0	3.55	3.08

a) the distance between the central carbon atoms of each ring b) the angle between the dipole vectors of each ring, which run through the central carbon atoms toward the nitrogen atoms c) the angle between the planes of each ring d) the average distance between the planes of each ring e) the slippage parameter describes the overlap of the two rings defined by the third side of the right triangle formed between the average perpendicular distance between the two rings and the line between the two central carbon atoms of each ring.

Thermal Analysis. Thermal gravimetric analysis was performed on a TA Instruments SDT 2960 under a steady stream of dry air. Compound **1** showed a weight loss at 138 °C that corresponds with a loss of the interstitial solvents: 3.26 H_2O and 1.79

DMF (15%, calcd. 17%). There is a second weight loss at 295 °C that corresponds with a loss of the coordination solvents: 3 H_2O and 1 DMF (10%, calcd. 11%). The powder remains stable until decomposition to calcium carbonate at 477 °C. Compound **2** shows a weight loss at ca. 156 °C that corresponds with a loss of the coordinated H_2O (5%, calcd. 5%) and a weight loss at ca. 318 °C that corresponds with a loss of the coordinated DMF (6 %, calcd. 6%). The compound decomposes into barium oxide above 420 °C. Compounds **3 - 6** have identical TGA plots with two features of loss of coordinated DMF (17%, calcd. 18%) at ca. 161 and 275 °C, with decomposition at 387 °C. Compound **7** shows a gradual weight loss between 80 and 412 °C that corresponds with a loss of the interstitial solvents (16%, calcd. 18%). The compound decomposes into uranium oxide after 412 °C.

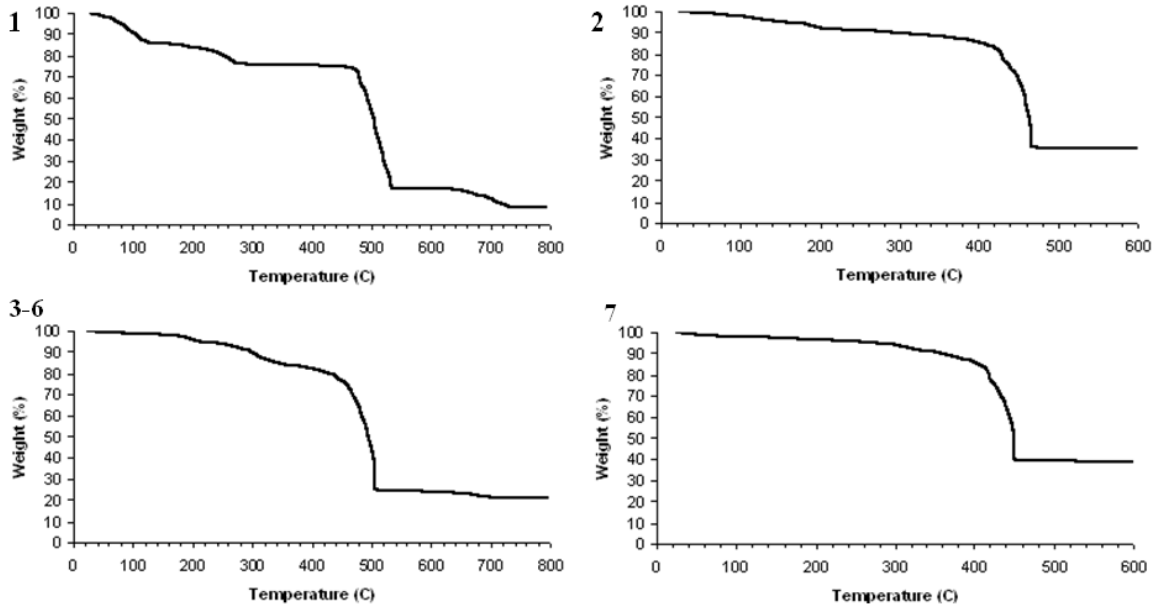

Figure 5.18. Thermal gravimetric analysis for compounds **1 – 7.**

Fluorescence. Compounds **1**, **2**, **3**, **6** and **8** exhibit solid-state luminescence dominated by the naphthalimide chromophore in the ligand (Figure 5.19). Based on the

excitation spectra, an excitation wavelength of 400 nm was used for all compounds except **6** (Tb), where 507 nm excitation was needed. A blue-green emission is observed where the maximum is slightly red-shifted with respect to the ligand in the case of the group 2 complexes **1** and **2** and slightly blue-shifted with respect to the ligand in the case of the lanthanum complex **3** and the thorium complex **8**. The terbium compound, **6**, had a similar broad emission as the other naphthalimide complexes, but red-shifted to the green-yellow region by ~75 nm.

Sensitization does occur for the europium complex, **5**, as seen in Figure 5.20. In a comparison to compound **3**, which is purely naphthalimide based fluorescence, the blue-green region decreases in intensity while the red region has intense well defined peaks correlating to Eu^{3+} emission.

Complexes containing cerium(III) or uranyl(VI), compounds **4** and **7**, have no solid state emission.

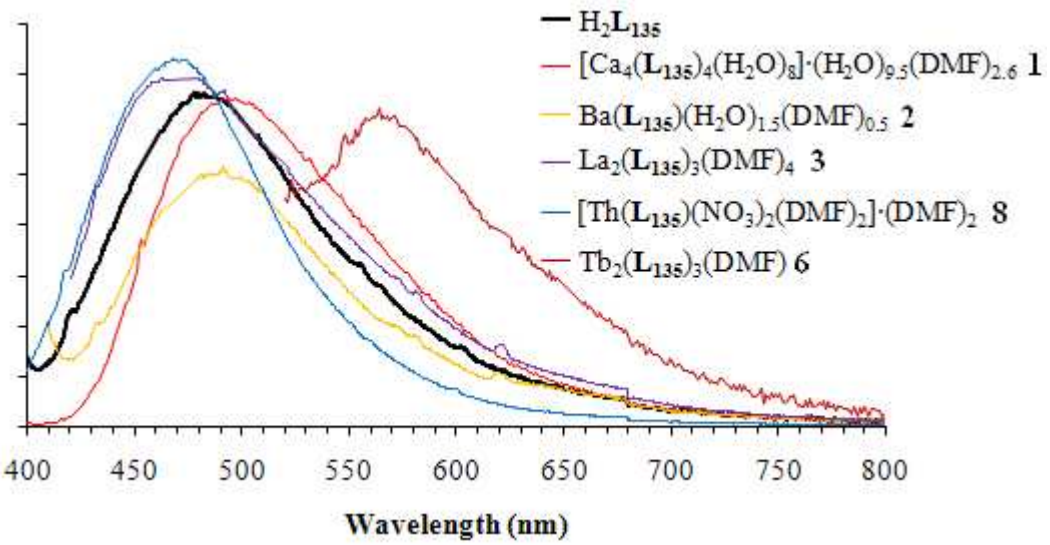

Figure 5.19. Fluorescence spectra of compounds **1**-**3**, **6**, **8** and the protonated ligand $H_2\mathbf{L_{135}}$.

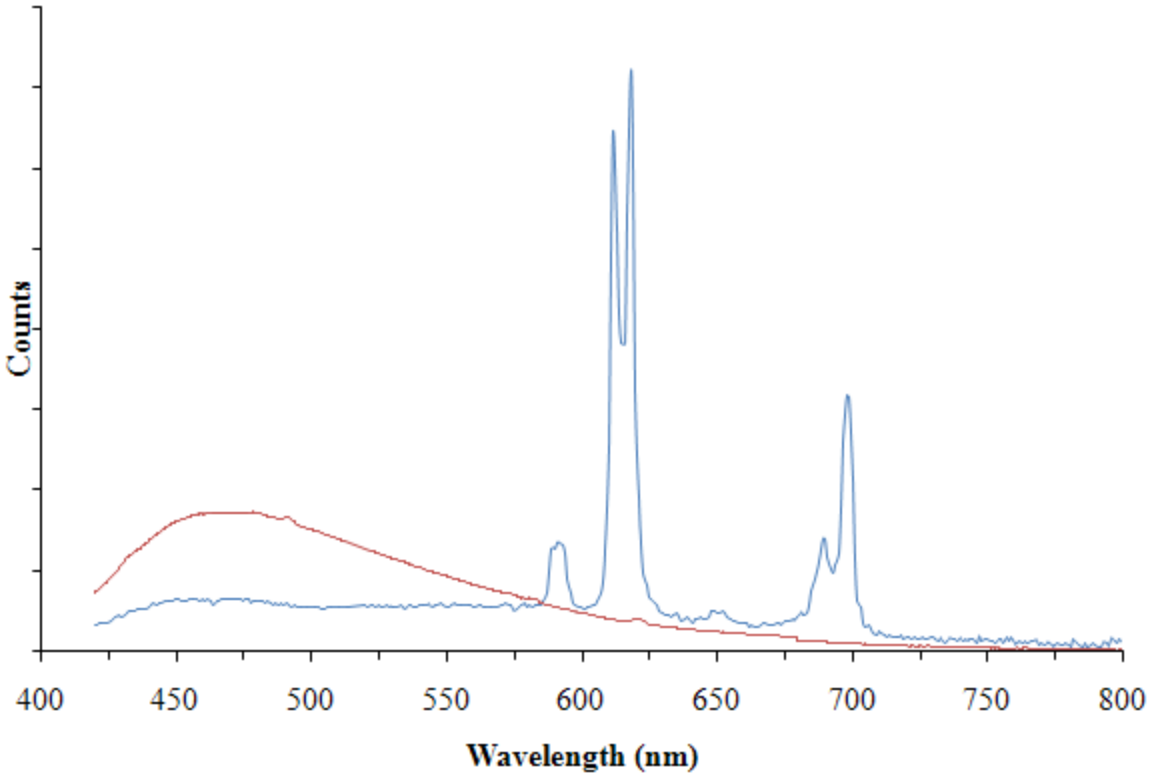

Figure 5.20. Fluorescence spectra of $Eu_2(\mathbf{L_{135}})_3(DMF)_4$ (**5**) in blue and $La_2(\mathbf{L_{135}})_3(DMF)_4$ (**3**) in red.

Discussion

The new ligand $\mathbf{L_{135}}^{2-}$ (Scheme 5.1) was synthesized and combined with a selection of metals from group 2 (Ca^{2+} and Ba^{2+}), lanthanides (La^{3+}, Ce^{3+}, Eu^{3+} and Tb^{3+}) and actinides (Th^{4+} and UO_2^{2+}) in order to study the impact of cation size and charge on the coordination environment and overall topology of the metal complexes. The key difference between $\mathbf{L_{135}}^{2-}$ and similar MOF ligands used by others[34–36] is the addition of the 1,8-naphthalimide supramolecular building block. This supramolecular tecton has shown a propensity to engage in $\pi\cdots$stacking interactions that have a significant influence on the solid state architecture, generating SMOF structures. In our previous work with group 1, 2 and lanthanide metals using less rigid, enantiopure ligands, *homochiral helices*

were observed either in helical rod SBUs or in the supramolecular organization of individual SBU helicates.[3,11,12,15]

The $\mathbf{L_{135}}^{2-}$ complexes of group 2 metals adopted two different SMOF structural types. Compound **1**, $[Ca_4(\mathbf{L_{135}})_4(H_2O)_8]\cdot(H_2O)_{9.5}(DMF)_{2.6}$, has one-dimensional (1D) rods of edge-shared calcium cations that interact with parallel rods only through π···π stacking to generate a 3D SMOF structure. Both *M* and *P* helical rod-shaped SBUs are present in the racemic crystals. A similar compound **[**$Ca(\mathbf{L_{ala}})_2(H_2O)]\cdot(H_2O)$, synthesized from enantiopure ligands, has a 1D homochiral helical rod-shaped SBU.[3] The SBUs from both calcium compounds have several points of connectivity with adjacent parallel SBUs via supramolecular nodes to form the 3D structure, which leaves channels occupied by disordered solvent.

Compound **2**, $Ba(\mathbf{L_{135}})(H_2O)_{1.5}(DMF)_{0.5}$, also has a rod-shaped SBU, but they are covalently bridged by the ligands to form 2D sheets that interact with adjacent sheets through π···π stacking to generate a 3D SMOF structure. The sheet-like structure is similar to others formed with group 1 metals when combined with the $\mathbf{L_{ser}}^-$ ligand, most notably K(**L**$_{\mathbf{ser}}$) and Cs(**L**$_{\mathbf{ser}}$).[11,18] Both $\mathbf{L_{ser}}^-$ and $\mathbf{L_{135}}^{2-}$ structures are formed by bridging edge-shared rod-shaped SBUs into sheets with naphthalimide rings on either side that interdigitate with adjacent sheets. A major difference is found in the supramolecular organization: the $\mathbf{L_{ser}}^-$ sheets are held together by continuous π···π stacking whereas the $\mathbf{L_{135}}^{2-}$ sheets have a space between each synthon occupied by disordered solvent (…-ring-ring-solvent-ring-ring-solvent-…). While the calcium and barium complexes are similar in their formation of edge-shared rod-shaped SBUs, the differences in 3D structure are most likely due to the larger ionic radius (1.14 Å compared to 1.49 Å) and coordination

number of barium. Barium also bares similarities to earlier sheet structures where the carbonyls of the naphthalimide ring are coordinated to the metal.[11,18]

The $\mathbf{L_{135}}^{2-}$ ligand forms a series of isostructural compounds based on binuclear SBUs, with La^{3+}, Ce^{3+}, Eu^{3+} and Tb^{3+}, despite the differences in cation size, ranging from 1.03 Å in the case of lanthanum(III) to 0.92 Å in the case of terbium(III). We have previously reported that a series of complexes formed between $\mathbf{L_{ser}}^{-}$ and a large range of lanthanides (La^{3+} through Dy^{3+}) had the same trinuclear, carboxylate-bonded helical structures.[15] In both complexes containing these ligands, we attribute the ability to prepare similar structures with metals of varying size to the accommodating and flexible nature of the π-stacking interactions. These lanthanide complexes form discrete SBUs as opposed to the 1D, rod-shaped SBUs that form for s-block metals. Interestingly, the structures of **3**-**6** contain our first case of C-H···π stacking between naphthalimide rings in SMOFs. These C-H···π stacking interactions occur within a sheet and do not disrupt the π···π stacking interactions between the sheets.

Both actinide (UO_2^{2+} and Th^{4+}) complexes form similar solid state structures with the $\mathbf{L_{135}}^{2-}$ ligand. These hard metals do not form edge- or corner-shared polyhedra and are exclusively bridged by carboxylates from the ligand into 1D ribbons, with π···π stacking generating only a 2D SMOF. Both metals have coordination environments with ligands other than $\mathbf{L_{135}}^{2-}$ that occupy part of the coordination sphere, O^{2-} in the case of U^{6+} and NO_3^- in the case of Th^{4+}. A recently reported uranyl complex with a 1,3-adamantanedicarboxylate ligand formed 1D ribbons similar to compound **7**.[24] The naphthalimide group affixed to the $\mathbf{L_{135}}^{2-}$ allows the 1D ribbons to extend to a 2D material through supramolecular interactions.

The complexes **1**, **2**, **3** and **8** have luminescence spectra based on the 1,8-naphthalimide moiety, with an intense broad emission in the blue-green region. While the group 2 complexes show the more typical slightly red-shifted spectra, the complexes with lanthanum(III) and thorium(III) have slightly blue-shifted spectra similar to previous complexes with $\mathbf{L_{ser}}^{-}$.[3,11] The terbium(III) complex **6** has the most red-shifted (~75 nm) peak out of any synthesized complex containing the naphthalimide group. Only for the europium complex **5** does the naphthalimide ligand act as a sensitizer for metal-based luminescence. The charge transfer between $\mathbf{L_{135}}^{2-}$ and Eu^{3+} is efficient enough that the ligand emission is decreased a significant amount while the europium emission is sharp and well-defined.

The remaining two complexes, **4** and **7** (Ce^{3+} and UO_2^{2+} based), are non-emissive. We have previously reported the ability of the cerium cation to quench naphthalimide fluorescence.[15] There have been a few reported cases of coordination polymers containing the uranyl cation and transition metals that have completely quenched fluorescence.[24,25,31] The fluorescence quenching mechanism for our cerium(III) and uranium(VI) complexes is most likely due to a charge transfer relaxation similar to those observed with transition metals.[37,38]

References

(1) Banerjee, D.; Parise, J. B. *Cryst. Growth Des.* **2011**, *11* (10), 4704–4720.

(2) Fromm, K. M. *Coord. Chem. Rev.* **2008**, *252* (8-9), 856–885.

(3) Reger, D. L.; Leitner, A.; Pellechia, P. J.; Smith, M. D. *Inorg. Chem.* **2014**, *53* (18), 9932–9945.

(4) Zhang, J.; Li, H.; Chen, P.; Sun, W.; Gao, T.; Yan, P. *J. Mater. Chem. C* **2015**, *3* (8), 1799–1806.

(5) Zhang, H.; Shan, X.; Zhou, L.; Lin, P.; Li, R.; Ma, E.; Guo, X.; Du, S. *J. Mater. Chem. C* **2013**, *1* (5), 888–891.

(6) Shelton, A. H.; Sazanovich, I. V.; Weinstein, J. A.; Ward, M. D. *Chem. Commun.* **2012**, *48* (22), 2749.

(7) Bonnet, C. S.; Devocelle, M.; Gunnlaugsson, T. *Org. Biomol. Chem.* **2012**, *10* (1), 126.

(8) Cook, T. R.; Zheng, Y. R.; Stang, P. J. *Chem. Rev.* **2013**, *113* (1), 734–777.

(9) Burrows, A. D.; Frost, C. G.; Mahon, M. F.; Richardson, C. *Angew. Chemie Int. Ed.* **2008**, *47* (44), 8482–8486.

(10) Williams, D. E.; Dolgopolova, E. A.; Pellechia, P. J.; Palukoshka, A.; Wilson, T. J.; Tan, R.; Maier, J. M.; Greytak, A. B.; Smith, M. D.; Krause, J. A.; Shustova, N. B. *J. Am. Chem. Soc.* **2015**, *137* (6), 2223–2226.

(11) Reger, D. L.; Leitner, A.; Smith, M. D.; Tran, T. T.; Halasyamani, P. S. *Inorg. Chem.* **2013**, *52* (17), 10041–10051.

(12) Reger, D. L.; Horger, J. J.; Smith, M. D.; Long, G. J.; Grandjean, F. *Inorg. Chem.* **2011**, *50* (2), 686–704.

(13) Reger, D. L.; Horger, J. J.; Debreczeni, A.; Smith, M. D. *Inorg. Chem.* **2011**, *50* (20), 10225–10240.

(14) Reger, D. L.; Debreczeni, A.; Smith, M. D. *Inorg. Chem.* **2011**, *50* (22), 11754–11764.

(15) Reger, D. L.; Leitner, A.; Smith, M. D. *Cryst. Growth Des.* **2015**. *15*(11), 5637-5644.

(16) An, J.; Shade, C. M.; Chengelis-Czegan, D. A.; Petoud, S.; Rosi, N. L. *J. Am. Chem. Soc.* **2011**, *133* (5), 1220–1223.

(17) Reger, D. L.; Debreczeni, A.; Horger, J. J.; Smith, M. D. *Cryst. Growth Des.* **2011**, *11* (9), 4068–4079.

(18) Reger, D. L.; Leitner, A.; Smith, M. D. *J. Mol. Struct.* **2015**, *1091*, 31–36.

(19) Reger, D. L.; Debreczeni, A.; Reinecke, B.; Rassolov, V.; Smith, M. D.; Semeniuc, R. F. *Inorg. Chem.* **2009**, *48* (18), 8911–8924.

(20) Reger, D. L.; Debreczeni, A.; Smith, M. D.; Jezierska, J.; Ozarowski, A. *Inorg. Chem.* **2012**, *51* (2), 1068–1083.

(21) Lam, A. W.-H.; Wong, W.-T.; Gao, S.; Wen, G.; Zhang, X.-X. *Eur. J. Inorg. Chem.* **2003**, *2003* (1), 149–163.

(22) Yang, X.; Jones, R. A.; Huang, S. *Coord. Chem. Rev.* **2014**, *273-274*, 63–75.

(23) Zhang, Y.; Price, J. R.; Karatchevtseva, I.; Lu, K.; Yoon, B.; Kadi, F.; Lumpkin, G. R.; Li, F. *Polyhedron* **2015**, *91*, 98–103.

(24) Thuéry, P.; Rivière, E.; Harrowfield, J. *Inorg. Chem.* **2015**, *54* (6), 2838–2850.

(25) Thuéry, P.; Harrowfield, J. *Inorg. Chem.* **2015**, *54* (13), 6296–6305.

(26) Shiri-Yekta, Z.; Nilchi, A.; Yaftian, M. R.; Yousefnia, H. *J. Radioanal. Nucl. Chem.* **2014**, *302* (3), 1143–1150.

(27) Severance, R. C.; Vaughn, S. A.; Smith, M. D.; zur Loye, H.-C. *Solid State Sci.* **2011**, *13* (6), 1344–1353.

(28) Ok, K. M.; Sung, J.; Hu, G.; Jacobs, R. M. J.; Hare, D. O. *J. Am. Chem. Soc.* **2008**, 3762–3763.

(29) Adelani, P. O.; Albrecht-Schmitt, T. E. *Inorg. Chem.* **2010**, *49* (12), 5701–5705.

(30) Chen, F.; Wang, C.; Li, Z.; Lan, J.; Ji, Y.; Chai, Z. *Inorg. Chem.* **2015**, *54* (8), 3829–3834.

(31) Wu, H. Y.; Wang, R. X.; Yang, W.; Chen, J.; Sun, Z. M.; Li, J.; Zhang, H. *Inorg. Chem.* **2012**, *51* (5), 3103–3107.

(32) Yin, M. C.; Ai, C. C.; Yuan, L. J.; Wang, C. W.; Sun, J. T. *J. Mol. Struct.* **2004**, *691* (1-3), 33–37.

(33) Oyang, L.; Sun, H.-L.; Wang, X.-Y.; Li, J.-R.; Nie, D.-B.; Fu, W.-F.; Gao, S.; Yu, K.-B. *J. Mol. Struct.* **2005**, *740*, 175–180.

(34) Wang, C.; Wang, Z.; Gu, F.; Guo, G. *J. Mol. Struct.* **2011**, *1004* (1-3), 39–44.

(35) Manos, M. J.; Kyprianidou, E. J.; Papaefstathiou, G. S.; Tasiopoulos, A. J. *Inorg. Chem.* **2012**, *51* (11), 6308–6314.

(36) Eubank, J. F.; Wojtas, L.; Hight, M. R.; Bousquet, T.; Kravtsov, V. C.; Eddaoudi, M. *J. Am. Chem. Soc.* **2011**, 17532–17535.

(37) Setlur, A. A.; Shiang, Joseph, J. *J. Phys. Chem. C* **2010**, *114*, 2792–2798.

(38) Shakhverdov, T. A. *Opt. Spectrosc.* **2003**, *95* (4), 571–580.

Appendix A: Copyright Permissions

Title: “Homochiral helical metal-organic frameworks of group 1 metals”

Author: Daniel L. Reger, Reger, D. L.; Leitner, A.; Smith, M. D.; Tran, T. T.; Halasyamani, P. S.

Publication: Inorganic Chemistry

Publisher: American Chemical Society

Date: August 14, 2013

Copyright 2013, American Chemical Society

PERMISSION/LICENSE IS GRANTED FOR YOUR ORDER AT NO CHARGE

This type of permission/license, instead of the standard Terms & Conditions, is sent to you because no fee is being charged for your order. Please note the following:

Permission is granted for your request in both print and electronic formats, and translations.

If figures and/or tables were requested, they may be adapted or used in part.

Please print this page for your records and send a copy of it to your publisher/graduate school.

Appropriate credit for the requested material should be given as follows: "Reprinted (adapted) with permission from (COMPLETE REFERENCE CITATION). Copyright (YEAR) American Chemical Society." Insert appropriate information in place of the capitalized words.

One-time permission is granted only for the use specified in your request. No additional uses are granted (such as derivative works or other editions). For any other uses, please submit a new request.

Title: “Framework Complexes of Group 2 Metals Organized by Homochiral Rods and π···π Stacking Forces: A Breathing Supramolecular MOF”

Author: Daniel L. Reger, Andrew Leitner, Perry J. Pellechia, and Mark D. Smith

Publication: Inorganic Chemistry

Publisher: American Chemical Society

Date: August 26, 2014

Copyright 2014, American Chemical Society

PERMISSION/LICENSE IS GRANTED FOR YOUR ORDER AT NO CHARGE

This type of permission/license, instead of the standard Terms & Conditions, is sent to you because no fee is being charged for your order. Please note the following:

Permission is granted for your request in both print and electronic formats, and translations.

If figures and/or tables were requested, they may be adapted or used in part.

Please print this page for your records and send a copy of it to your publisher/graduate school.

Appropriate credit for the requested material should be given as follows: "Reprinted (adapted) with permission from (COMPLETE REFERENCE CITATION). Copyright (YEAR) American Chemical Society." Insert appropriate information in place of the capitalized words.

One-time permission is granted only for the use specified in your request. No additional uses are granted (such as derivative works or other editions). For any other uses, please submit a new request.

Title: “Homochiral, Helical Coordination Complexes of Lanthanides(III) and Mixed-Metal Lanthanides(III): Impact of the 1,8-Naphthalimide Supramolecular Tecton on Structure, Magnetic Properties, and Luminescence”

Author: Daniel L. Reger, Andrew Leitner, Mark, D. Smith

Publication: Crystal Growth & Design

Publisher: American Chemical Society

Date: October 12, 2015

Copyright 2015, American Chemical Society

PERMISSION/LICENSE IS GRANTED FOR YOUR ORDER AT NO CHARGE

This type of permission/license, instead of the standard Terms & Conditions, is sent to you because no fee is being charged for your order. Please note the following:

Permission is granted for your request in both print and electronic formats, and translations.

If figures and/or tables were requested, they may be adapted or used in part.

Please print this page for your records and send a copy of it to your publisher/graduate school.

Appropriate credit for the requested material should be given as follows: "Reprinted (adapted) with permission from (COMPLETE REFERENCE CITATION). Copyright (YEAR) American Chemical Society." Insert appropriate information in place of the capitalized words.

One-time permission is granted only for the use specified in your request. No additional uses are granted (such as derivative works or other editions). For any other uses, please submit a new request.

This is a License Agreement between Andrew Leitner ("You") and Elsevier ("Elsevier") provided by Copyright Clearance Center ("CCC"). The license consists of your order details, the terms and conditions provided by Elsevier, and the payment terms and conditions.

Supplier	Elsevier Limited The Boulevard,Langford Lane Kidlington,Oxford,OX5 1GB,UK
Registered Company Number	1982084
Customer name	Andrew Leitner
Customer address	631 Sumter St. COLUMBIA, SC 29205
License number	3733690695108
License date	Oct 21, 2015
Licensed content publisher	Elsevier
Licensed content publication	Journal of Molecular Structure
Licensed content title	Cesium complexes of naphthalimide substituted carboxylate ligands: Unusual geometries and extensive cation-π interactions
Licensed content author	Daniel L. Reger,Andrew Leitner,Mark D. Smith
Licensed content date	5 July 2015
Licensed content volume number	1091
Number of pages	6
Start Page	31
End Page	36
Type of Use	reuse in a thesis/dissertation

Portion	full article
Format	both print and electronic
Are you the author of this Elsevier article?	Yes
Will you be translating?	No
Title of your thesis/dissertation	Supramolecular Coordination Networks of s- and f-Block Metals Featuring the 1,8-Naphthalimide Tecton
Expected completion date	Nov 2015
Estimated size (number of pages)	170
Elsevier VAT number	GB 494 6272 12
Permissions price	0.00 USD
VAT/Local Sales Tax	0.00 USD / 0.00 GBP
Total	0.00 USD